Εθνικό Μετσόβιο Πολυτεχνείο

Διπλωματική Εργασία

Υπολογιστική προσέγγιση στον υπολογισμό της ηλικίας του αέρα, ως παράμετρος της ποιότητας του αέρα

Συγγραφέας:
Νικόλαος Μπέλτσος

Επιβλέπων:
Δημήτριος Μπούρης

Εργαστήριο Τεχνολογικών Καινοτομιών Προστασίας Περιβάλλοντος
Σχολή Μηχανολογών Μηχανικών, ΕΜΠ

Αθήνα, Οκτώβριος 2023

National Technical University of Athens

Diploma Thesis

A computational approach to the calculation of age of air, as a parameter of air quality

Author: Nicholas Beltsos

Supervisor: Dimitrios Bouris

Laboratory of Innovative Environmental Technologies School
of Mechanical Engineering, NTUA

Athens, October 2023

Preface

The current thesis was written for the Laboratory for Innovative Environmental Technologies (LIET) of the School of Mechanical Engineering in the National Technical University of Athens (NTUA) during the academic year 2022-2023 under the supervision of Professor Dimitrios Bouris. The aim of the thesis is the development of a numerical simulation tool that calculates the age of air inside a building.

At this point, I would like to express my deepest gratitude to my professor, Dimitri Bouri, for his invaluable guidance, patience and adaptive flexibility over the entire process of writing this thesis. I would also like to thank my parents for their unwavering love and support throughout my academic journey.

Statement of Responsibility for Plagiarism and Intellectual Property Theft

I have read and understood the rules regarding plagiarism and the proper citation of sources outlined in the Guidelines for Thesis Writing. I hereby declare that, to the best of my knowledge, the content of this work is the result of my own effort, and I have provided references to all sources used.

Nicholas Beltsos

Abstract

The primary objective of this thesis is to develop a numerical tool capable of calculating the age of air (AOA) at various locations within a building. The age of air is a crucial parameter that provides insights into the freshness of indoor air, enabling the assessment of ventilation effectiveness. Many of the common parameters used in assessing ventilation ignore the impact of molecular and turbulent diffusion, often proving inadequate when incomplete mixing conditions exist. In scenarios where air mixing is not ideal, the air entering specific areas comprises a blend of recirculated and fresh air, making it challenging to describe the system's behavior accurately. To characterize the freshness and dilution capacity of air at a particular point, we rely on its "age," which proves to be a valuable metric.

Numerous approaches to determine the age of air have been explored, both experimentally through tracer gas techniques and numerically. The primary numerical approach involves solving a transport equation, necessitating knowledge of the velocity field and fluid properties. In this thesis, we introduce a software solution that employs Computational Fluid Dynamics (CFD) techniques to solve this transport equation for steady turbulent flows. An important additional requirement was the compatibility of the developed Fortran code with the laboratory's existing Computational Fluid Dynamics (CFD) software. This compatibility was crucial to facilitate the integration of the new code into the laboratory's workflow and leverage any existing resources effectively.

The software was applied in multiple test cases, yielding consistent results with expected airflow patterns. Furthermore, through a series of simulations on building models, several points of interest were identified regarding the distribution of age of air within them and the effectiveness of their natural ventilation. Lastly, during the course of the research, certain areas for improvement and enhancement have been identified. These areas offer opportunities to refine the software's performance and expand its capabilities.

Περίληψη

Ο κύριος στόχος αυτής της Διπλωματικής εργασίας είναι να αναπτυχθεί ένα αριθμητικό εργαλείο που να υπολογίζει την ηλικία του αέρα σε διάφορα σημεία εντός ενός κτιρίου. Η ηλικία του αέρα είναι μια χρήσιμη παράμετρος που παρέχει πληροφορίες σχετικά με το πόσο «φρέσκος» είναι ο αέρας στο εσωτερικό ενός κτιρίου, επιτρέποντας την αξιολόγηση της αποτελεσματικότητας του αερισμού. Πολλές από τις διαδεδομένες παραμέτρους που χρησιμοποιούνται στην αξιολόγηση του αερισμού, αγνοούν την επίδραση της μοριακής και τυρβώδους διάχυσης και συχνά αποδεικνύονται ανεπαρκείς, όταν υπάρχουν ατελείς συνθήκες ανάμειξης. Σε σενάρια όπου η ανάμειξη του αέρα δεν είναι ιδανική, ο αέρας που εισέρχεται σε συγκεκριμένα σημεία αποτελεί ένα μείγμα από ανακυκλωμένο και «φρέσκο» αέρα, καθιστώντας δύσκολη την ακριβή περιγραφή της συμπεριφοράς του συστήματος. Για να χαρακτηριστεί η «φρεσκάδα» του αέρα σε ένα συγκεκριμένο σημείο, βασιζόμαστε στην «ηλικία» του, που αποδεικνύεται ότι είναι ένας πολύτιμος δείκτης.

Έχουν εξερευνηθεί πολλές προσεγγίσεις για τον προσδιορισμό της ηλικίας του αέρα, τόσο πειραματικές μέσω τεχνικών με αέρια-δείκτες όσο και αριθμητικές. Η κύρια αριθμητική

προσέγγιση περιλαμβάνει την επίλυση μιας εξίσωσης μεταφοράς, που απαιτεί γνώση του πεδίου ταχύτητας και της συνεκτικότητας. Σε αυτή την εργασία, παρουσιάζεται η ανάπτυξη και εφαρμογή ενός λογισμικού που χρησιμοποιεί τεχνικές Υπολογιστικής Ρευστομηχανικής (CFD) για να επιλύσει αυτήν την εξίσωση μεταφοράς για μόνιμες τυρβώδεις ροές. Ένα πρόσθετο σημαντικό απαιτούμενο της παρούσας εργασίας, είναι η συμβατότητα του αναπτυγμένου κώδικα Fortran με το υπάρχον λογισμικό CFD του Εργαστηρίου Τεχνολογικών Καινοτομιών Προστασίας Περιβάλλοντος. Αυτή η συμβατότητα είναι σημαντική για τη διευκόλυνση της ενσωμάτωσης του νέου κώδικα στη ροή εργασιών του εργαστηρίου και την αποτελεσματική χρήση των υπαρχόντων πόρων.

Το λογισμικό εφαρμόστηκε σε πολλαπλές περιπτώσεις δοκιμής, δίνοντας αποτελέσματα συνεπή με τα αναμενόμενα μοτίβα ροής. Επιπλέον, μέσα από μια απο μια σειρά προσομοιώσεων σε μοντέλα κτιρίων, εντοπιστήκαν αρκετά σημεία ενδιαφέροντος ως προς την κατανομή της ηλικίας του αέρα στο εσωτερικό τους και την αποτελεσματικότητα του φυσκού αερισμού τους. Τέλος, κατά τη διάρκεια της έρευνας, προσδιορίστηκαν ορισμένα περιοχές για βελτίωση και εξέλιξη του υπολογιστικού εργαλείου. Αυτές οι περιοχέςαποτελούν ευκαιρία για περαιτέρω ενίσχυση της απόδοσης του λογισμικού και τη διεύρυνση των δυνατοτήτων του.

Table of Contents

Table of Figures

Chapter 1: Introduction

1.1 Outline of the Thesis

In the first chapter the focus is on introducing the significance of indoor air quality in our daily lives. It emphasizes the crucial role of ventilation systems in maintaining and improving air quality indoors. Furthermore, this chapter outlines the existing standards and regulations that define the criteria for effective ventilation. Lastly, it provides an overview of the prior research studies that have contributed to the adoption of "age of air" as a pivotal parameter for evaluating ventilation effectiveness. The second chapter is dedicated to clarifying some key concepts in fluid mechanics. The third and fourth chapters of the thesis are dedicated to outlining the concept of age of air and its mathematical background. The next two chapters describe the computational approach that was used to develop the software.

The last two chapters are dedicated to test cases. Initially, the software was tested using simple test cases often with well-defined analytical solutions. This step was crucial to establish the software's reliability and correctness in fundamental scenarios. Subsequently, the software underwent a more comprehensive testing phase, where it was applied to simulate airflow within various building configurations. These real-world cases represented complex indoor environments with different architectural layouts and flow characteristics. By subjecting the software to these diverse building configurations, it was possible to assess its performance under more challenging and realistic conditions.

1.2 Indoor Air Quality (IAQ)

Unfortunately, air pollution exists inside a variety of interior environments in which people live and work, such as industrial workplaces, office buildings, schools, hospitals, tunnels, mines, private homes and apartment buildings. Indoor Air Quality (IAQ) pertains to the quality of the air within and in the vicinity of buildings and structures, with a particular emphasis on how it affects the well-being and comfort of the individuals in those spaces. Good indoor air quality (IAQ) can be described as air that does not contain harmful concentrations of known contaminants. These contaminants or pollutants typically encompass gaseous elements like carbon dioxide (emanating from occupants and combustion devices), volatile organic compounds (released by substances like carpet adhesives), odors, and particulate matter. Maintaining good IAQ is crucial for safeguarding the well-being and comfort of individuals inhabiting the space.

1.2.1 Common Contaminants and Related Health Issues

According to The Chartered Institution of Building Services Engineers (CIBSE) [1], common contaminants can be divided into the following categories:

Gaseous pollutants

Common gaseous contaminants present in indoor environments encompass carbon dioxide (CO_2), carbon monoxide (CO), nitrogen oxides (NO and NO_2), sulfur dioxide, ozone (O_3), and, in specific locations, naturally occurring radon gas.

- **Carbon dioxide**, perhaps the most prevalent pollutant, is exhaled as a metabolic byproduct and emanates from appliances like gas stoves and boilers. While it is non-toxic under

normal conditions, elevated concentrations (above 10,000 ppm) can induce drowsiness and, at significantly higher levels, unconsciousness.

- Conversely, **carbon monoxide** poses a high toxicity risk at low concentrations (above 86 ppm). It forms when there is insufficient oxygen for combustion or in the case of malfunctioning combustion appliances [2]. External sources, particularly vehicles, can also contribute to its presence. Due to its poisonous nature and the potential for formation in tightly sealed buildings,
- **Nitrogen oxides**, specifically NO and NO_2, are generated during combustion, especially at elevated temperatures. Sulfur dioxide is a byproduct of burning sulfur-containing fuels, such as fuel oil.
- **Ozone** is produced when sunlight interacts with nitrogen oxides. Nitrogen oxides, sulfur dioxide, and ozone can irritate the respiratory system [3].
- **Radon** is emitted by certain types of rocks, like granite. While radon gas itself has limited adverse effects (as it can be blocked by relatively thin materials), associated radioactive isotopes released during the decay process can be carcinogenic if inhaled [4]. Special precautions, such as low permeability membranes and extraction systems, are necessary in areas with high radon concentrations to prevent its seepage into buildings.

Emission rates for these pollutants can be determined under specific conditions, such as varying activity levels or combustion rates in boilers. Knowing the emission rate enables the calculation of the necessary ventilation to dilute pollutant concentrations to safe levels.

Volatile organic compounds (VOCs)

Volatile organic compounds (VOCs) encompass substances like benzene, formaldehyde, and trichloroethylene (TCE):

- **Benzene**: This compound serves as a solvent and can be found in various products such as paints, plastics, inks, and rubber.
- **Formaldehyde**: Released by laminates, paints, and adhesives, formaldehyde is commonly encountered in indoor environments.
- **Trichloroethylene (TCE)**: TCE is employed in the manufacturing of inks, paints, lacquers, and adhesives.

Many VOCs are characterized by unpleasant odors, and some of them possess carcinogenic properties, posing health risks to individuals exposed to them in indoor settings [5].

Odors

Occasionally, pinpointing the reasons behind complaints regarding inadequate indoor air quality (IAQ) can be challenging. For instance, concentrations of recognized pollutants may fall below established thresholds or recommended short-term exposure limits. Nevertheless, some of these substances can give rise to odors, including some that might be displeasing and lead to grievances from occupants.

The origins of these odors encompass various factors. Cooking activities can emit distinct odors, as can the decay of food items, unsanitary appliances like toilets and sinks, drainage systems for soil and wastewater, building materials, furnishings, and even human activities, such as perspiration. These odors often consist of combinations of volatile organic compounds (VOCs), water vapor, and fragrant gases. When cooking odors are effectively contained using exhaust ventilation systems within hoods and other odors are prevented from infiltrating a building through the use of vapor barriers and well-sealed enclosures, the primary sources of indoor odors are typically attributed to human presence and emissions from building materials and furnishings.

Particulates

Particulates are tiny particles that originate from various sources, including human occupants, combustion processes, and external factors like vegetation and vehicle emissions. They can also be emitted from materials such as clothing, carpets, wallboard, aerosol sprays, dust mites, insects, and molds [6]. Among these, biogenic pollutants resulting from biological processes (such as fungi, molds, mites, bacteria, viruses, and pollen) are responsible for many health issues, including lung irritation, bronchial asthma, and allergic rhinitis. Additionally, toxic particulates like asbestos fibers and tobacco-related products pose health risks.

These particles typically vary in size, ranging from 0.1 to 10,000 micrometers (μm). Particularly critical sizes are those below 10 μm and 2.5 μm, commonly referred to as PM10 and PM2.5, respectively.

Water vapor

Water vapor can be regarded as a contaminant since its existence elevates relative humidity levels and encourages the development of mold [7]. Moreover, it can influence the rate at which volatile organic compounds (VOCs) are released. Water vapor is emitted by individuals and originates from activities such as laundry, cooking, and the operation of combustion appliances.

1.2.2 Additional Risks Associated with Bad IAQ

Health consequences stemming from indoor air pollutants can manifest either shortly after exposure or potentially many years later.

- **Immediate Effects**: Certain health consequences may become apparent shortly after a single exposure or repeated exposures to indoor pollutants. These immediate effects encompass irritation of the eyes, nose, and throat, as well as symptoms such as headaches, dizziness, and fatigue. Typically, these immediate effects are of short duration and amenable to treatment. In some instances, addressing these symptoms may involve simply removing the individual from the source of pollution, if it can be identified. Additionally, shortly after exposure to specific indoor air pollutants, symptoms associated with certain diseases, such as asthma, may emerge, be exacerbated, or worsen [8]. The likelihood of immediate reactions to indoor air pollutants hinges on various factors, including a person's age and existing medical conditions. In some cases, an individual's response to a pollutant is contingent on their unique sensitivity, which can vary significantly from person to person. After repeated or high-level exposures, some individuals can develop sensitivities to biological or chemical pollutants. Certain immediate effects can resemble symptoms associated with colds or other viral illnesses, making it challenging to ascertain whether the symptoms result from indoor air pollution exposure. Hence, it is vital to take note of when

and where these symptoms occur. For instance, if symptoms subside or disappear when an individual is away from a specific area, efforts should be made to identify potential indoor air sources that could be contributing to the issues. Additionally, inadequate outdoor air supply or prevailing conditions related to heating, cooling, or humidity indoors can exacerbate some effects.

- **Long-Term Effects**: Some health consequences may become evident years after exposure has occurred, or they may manifest only after extended or repeated exposure periods. These effects encompass certain respiratory ailments, heart conditions, and cancer, which can be profoundly disabling or even fatal. It is advisable to take measures to enhance indoor air quality in your home, even if symptoms are not currently noticeable [9].

Although indoor air commonly contains pollutants that can lead to various adverse effects, there is significant uncertainty regarding the specific concentrations or durations of exposure required to trigger particular health issues. Moreover, individuals can respond very differently to exposure to indoor air pollutants. Individual sensitivity represents a significant variable in the complex interplay of factors that influence the well-being of building occupants.

Vulnerability to the health impacts of airborne pollutants is most pronounced in infants, the elderly, and individuals with underlying health conditions. Among these, immune-suppressed individuals such as AIDS patients and organ transplant recipients, as well as those with genetic disorders like lupus erythematosus, exhibit heightened sensitivity to common colds. Excessive alcohol consumption renders individuals more susceptible to air contaminants that can affect the liver. People with dry skin are at increased risk of further skin dryness and chemical penetration. Smoking tobacco products weakens the body's defense mechanisms. Some medications can amplify the effects of environmental exposures. Additionally, individuals with preexisting conditions, such as lung damage from fires, may experience heightened reactions to airborne contaminants. Additional research is necessary to gain a better understanding of the health effects associated with exposure to typical pollutant concentrations found in homes and those stemming from higher concentrations occurring for short durations.

Another important factor which affects the different health risks of bad IAQ is the duration of exposure. In office buildings, people are typically exposed for 8 to 10 hours a day, five days a week. In residential settings, exposure can extend to all the hours of the day, every day. Since some substances can accumulate in the body over time, continuous 24-hour exposures can lead to a buildup that may affect health. Additionally, there are other environments where extended exposure times should be considered, such as hospital rooms, hotels, psychiatric wards, and prison cells.

Another complex syndrome linked to bad IAQ, is that of **Sick Building Syndrome (SBS)**. SBS is a term used to describe a collection of non-specific symptoms that individuals experience while spending time in a particular building. These symptoms typically occur when occupants are in the building and improve or disappear when they leave. SBS does not have a specific, identifiable cause like a contagious disease. Instead, it is associated with a combination of factors related to the indoor environment. Common symptoms of SBS, according to the World Health Organization (WHO) [10] are the following:

- Respiratory Irritation: This can include symptoms like coughing, sneezing, throat irritation, and a runny or stuffy nose.

- Eye and Skin Irritation: Occupants may experience watery or itchy eyes, skin rashes, or general discomfort.
- Headaches: Frequent or persistent headaches are a common complaint among individuals with SBS.
- Fatigue: Occupants often report feeling unusually tired or fatigued while inside the building.
- Difficulty Concentrating: Some individuals may have trouble focusing or experience a decrease in cognitive function.
- General Discomfort: A sense of discomfort, unease, or malaise is often associated with SBS.

Additionally, bad indoor air quality can contribute to the **spread of diseases** like pulmonary tuberculosis (TB) [11], severe acute respiratory syndrome (SARS) [12], COVID19 and the common cold [13]. Poorly ventilated indoor spaces can allow respiratory droplets containing the virus to accumulate in the air. When an infected person talks, coughs, or sneezes, these droplets can linger in the environment. Inadequate ventilation fails to dilute and remove these particles, increasing the risk of exposure to others. In indoor environments with stagnant air or inadequate ventilation, droplets can remain suspended for extended periods, potentially exposing individuals to the virus even at distances beyond the typical 6-feet (2-meter) recommendation.

In conclusion, unacceptable indoor air quality (IAQ) can pose both immediate and long-term health risks, reduce the well-being and contribute to lost productivity and absenteeism at work. At the same time, indoor air pollution may cause diverse symptoms and illnesses, including SBS and increase the risk of disease transmission.

1.2.3 Benefits of Good IAQ

According to the American Society of Heating, Refrigerating and Air-Conditioning Engineers (ASHRAE) the benefits of good IAQ can be divided into the following categories:

- Category 1: Health and Well-Being
    - Respiratory Health: Good IAQ reduces the risk of respiratory diseases, such as asthma and allergies. Discuss the role of reduced allergens, pollutants, and irritants in maintaining healthy respiratory systems.
    - Cardiovascular Health: Examine the links between IAQ and cardiovascular health, highlighting the potential reduction in heart diseases and related health costs.
    - Cognitive Function: Explore research on the influence of IAQ on cognitive function, focusing on improved concentration, decision-making, and academic performance.
    - Mental Health: Discuss the psychological benefits of clean indoor air, including reduced stress, anxiety, and depression, and the implications for overall well-being.
- Category 2: Productivity and Performance
    - Occupational Productivity: Analyze studies demonstrating how good IAQ in workplaces leads to increased employee productivity, reduced absenteeism, and improved job satisfaction.
    - Educational Outcomes: Explore the impact of IAQ on student learning, discussing the connection between well-ventilated classrooms and academic achievements.

    - Healthcare Environments: Highlight the significance of IAQ in healthcare settings, emphasizing its role in patient recovery rates and healthcare worker well-being.
- Category 3: Energy Efficiency and Sustainability
    - Energy Conservation: Discuss the relationship between IAQ improvements and energy-efficient building design, showcasing strategies that promote both sustainability and occupant comfort.
    - Green Building Standards: Explore how good IAQ contributes to achieving green building certifications and the growing demand for sustainable, healthy structures.
- Category 4: Economic Implications
    - Healthcare Savings: Examine the potential healthcare cost reductions associated with improved IAQ, considering the economic benefits for individuals and society.
    - Productivity Gains: Calculate the economic value of increased productivity resulting from better IAQ in commercial and educational settings.
    - Energy Cost Savings: Analyze the financial advantages of energy-efficient IAQ strategies, taking into account reduced energy consumption and operational costs.

1.3 Role of Ventilation in Enhancing IAQ

Ventilation is a crucial element in ensuring good indoor air quality (IAQ) and maintaining comfortable thermal conditions. Specifically, ventilation serves several purposes, including:

- Supplying fresh air for metabolic processes and for diluting and eliminating indoor pollutants.
- Removing contaminants at their source, such as kitchen and bathroom exhaust systems and industrial fume hoods.
- Meeting the combustion requirements of appliances like gas stoves, boilers, and unvented heaters.
- Distributing conditioned air for heating or cooling purposes.
- Establishing pressure differentials within spaces to prevent the infiltration of external pollutants or contaminants between areas (e.g., maintaining the cleanliness of integrated circuits in cleanrooms).
- Pre-cooling building fabric (e.g. night venting of naturally ventilated spaces.

Ventilation can be propelled by either natural means (referred to as natural ventilation) or through the use of a fan (known as mechanical ventilation).

1.3.1 Natural Ventilation

Natural ventilation relies on natural forces like wind and buoyancy to circulate outdoor air through a building and remove indoor air pollutants. It utilizes the inherent properties of air movement without the need for mechanical devices. It is achieved through openings like windows, doors, vents, and rooftop openings. Outdoor air enters the building through these openings, while warm indoor air rises and exits through higher openings, creating a natural airflow pattern.

Advantages of NV include:

- Energy Efficiency: Natural ventilation is energy-efficient since it doesn't rely on mechanical fans or systems, reducing operational costs.
- Cost-Effective: Initial installation costs are typically lower compared to mechanical systems.
- Environmentally Friendly: It reduces the building's carbon footprint by minimizing energy consumption.
- Connection to Nature: It provides a direct connection to the outdoor environment, allowing occupants to experience natural airflow and outdoor views.

There are however some inherent challenges with utilizing NV:

- Limited Control: Natural ventilation is highly dependent on external environmental conditions, such as wind direction and speed. It may not always meet indoor air quality (IAQ) standards.
- Inconsistent Performance: Effectiveness varies based on building design, orientation, and location.
- Security and Noise: Openings for natural ventilation may pose security risks and allow outdoor noise to enter.

1.3.2 Mechanical Ventilation

Mechanical ventilation is an active ventilation strategy that uses mechanical equipment, such as fans or blowers, to control and facilitate the movement of indoor and outdoor air. It provides precise control over airflow rates.

Advantages:

- Control: Mechanical ventilation allows for precise control of ventilation rates, ensuring consistent IAQ regardless of external conditions.
- Versatility: It can be customized for various building types and sizes, making it suitable for residential, commercial, and industrial applications.
- Air Filtration: Mechanical systems can incorporate air filtration to remove particles and pollutants.
- Heat Recovery: Advanced systems, like heat recovery ventilation (HRV) and energy recovery ventilation (ERV), recover heat or energy from exhaust air, improving energy efficiency.

Challenges:

- Energy Consumption: Mechanical systems require energy for operation, which can lead to higher energy bills.
- Maintenance: Regular maintenance is essential to ensure efficient and reliable operation.
- Initial Costs: Installation costs can be higher compared to natural ventilation.

1.3.3 Mixed-Mode Ventilation

Mixed-mode ventilation combines elements of both natural and mechanical ventilation within the same building or space, offering flexibility and energy savings. It allows occupants to choose between natural and mechanical ventilation based on their preferences and comfort needs. In mixed-mode systems, windows and mechanical ventilation systems work in tandem. When outdoor

conditions are favorable (e.g., mild temperatures and low pollution levels), occupants can open windows for natural ventilation. During adverse conditions (e.g., extreme heat or cold), mechanical systems take over to maintain comfort.

Advantages:

- Energy Efficiency: Mixed-mode systems optimize energy use by using natural ventilation when possible and switching to mechanical ventilation when needed.
- Occupant Comfort: They offer occupants control over their environment, accommodating individual preferences.
- Backup Ventilation: Mechanical systems provide backup ventilation during extreme conditions, ensuring IAQ and thermal comfort.

Challenges:

- Complex Controls: Mixed-mode systems require sophisticated controls to seamlessly transition between natural and mechanical ventilation.
- Occupant Education: Occupants must be educated on how to operate the system effectively to maximize its benefits.
- Initial Investment: Installation costs may be higher due to the integration of both natural and mechanical components.

In summary, natural, mechanical, and mixed-mode ventilation each offer unique advantages and challenges. The choice of ventilation strategy depends on building design, environmental conditions, and occupant needs.

1.4 Standards and Regulations

There are several existing standards and guidelines that address ventilation for good indoor air quality. These standards are developed by organizations like ASHRAE (American Society of Heating, Refrigerating and Air-Conditioning Engineers), ANSI (American National Standards Institute), ISO (International Organization for Standardization) and other industry-specific bodies. Here are some notable standards:

- ANSI/ASHRAE Standard 62.1, titled "Ventilation for Acceptable Indoor Air Quality," was first introduced in 1973. This standard sets forth the minimum requirements for ventilation and other indoor air quality (IAQ) considerations in non-residential and non-healthcare buildings. Its prescribed outdoor air ventilation rates have been incorporated into widely used building codes in the United States, such as the International Mechanical Code and Uniform Mechanical Code. Additionally, numerous green building programs, including LEED (Leadership in Energy and Environmental Design), make reference to this standard.
- ANSI/ASHRAE Standard 62.2, known as "Ventilation and Acceptable Indoor Air Quality in Residential Buildings," was initially published in 2003. This standard specifically addresses ventilation requirements in residential structures. Minimum ventilation criteria from this standard have been adopted into various building codes, including California's Title 24. Moreover, it serves as a reference in sustainability programs like LEED for Homes and the U.S. Environmental Protection Agency's Indoor AirPlus initiative.
- ANSI/ASHRAE/ASHE Standard 170, titled "Ventilation of Health Care Facilities." Standard 170, developed in 2017, consolidates several previously separate documents utilized across

North America into one comprehensive standard. It has become widely incorporated into building codes to establish ventilation guidelines for hospitals and other healthcare facilities.

- ANSI/ASHRAE/ICC/USGBC/IES Standard 189.1, named "Standard for the Design of High-Performance, Green Buildings Except Low-Rise Residential Buildings," was created in collaboration with organizations like USBGC (U.S. Green Building Council), the International Code Council, and the Illuminating Engineering Society. This standard, initially issued in 2017, outlines IAQ requirements that extend beyond those found in Standard 62.1. It was developed for potential adoption into voluntary green and sustainable rating systems, green building incentive programs, and local building regulations. Notably, the 2017 version of this standard serves as the technical foundation for the 2018 International Green Construction Code.
- ISO 16814 - Building environment design - Indoor air quality - Part 1: Indoor air quality, system design, and verification. This international standard provides guidance on designing HVAC systems to achieve good indoor air quality. It addresses system design, verification, and documentation.

Regulations and guidelines related to ventilation for good indoor air quality vary by country and region. These regulations are typically enforced by governmental agencies responsible for public health, building codes, and environmental protection. Here are some examples of existing regulations and guidelines in different regions:

United States:

- ASHRAE Standards: The American Society of Heating, Refrigerating and Air-Conditioning Engineers (ASHRAE) publishes standards such as ASHRAE Standard 62.1 and 62.2, which provide ventilation requirements for non-residential and residential buildings, respectively. These standards are often referenced in building codes.
- Occupational Safety and Health Administration (OSHA): OSHA regulations include requirements for ventilation in workplaces to protect workers' health and safety.
- Environmental Protection Agency (EPA): EPA guidelines address indoor air quality in various settings, including schools. The EPA's Indoor AirPlus program provides guidelines for builders to improve indoor air quality in homes.
- Local Building Codes: Many U.S. states and municipalities have adopted building codes that incorporate ventilation requirements to ensure good indoor air quality.

European Union:

- EN Standards: European standards (EN) related to indoor air quality and ventilation are used as guidelines for member states. These standards cover aspects like ventilation rates, filtration, and thermal comfort.
- EU Directives: The EU has directives related to indoor air quality and ventilation in buildings, including the Energy Performance of Buildings Directive and the Indoor Air Quality Directive. These directives set requirements for member states to improve indoor air quality in buildings.

Canada:

- National Building Code (NBC): Canada's National Building Code includes provisions for ventilation in buildings, including requirements for fresh air intake, exhaust, and air distribution systems.
- Provincial and Territorial Building Codes: Provinces and territories in Canada may have their own building codes with specific ventilation requirements.

Australia:

- National Construction Code (NCC): The NCC, which includes the Building Code of Australia (BCA), provides guidelines and requirements for building ventilation and indoor air quality.
- State and Territory Regulations: Different states and territories in Australia may have additional regulations related to ventilation in buildings.

United Kingdom:

- Building Regulations: In the UK, Building Regulations provide requirements for ventilation in buildings to ensure good indoor air quality.
- Chartered Institution of Building Services Engineers (CIBSE): CIBSE publishes guidance on building services, including ventilation, to support compliance with regulations.

It's important to note that these regulations and guidelines are subject to updates and revisions. Building professionals, including architects, engineers, and contractors, must stay informed about the latest requirements in their specific regions to ensure compliance and promote good indoor air quality.

1.5 Overview of Existing Research

Quantifying ventilation efficiency is a critical aspect of indoor air quality (IAQ) research and building design. This process involves assessing how effectively ventilation systems bring in fresh outdoor air and remove indoor pollutants. Assessing ventilation effectiveness is an interdisciplinary field of research that involves a variety metrics and measurement techniques.

1.5.1 Common Ventilation Metrics and Measurement Techniques

Several key metrics are commonly used to assess ventilation effectiveness and indoor air quality (IAQ):

- **Ventilation Rate (VR)**: This metric quantifies the rate at which outdoor air is introduced into a space and is typically measured in liters per second (L/s) or cubic feet per minute (CFM). Ventilation rate is a fundamental metric for ensuring adequate fresh air supply to dilute indoor pollutants.
- **Air Change Rate (ACH)**, also seen as specific airflow rate, is a fundamental metric for quantifying ventilation efficiency. ACH represents the number of times the entire volume of air within a space is replaced with outdoor air per hour. ACH proves to have certain limitations in describing real flows, where the ideal piston flow (this flow model will be discussed in the next Chapter) often does not apply. Generally, however, a higher ACH indicates more frequent air exchanges and better dilution of indoor pollutants. ACH of ventilated zone is defined as the ratio of the volumetric flow at the inlet, $Q\left[\frac{m^3}{h}\right]$ over the indoor air volume, $V[m^3]$ and is typically measured in $[h^{-1}]$:

$$ACH = \frac{Q}{V} \tag{1.1}$$

- **Reference Time (τ_{ref}),** is not a new metric but simply the reciprocal of ACH. However, in many applications that assess the IAQ, the interest lies in the time that has elapsed since the air entered the building. It is worth noting that in a real flow the time taken to replace the air in the space is greater than the reference time. Despite that, it remains a convenient metric for many ventilation applications. It is measured in seconds and can be defined as:

$$\tau_{ref} = \frac{1}{ACH} \tag{1.2}$$

- **Carbon Dioxide (CO_2) Concentration**: Monitoring CO_2 levels is a common way to assess indoor air quality. Elevated CO_2 levels can indicate inadequate ventilation because humans exhale CO_2, and high levels may lead to discomfort and reduced cognitive function.

Some of the most common methods for measuring the above metrics include the use of a tracer gas. Tracer gas methods are used to assess indoor air quality and ventilation effectiveness by introducing a known quantity of a tracer gas into a space and measuring its concentration change over time. It's important to note that tracer gas methods require careful planning, proper calibration of equipment, and consideration of factors such as the release location and measurement locations to ensure accurate results. These methods are based on the principle of dilution, and several techniques can be employed:

- **Tracer Gas Dilution Method**: A known quantity of a tracer gas (e.g., sulfur hexafluoride, SF6) is released into the indoor environment. The tracer gas should be inert, non-toxic, and non-flammable. The initial concentration of the tracer gas is measured at a specific location within the space. The concentration of the tracer gas is continuously monitored over time at the same location. Using the change in concentration, the ventilation rate (the rate at which outdoor air is entering the space) is calculated based on the principle of dilution. The VR can be determined using equations such as the mass balance equation. Based on the way the tracer gas is introduced, we can apply the Dilution method using one of the following techniques:
    - **Constant Injection Technique**: In this method, a tracer gas is continuously released into the indoor space at a constant rate from a controlled source. Sensors are placed at various locations within the space to monitor the concentration of the tracer gas over time. The steady-state concentration is used to calculate the ventilation rate, providing information about the overall air change rate.
    - **Step-Down Technique**: The step-down tracer gas dilution method involves releasing a known quantity of tracer gas into the indoor space at a relatively high concentration. Sensors are strategically placed to monitor the decreasing concentration of the tracer gas over time. The rate at which the tracer gas concentration decreases is used to calculate the ventilation rate, providing information about the effectiveness of the ventilation system.
    - **Step-Up Technique**: In contrast to the step-down method, the step-up tracer gas dilution method starts with a low concentration of tracer gas, typically close to background levels. An external source increases the concentration of the tracer gas within the space. Sensors placed within the space monitor the rising concentration of the tracer gas. By analyzing the rate of increase in concentration, ventilation rates can be estimated.

- **Pulse Technique**: The pulse tracer gas dilution method involves introducing a short burst or pulse of tracer gas into the indoor environment. Sensors placed within the space quickly capture the rise and fall of the tracer gas concentration. This method is useful for assessing transient conditions, such as the impact of opening doors or windows or the response of the ventilation system to sudden changes. By analyzing the response time and peak concentration of the tracer gas pulse, ventilation rates and air exchange effectiveness can be determined.

- **Tracer Gas Decay Method**: Similar to the dilution method, a known quantity of a tracer gas is introduced into the indoor space. The initial concentration of the tracer gas is measured. Instead of continuous monitoring, the concentration of the tracer gas is monitored intermittently. The decay rate of the tracer gas concentration is determined. The calculation is typically performed using the exponential decay formula:

$$VR = \left(\frac{Q}{V}\right) \ln\left(\frac{C_0}{C(t)}\right) \tag{1.3}$$

Where:
$VR =$ Ventilation rate (air changes per hour or cubic feet per minute)
$Q =$ Tracer gas release rate (in cubic feet per minute)
$V =$ Volume of the space (in cubic feet)
$C_0 =$ Initial concentration of the tracer gas
$C(t) =$ Concentration of the tracer gas at time t

Measurements of local ventilation efficiency using the tracer gas technique have been carried out in full-scale rooms [14] [15] as well as using scale models [16].

1.5.2 The Significance of Additional Ventilation Metrics

Although the aforementioned metrics have been extensively and successfully used to control concentration of contaminants, they have limitations in assessing certain aspects of IAQ. More specifically, they do not take into consideration how well the indoor air is mixed and they often fail to identify areas of stagnation, where air doesn't circulate well.
To address these issues, a new parameter of IAQ was introduced in the early 1980s called the age of air (AOA). Among the first people define the quantity of AOA in the context of assessing ventilation was M. Sandberg in 1981. The idea behind this metric is to measure the freshness of air based on how long an air parcel remains in a room, with shorter times indicating better local ventilation [17] [18]. In a room where air is not perfectly mixed, the air introduced into any section of the room is a combination of both recirculated and outside air, making it more challenging to analyze the system's dynamics. The "freshness" of the air and its ability to dilute at a specific location are quantified by its "age." The air's age at that particular point is determined as the time "z" that has passed since it entered the room.

1.5.3 Determination of the Mean AOA

Local mean age of air (local AOA) can be determined through experimental means employing tracer gas techniques or calculated numerically using computational fluid dynamics (CFD) methods.

In tracer gas methods, a known amount of tracer gas is introduced into a space following a predefined pattern. The change in tracer gas concentration over time is then measured to determine the age of the air. For instance, one method involves filling a ventilated room with tracer

gas, then removing it. The subsequent decay in tracer gas concentration, caused by the infiltration of outdoor fresh air into the room, is recorded, and the local AOA is derived from the area under the transient concentration curve [19]. In another example, Fisk et al. [20] employed a step-up technique using sulfur hexafluoride (SF6) tracer gas to assess age of air and compare ventilation effectiveness in laboratory experiments. Jung and Zeller [21] concurrently utilized SF6 and nitrous oxide (N2O) tracer gases with step-up, step-down, and pulse techniques in a mechanically ventilated laboratory room to explore practicality and reproducibility.

Alternatively, local MAA can be determined through numerical modeling rather than experimental measurements. Numerical simulations offer advantages in assessing room airflow, considering factors such as wind and buoyancy effects, individually and collectively [22]. There are two numerical approaches for predicting MAA:

- the transient method, which is based on results from experimental tracer gas methods;
- the steady-state method, which is based on the steady-state solutions of airflow equations and requires the resolution of an additional transport equation using CFD techniques;

Li et al. [23] compared these numerical methods and found that the transient and steady-state methods were reliable for predicting local mean AOA, with the transient method requiring more computational time for a complete solution. With advancements in computer technology and commercial CFD software, local mean AOA is increasingly calculated numerically in various enclosed spaces, including clean or hospital rooms [24] [25], traditional ventilated rooms [22] [26] [27] and unconventional locations like deep coal mines [28], underground car parks [29]and large open spaces such as estuaries [30]. In most of these studies, the steady-state method was employed, solving an additional partial differential equation to describe the transport of a scalar known as "age of air". Kato and Murakami [31] developed AOA calculations for steady-state and concentration distribution analysis in CFD-based simulations, defining it as SVE3. In contrast, SVE1 represents the average concentration or residence time of contaminants at a specific location in a room [32]. Similarly, Gan [33] conducted computations for a single room featuring flow driven by buoyancy through a solitary opening. Lube et al. [34] documented a comparable scenario with a transient solution using URANS.

Chapter 2: Key Concepts in Fluid Mechanics

2.1 Fluid as a Continuum

A fluid is comprised of numerous molecules in constant motion and collision, giving it a seemingly discontinuous nature at the molecular level. However, our focus shifts from individual molecules to their average behavior in fluid mechanics. We treat the fluid as a continuous medium, referred to as a 'continuum,' neglecting its discrete molecular structure. This allows us to discuss fluid properties at specific points, enabling mathematical descriptions using differential calculus, including the application of Newton's Laws of Motion.

The foundational assumption behind the continuum hypothesis is that we can define an exceedingly small element where properties become independent of volume size, satisfying the requirements of differential calculus. Fortunately, this assumption holds for most fluids under typical conditions in ventilation, as these small elements still contain a vast number of molecules.

2.2 Types of Flow

There are several types of flow in fluid dynamics, each characterized by its specific behavior and characteristics. Flows can be laminar, transitional, turbulent, steady or unsteady, and various combinations of these. A very useful indicator that helps us determine the type of flow, is the Reynolds number.

Different flow types are often associated with different values of Reynolds number, Re:

$$Re = \frac{\rho\, UL}{\mu} \tag{2.1}$$

where U and L are, respectively, a representative velocity and length of the flow under consideration. The Reynolds number is a measure of the ratio between dynamic and viscous forces and provides insights into the flow's nature. Ventilation flows typically exhibit low Reynolds numbers, indicating significant viscous effects.

2.2.1 Laminar, Transitional and Turbulent Flows

Laminar, transitional, and turbulent flows are distinct types of fluid flow behaviors characterized by their respective patterns of fluid motion and levels of turbulence:

- **Laminar flow** is a type of fluid motion characterized by smooth, orderly, and well-defined streamlines. In laminar flow, adjacent layers of fluid flow in parallel, and there is minimal mixing or turbulence between them. This flow type typically occurs at low flow velocities and low Reynolds numbers. It is often associated with a predictable and stable flow pattern.
- **Transitional flow** is an intermediate state between laminar and turbulent flow. In transitional flow, there is a mix of laminar and turbulent characteristics within the fluid. It may include irregular fluctuations in velocity and pressure, as well as occasional vortex formation. Transitional flow occurs as a result of increasing flow rates or changes in fluid properties, causing the flow to become unstable and transition from laminar to turbulent behavior.

- **Turbulent flow** is characterized by chaotic, irregular, and unpredictable fluid motion. In turbulent flow, eddies, vortices, and fluctuations in velocity and pressure are prevalent throughout the flow field. Turbulent flow typically occurs at higher flow velocities and high Reynolds numbers. It results from the dominance of inertial forces over viscous forces, leading to vigorous mixing and energy dissipation within the fluid.

2.2.2 Steady and Unsteady Flows

Steady and unsteady flows are two categories that describe the behavior of fluid motion with respect to time:

- **Steady flow** is a type of fluid motion where the velocity, pressure, temperature, and other fluid properties at any given point within the flow field remain constant with time. In other words, in a steady flow, the flow variables do not change as time progresses. This means that the flow is consistent and unchanging over time. Steady flows are common in many engineering applications where a system has reached a stable and continuous state. For example, the flow of water through a well-designed pipe system with a constant flow rate can exhibit steady flow because the fluid properties remain constant at any point within the pipe.
- **Unsteady flow**, also referred to as transient flow, is the opposite of steady flow. In unsteady flow, the fluid properties, such as velocity, pressure, and temperature, change with time at various points within the flow field. This means that the flow is not consistent or stable over time, and it can vary in response to external factors or changes in boundary conditions.

Turbulent flows are strictly speaking always unsteady, but in many applications, turbulent flows can be considered steady. To do that we will have to assume that the non-random component is constant. Thus, an instantaneous velocity component u can be expressed in the form

$$u(x,t) = \bar{u}(x) + u'(x,t) \tag{2.2}$$

where $\bar{u}$ is the steady (constant) component and u' is the random turbulent fluctuation.

2.3 Transport Mechanisms

Transport of quantities by a fluid takes place by advection (convection) and molecular diffusion. Convection is the process of mass transfer within a fluid due to the bulk motion of the fluid itself.

Molecular diffusion in the context of air flow refers to the movement of individual gas molecules within a flowing air stream. In a flowing air stream, individual gas molecules are in constant random motion due to their thermal energy. They move in all directions with varying speeds. Molecular diffusion in air flow occurs when there is a difference in the concentration of a specific gas component between two regions within the air stream. This difference in concentration is called a concentration gradient. Gas molecules tend to move from regions of higher concentration to regions of lower concentration due to random collisions and interactions. This movement is driven by the concentration gradient and is a fundamental property of gases. The rate of molecular diffusion in air flow depends on several factors:

- Concentration Gradient: A steeper concentration gradient results in faster diffusion, meaning that gas molecules will move more rapidly from areas of high concentration to areas of low concentration.

- Temperature: Higher temperatures increase the kinetic energy of gas molecules, leading to increased molecular motion and faster diffusion.
- Molecular Properties: The size and shape of gas molecules influence their diffusion rates. Smaller and lighter molecules tend to diffuse more quickly than larger and heavier ones.

The transport by molecular diffusion is given by Fick's law. In one dimensional form, the mass flow per unit area in the x direction is given by

$$-D_m\left(\frac{dc}{dx}\right) \tag{2.3}$$

where $\frac{dc}{dx}$ is the rate of change of mass concentration with x and D_m is a property of the contaminant, known as the molecular diffusion coefficient (diffusivity) in air. The negative sign represents that mass flows from higher concentrations to lower concentrations.

It is a key process that influences the dispersion and mixing of gases in the atmosphere or within confined spaces, such as ventilation systems, and it plays a significant role in various scientific, engineering, and environmental applications.

2.4 Paths and Streamlines

According to the continuum hypothesis, each point within a flow has an associated velocity vector. While a point is not a physical entity, we can imagine a hypothetical "particle" that coincides with a specific point at a particular moment. If we know the velocity field at each time-step, we can ascertain the path this particle follows. In the case of a steady flow, this path traces what we call a "streamline." All particles passing through a given point follow the same streamline.

In a steady flow, the streamline is tangential everywhere to the resultant velocity. This definition holds even in unsteady flows, allowing us to define an instantaneous streamline. However, this concept differs from the actual path. In cases where unsteadiness arises from turbulence, the time-averaged streamline can be determined using time-averaged velocities. It's important to note that no real particle will precisely follow this path, as the likelihood of this happening is exceedingly low.

These concepts of paths and streamlines are pertinent to the concept of the "age of air." The hypothetical particle mentioned earlier is not a tangible particle in the conventional sense, as its composition changes continuously due to molecular diffusion. In terms of motion, this doesn't significantly impact our understanding because the exchanged molecules possess identical physical properties within the air. However, when considering their age, molecular diffusion takes on a new significance.

2.5 Two Ideal Flow Models

Piston flow and perfect mixing are two contrasting models in fluid dynamics that describe different ways substances are distributed within a system, like a building.

- **Piston flow**, also known as plug flow or streamline flow, is a theoretical concept where substances move through a system in a continuous, unidirectional manner, without any mixing or dispersion. This represents an idealized flow, primarily because molecular diffusion is an inherent factor, and near the walls, the velocity distribution must deviate

from uniformity due to the no-slip condition. In piston flow, mixing is entirely absent, with all incoming elements reaching the outlet simultaneously.

- **Perfect mixing** is the opposite to piston flow. Perfect mixing, as the name implies, represents a situation where substances within a system are uniformly and instantaneously mixed, resulting in a homogeneous distribution of properties throughout the system. The dispersion and mixing of different gases is mainly driven by molecular diffusion. In practical applications, achieving this condition can be approximated by utilizing mixing fans.

Real-world systems often fall somewhere between these two extremes, depending on factors like geometry, flow rates, and mixing mechanisms.

Chapter 3: Contaminant Transport

3.1 Introduction

Contaminants are gaseous pollutants whose presence in indoor environments can negatively affect IAQ. Contaminants are carried away from their source by the airflow inside the room (convection) and by the natural scattering of molecules (molecular diffusion). This results in the dispersion of contaminant levels within each room, creating a concentration field. As this process occurs, contaminants are thinned out and expelled from the room through openings in the building's structure. This dilution and removal of pollutants are the key roles of ventilation in maintaining good indoor air quality when dealing with internal sources

The objective of this chapter is to derive the transport equations that describe the concentration of a contaminant at a point, by applying the principle of mass conservation. Understanding the transport of contaminants is crucial for establishing the mathematical background that governs the concept of AOA.

3.2 Concentration at a Point

Theoretical models for contaminant transport are based on the idea that we can treat the concentration of contaminants as a continuous function across space. On that basis, we can define the concentration at a specific point in that space. To do this, we need to consider a small volume centered around a specific point.

We can define the concentration of a contaminant c at a point as the ratio of the mass of contaminant over volume of the mixture:

$$c = \frac{m}{\Delta V}\,, \tag{3.1}$$

where m is the mass of contaminant in the small volume ΔV surrounding the point.

The concentration can also be expressed as the number of molecules per unit volume,

$$n = \frac{N}{\Delta V} \tag{3.2}$$

where N is the number of molecules of contaminant in the volume. The concentration c is equal to n multiplied by the molecular weight of the contaminant.

3.3 Transport Equation for Concentration at a Point

We will use the principle of mass conservation in terms of the concentration and the velocities at a point, in order to arrive at a partial differential transport equation for c. For that we will define a rectangular parallelepiped with dimensions dx, dy, dz (control volume) and the point at the center of that parallelepiped whose concentration is c and its velocity is described by the (u, v, w) vector,

as shown in figure (1).

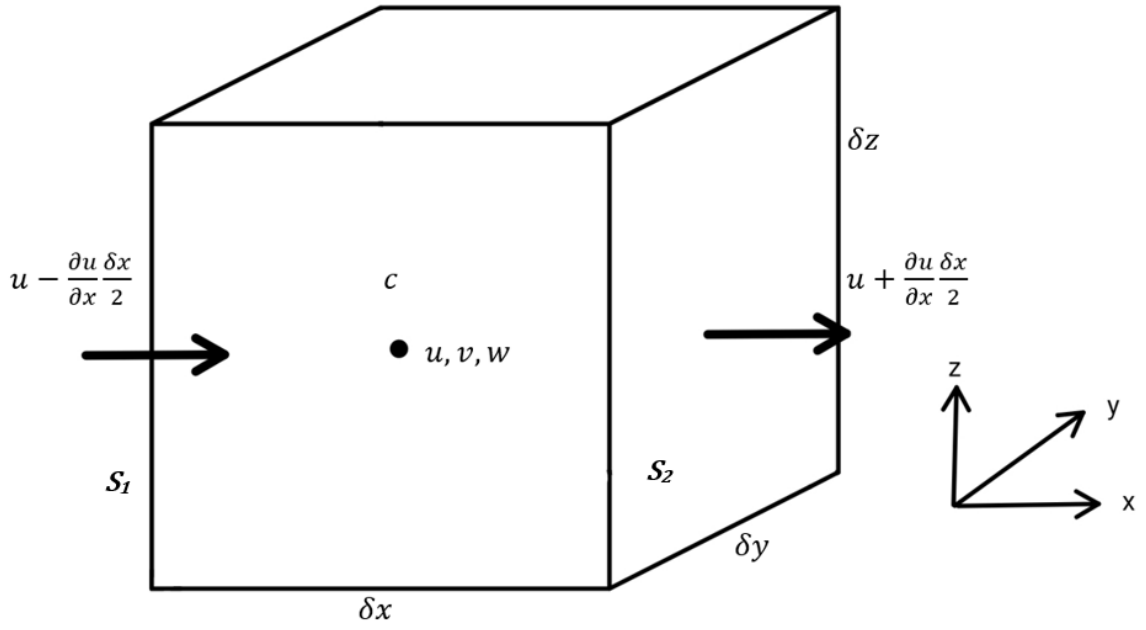

Figure 1: Control Volume

We will also make the following assumptions:

- The dimensions of the control volume dx, dy, dz are very small
- The studied time change dt is very small
- There is no release of contaminant inside the control volume

According to Etheridge [35] the mass conservation principle for a contaminant is stated as:

The rate of increase with time of the mass contained within a control volume fixed in space is equal to the net inward mass flow rate through the surfaces of the control volume plus the rate at which the contaminant is released within the volume.

The rate of increase with time of the mass contained within the control volume can be mathematically described by the following integral:

$$\frac{\partial}{\partial t}\oint_V c.\, dV \tag{3.3}$$

One, can simplify the integral (3.3) by taking into consideration our assumptions about the very small control volume and the very small time-step. On that basis, the increase of the mass inside a very small control volume, within a very small time-step dt can be written as:

$$\delta x \cdot \delta y \cdot \delta z \frac{\partial c}{\partial t}\ \delta t \tag{3.4}$$

As discussed on the previous chapter, mass flow in fluid mechanics takes place by the mechanisms of convection and molecular diffusion. For that reason, the mass flow rate through the surfaces of the volume has two components, one for convection and one for molecular diffusion.

The convection component of the mass flow rate through the volume along the x-axis can be written mathematically as follows:

$$\oint_{S1} uc \cdot dA - \oint_{S2} uc \cdot dA \tag{3.5}$$

The term (3.5) applied to our control volume can be written as:

$$\left(u - \frac{\partial u}{\partial x}\frac{\delta x}{2}\right)\left(c - \frac{\partial c}{\partial x}\frac{\delta x}{2}\right)\delta y.\delta z - \left(u + \frac{\partial u}{\partial x}\frac{\delta x}{2}\right)\left(c + \frac{\partial c}{\partial x}\frac{\delta x}{2}\right)\delta y.\delta z \tag{3.6}$$

By assuming the terms δx^2 to be negligible, we can further simplify the term (3.6) as follows:

$$-\left(c\frac{\partial u}{\partial x} + u\frac{\partial c}{\partial x}\right)\delta x.\delta y.\delta z \tag{3.7}$$

which describes the mass flow of contaminant in the x-dimension into the control volume due to convection. Similar mathematical expressions apply for the other dimensions

As discussed in the previous chapter, the transport of a passive contaminant by molecular diffusion is given by Fick's law. Applying equation (2.3) to describe the diffusion component of flow rate through the volume along the x-axis, we get:

$$-D_{\mathrm{m}}\oint_{S1}\frac{\partial c}{\partial x}dA + D_{\mathrm{m}}\oint_{S2}\frac{\partial c}{\partial x}dA \tag{3.8}$$

where D_m is the molecular diffusion coefficient. The term (3.8) applied to our control volume can be written as:

$$-D_{\mathrm{m}}\left(\frac{\partial c}{\partial x} - \frac{\partial^2 c}{\partial x^2}\frac{\delta x}{2}\right)\delta y \cdot \delta z + D_{\mathrm{m}}\left(\frac{\partial c}{\partial x} + \frac{\partial^2 c}{\partial x^2}\frac{\delta x}{2}\right)\delta y \cdot \delta z \tag{3.9}$$

After excluding the higher order terms, we get:

$$D_{\mathrm{m}}\left(\frac{\partial^2 c}{\partial x^2}\right)\delta x \cdot \delta y \cdot \delta z \tag{3.10}$$

which describes the diffusion flow rate in the x-direction. Similar mathematical expressions apply for the other dimensions.

Thus, the mass that has entered the control volume in the x-dimension in time dt due to convection and diffusion is the sum of terms (3.7) and (3.10):

$$-\left(c\frac{\partial u}{\partial x} + u\frac{\partial c}{\partial x} - D_{\mathrm{m}}\frac{\partial^2 c}{\partial x^2}\right)\delta x \cdot \delta y \cdot \delta z \cdot \delta t \tag{3.11}$$

Similar mathematical expressions apply for the other dimensions. If we sum the terms of mass flow for all dimensions, we would get the total inward mass flow through the surfaces of the control volume:

$$-c\left(\frac{\partial u}{\partial x}+\frac{\partial v}{\partial y}+\frac{\partial w}{\partial z}\right)-\left(u\frac{\partial c}{\partial x}+v\frac{\partial c}{\partial y}+w\frac{\partial c}{\partial z}\right)+D_{\mathrm{m}}\left(\frac{\partial^2 c}{\partial x^2}+\frac{\partial^2 c}{\partial y^2}+\frac{\partial^2 c}{\partial z^2}\right) \tag{3.12}$$

Applying the mass conservation principle, the total inward mass flow, described by term (3.12), should be equal the increase of mass in the control volume, described by the term (3.4). Equating these terms gives us:

$$\frac{\partial c}{\partial t}=-c\left(\frac{\partial u}{\partial x}+\frac{\partial v}{\partial y}+\frac{\partial w}{\partial z}\right)-\left(u\frac{\partial c}{\partial x}+v\frac{\partial c}{\partial y}+w\frac{\partial c}{\partial z}\right)+D_{\mathrm{m}}\left(\frac{\partial^2 c}{\partial x^2}+\frac{\partial^2 c}{\partial y^2}+\frac{\partial^2 c}{\partial z^2}\right) \tag{3.13}$$

However, the mass conservation for the air takes the form:

$$\frac{\partial u}{\partial x}+\frac{\partial v}{\partial y}+\frac{\partial w}{\partial z}=0 \tag{3.14}$$

This allows us to simplify equation (3.13) as follows:

$$\frac{\partial c}{\partial t}=-\left(u\frac{\partial c}{\partial x}+v\frac{\partial c}{\partial y}+w\frac{\partial c}{\partial z}\right)+D_{\mathrm{m}}\left(\frac{\partial^2 c}{\partial x^2}+\frac{\partial^2 c}{\partial y^2}+\frac{\partial^2 c}{\partial z^2}\right) \tag{3.15}$$

3.4 Boundary Conditions

We will divide the boundary conditions in three types:

- At solid surfaces. In this region, the mass flow in the direction normal to the surface is equal to zero. According to Fick's Law this leads to the following expression:

  $$\frac{\partial c}{\partial n}=0 \tag{3.16}$$

  where n denotes the normal direction.

- At an inlet. Here, concentration is set to be equal to the concentration in the supply air, c_{in}:

  $$c=c_{in} \tag{3.17}$$

  it is worth noting that c_{in} can vary in time and space.

- At outlets. Here the actual values form part of the solution so it is necessary to specify gradients. For example

  $$\frac{\partial c}{\partial x}=0 \tag{3.18}$$

3.5 Transport Equations for Turbulent Flow

In general, the velocity vector (u, v, w) varies with time. Specifically, in turbulent flows however we separate each velocity component into two parts, namely a coherent part, $\bar{u}(t)$ and a random turbulent part, $u'(t)$. As discussed in section (2.3), in a steady turbulent flow, $\bar{u}(t)$ is considered constant and is written as the time-averaged value $\bar{u}$. Thus, the velocity component u(t) can be written as follows:

$$u(t)=\bar{u}+u'(t) \tag{3.19}$$

Similar expressions apply for the other components. On that basis, we can also express the instantaneous concentration a similar way. That is:

$$c(t) = \bar{c} + c'(t) \tag{3.20}$$

Substituting equations (3.19) and (3.20) into equation (3.15) and taking the time average leads to the Reynolds-averaged equation for the time-averaged concentration at a point, $\bar{c}$:

$$\frac{\partial \bar{c}}{\partial t} = -\bar{u}\frac{\partial \bar{c}}{\partial x} - \bar{v}\frac{\partial \bar{c}}{\partial y} - \bar{w}\frac{\partial \bar{c}}{\partial z} + D_{\mathrm{m}}\left(\frac{\partial^2 \bar{c}}{\partial x^2} + \frac{\partial^2 \bar{c}}{\partial y^2} + \frac{\partial^2 \bar{c}}{\partial z^2}\right) - \left(\frac{\partial \overline{u'c'}}{\partial x} + \frac{\partial \overline{v'c'}}{\partial y} + \frac{\partial \overline{w'c'}}{\partial z}\right) \tag{3.21}$$

The $\overline{u'c'}$ terms in equation (3.21) represent convection as a result of correlations between the concentration fluctuations and the turbulent velocity fluctuations. In order to solve this equation, we will have to relate $\overline{u'c'}$ to other properties of the flow, similar to the turbulence models used in the Reynolds Averaged Navier Stokes (RANS) equations. It is important to clarify that in equation (3.21), the mean concentration $\bar{c}$ can change with time, although very slowly. Its variation in time is often a result of variations in the strength of the contaminant source. On the other hand, the fluctuation $c'(t)$ is of much higher frequency and is associated with random velocity fluctuations due to turbulence. This major difference in time-scale allow us to use modelling similar the ones used for turbulence.

In these models, the terms corresponding to turbulent transport of momentum are related to mean velocity gradients by semi-empirical turbulent diffusion coefficients, μ_t. If we apply a similar approach for concentration, we can define turbulent diffusion coefficients for concentration. These are:

$$D_x = -\frac{\overline{u'c'}}{\frac{\partial \bar{c}}{\partial x}}, \qquad D_y = -\frac{\overline{v'c'}}{\frac{\partial \bar{c}}{\partial y}}, \qquad D_z = -\frac{\overline{w'c'}}{\frac{\partial \bar{c}}{\partial z}} \tag{3.22}$$

Substituting in (3.21) gives:

$$\frac{\partial \bar{c}}{\partial t} = -\bar{u}\frac{\partial \bar{c}}{\partial x} - \bar{v}\frac{\partial \bar{c}}{\partial y} - \bar{w}\frac{\partial \bar{c}}{\partial z} + \frac{\partial}{\partial x}\left((D_x + D_{\mathrm{m}})\frac{\partial \bar{c}}{\partial x}\right) + \frac{\partial}{\partial y}\left((D_y + D_{\mathrm{m}})\frac{\partial \bar{c}}{\partial y}\right) + \\ + \frac{\partial}{\partial z}\left((D_z + D_{\mathrm{m}})\frac{\partial \bar{c}}{\partial z}\right)\Bigg) \tag{3.23}$$

At this point we can assume that turbulence is isotropic which means that it behaves uniformly, regardless of the orientation or direction in which it's measured. This assumption simplifies the analysis of turbulent flows by considering turbulence statistics to be the same in all directions. While this simplification doesn't perfectly represent real-world turbulence, it aids in mathematical modeling and understanding turbulent behavior. Based on this assumption, the three diffusion coefficients at a point are equal, D_{j} and are related to $\mu_{\mathrm{t}}$by:

$$\frac{\mu_{\mathrm{t}}}{\rho D_{\mathrm{j}}} = \mathrm{Sc}_{\mathrm{t}} \tag{3.24}$$

where Sc_t is the turbulent Schmidt number.

Chapter 4: The Theory of Age of Air

4.1 Introduction

The age of the air offers valuable insights into indoor air quality and plays a central role in optimizing ventilation for health, energy efficiency, and occupant comfort. In the context if this thesis, age of air is used to evaluate how well natural ventilation systems are working. For example, a more efficient system will result in lower air ages for a given fresh-air flow rate compared to a less effective one.

Age of air is the time that has passed since outdoor air entered a space through an opening in the building envelope. It depends on the velocity of the air movement as well as the molecular diffusion. This is different from contaminant concentration, which also relies on the location and nature of the contaminant source. In this regard, age of air is a simpler and more general indicator of air quality compared to measuring contaminant concentration at a single point.

As explained in the previous chapter, a single point represents a very tiny control volume, and the concentration of a contaminant at that point is essentially the number of contaminant molecules within that small space divided by its volume. We use the same approach when dealing with age of air, however unlike contaminants, the control volume only contains air molecules.

What sets the air molecules apart is that each one has a unique entry time into the room. This characteristic remains constant as the molecules move through the room. Air age simply measures the time difference between the current time and the time each air molecule entered the room.

4.2 The Challenges in Determining the Age of Air

Any approach to the numerical determination of the age of air will face two main challenges:

- accounting for molecular diffusion (especially in steady flows)
- accounting for turbulent fluctuations in unsteady flows

To better understand these challenges, we will consider a steady flow in a room and a particle that follows a specific streamline, as shown in figure (2). In engineering applications, one can calculate the velocity field within a room using Computational Fluid Dynamics (CFD). With these results, streamlines can be generated, allowing us to determine the time it takes for a hypothetical particle (or point) to travel from the inlet to a specific point, called "P." Although this value would seem to be the age at point P, this is not the case. What this assumption neglects, is the influence of molecular diffusion on the age. In other words, the flow's kinematics alone cannot fully determine the age, as molecular diffusion effects haven't been considered in the age calculation. To address this, we need to take into account a small control volume of air surrounding the point and consider the changes in the composition of molecules that have occurred since the air entered the space. This involves looking at mass transport, similar to how we calculate the transport of contaminants.

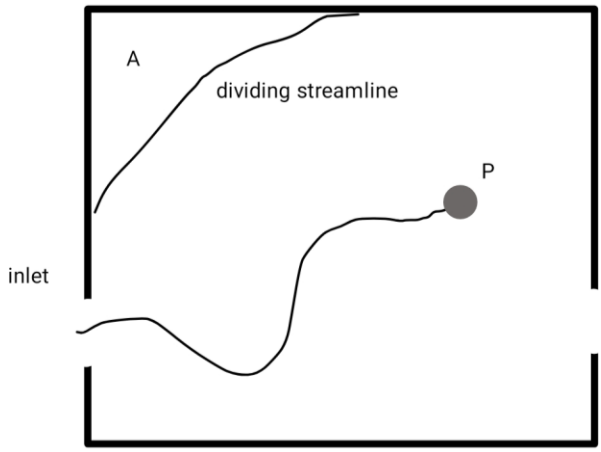

Figure 2: Streamlines in a steady flow

One might argue that molecular diffusion has a negligible impact compared to convection by the velocity field. However, this argument isn't always valid, as illustrated by the circulation region marked as "A" in the above figure. This region is enclosed due to the separation and reattachment of streamlines, forming a closed area known as a "separation bubble." If we disregard molecular diffusion, no air would be transported across the dividing streamline into this region, resulting in an infinite age. However, in reality, the age is finite due to the influence of molecular diffusion across the streamline surface. If the flow in the room is turbulent (i.e. unsteady), the path followed by the hypothetical particle will vary with time, as indicated in the figure below.

If one were to compute the velocity field at extremely small time-steps, it would be possible to construct particle paths and track how age varies with time. This computational technique is known as Direct Numerical Simulation (DNS). However, similar to steady flow calculations, there is the drawback of neglecting molecular diffusion when calculating age. Nevertheless, turbulent diffusion, which is a much more dominant transport mechanism, mitigates the significance of neglecting molecular diffusion, particularly in areas close to solid surfaces where turbulent fluctuations tend to approach zero. Unfortunately, employing DNS for calculating instantaneous flow fields isn't practical for design purposes. Instead, Computational Fluid Dynamics (CFD) is commonly used to determine mean streamlines. It's important to note that the impact of turbulent diffusion isn't accounted for when calculating ages based on mean streamlines. Until the point where calculating unsteady flow fields becomes a feasible option, an alternative approach is necessary.

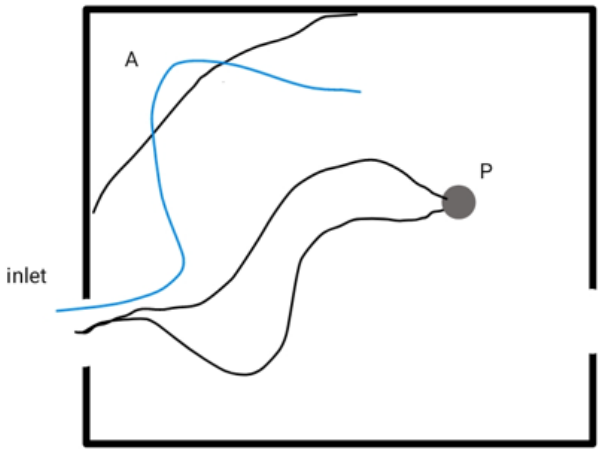

Figure 3: Paths traced out by particles in turbulent flow

The streamline depicted in figure (3) essentially resembles a streamtube with a very small cross-section. In the realm of continuum fluid mechanics, a material element is defined by tracking the movement of the points forming its external boundaries. As a small element of the streamtube moves from the inlet to point P, its shape undergoes changes, but the quantity of matter it contains remains constant. However, the composition of this matter changes due to molecular diffusion, involving the exchange of air molecules across the boundaries. Each molecule can be uniquely identified by the time it entered the space, which remains a fixed property of the molecule (assuming it doesn't re-enter the space). Consequently, the principle of conservation of mass can be applied to molecules within a specified entry time range. This approach forms the basis for deriving transport equations for age.

4.3 Age of air at a Point

In order to define the age at a point, we will need to consider a small volume, ΔV, surrounding the point. Every molecule contained in that control volume, will have entered the room at a certain time, t_{ent}. The age of a molecule, τ, at a specific time t is defined as:

$$\tau = t - t_{ent} \tag{4.1}$$

If we consider that there are $N_{\Delta V}$ air molecules in ΔV, there is a distribution of ages within ΔV. Assuming that $N_{\Delta V}$ is very large, we can define a continuous frequency function that describes the fraction of molecules within ΔV with ages lying between τ and $\tau + \Delta\tau$. This is expressed in terms of the frequency function (distribution), $f_a(\tau)$, which is defined by

$$(\text{fraction of molecules with age between } \tau \text{ and } \tau + \Delta\tau) = f_a(\tau)\,\Delta\tau \tag{4.2}$$

where $f_a(\tau)$ is a continuous function of τ.

Frequency distributions display two important properties:

- the area under the $f_a(\tau)$ curve is equal to 1, because all of the molecules are included, so

$$\int_0^\infty f_a(\tau)\, d\tau = 1 \tag{4.3}$$

- the mean value of the age of molecules in ΔV is given by:

$$\tau_\alpha = \int_0^\infty f_a(\tau) \cdot \tau\, d\tau \tag{4.4}$$

The quantity τ_α is known as the spatial average of τ in the volume ΔV surrounding the point. In the continuum hypothesis, τ_α is independent of the size of ΔV as ΔV tends to zero. For that reason, it is referred to as the age at a point or local mean age of air. In the following chapters we will often use the term age of air (AOA) interchangeably with the terms local mean age of air and age of air at a point.

The time a molecule spends in a room before exiting at an outlet is referred to as its residence time. Each molecule within the room has its own associated residence time at any given location. The average residence time of molecules at a specific point is represented as $\langle \tau_r \rangle$.

It also possible to define the room average age of air. This requires knowledge of the spatial distribution of τ_α, and can be found by averaging τ_α over the volume. The room average age $\langle \tau_\alpha \rangle$ (or $\langle \overline{\tau_\alpha} \rangle$) is the spatial average of the age over the room volume:

$$\langle \tau_\alpha \rangle = \frac{1}{V_{tot}} \oint \tau_a dV \tag{4.5}$$

It is shown that, for steady flow, the residence time $\langle \tau_r \rangle$ is simply twice the room average age $\langle \tau_\alpha \rangle$ [35].

4.4 Transport Equations for AOA at a Point

We will obtain the transport equations for AOA at a point by expanding on the equations that were derived in the previous chapter for the contaminant transport.

As discussed in Section 3.2, the concentration at a point, can be defined in terms of mass of contaminant per unit volume, denoted as c but also in terms of number of molecules per unit volume, denoted as n. Since both of these definitions are valid and can be used interchangeably, we will replace the variable c in equation (3.15) with the number of contaminant molecules per unit volume, n. By doing so, we get:

$$\frac{\partial n}{\partial t} = -u\frac{\partial n}{\partial x} - v\frac{\partial n}{\partial y} - w\frac{\partial n}{\partial z} + D_{\mathrm{m}}\left(\frac{\partial^2 n}{\partial x^2} + \frac{\partial^2 n}{\partial y^2} + \frac{\partial^2 n}{\partial z^2}\right) \tag{4.6}$$

In a given volume ΔV, we can refer to the concentration of molecules, n_{ent} that entered between time t_{ent} and $t_{ent} + \Delta t$. This means that the number of molecules that entered the volume in the specified time range are $(n_{ent} * \Delta V)$. The frequency distribution for $t_{ent}$is denoted by f_{ent} and since there is a total number of $N_{\Delta V}$ air molecules in the volume, n_{ent} is related to f_{ent} by the following expression:

$$n_{\mathrm{ent}} = f_{\mathrm{ent}} \cdot \Delta t \frac{N_{\Delta V}}{\Delta V} \tag{4.7}$$

Substitution into equation (4.6) gives the transport equation for f_{ent}:

$$\frac{\partial f_{\text{ent}}}{\partial t} = -u\frac{\partial f_{\text{ent}}}{\partial x} - v\frac{\partial f_{\text{ent}}}{\partial y} - w\frac{\partial f_{\text{ent}}}{\partial z} + D_{\text{m}}\left(\frac{\partial^2 f_{\text{ent}}}{\partial x^2} + \frac{\partial^2 f_{\text{ent}}}{\partial y^2} + \frac{\partial^2 f_{\text{ent}}}{\partial z^2}\right) \tag{4.8}$$

According to equation (4.4) the mean entry time for the molecules at a point, t_{entp}, is:

$$t_{\text{entp}} = \int_{-\infty}^{t} f_{\text{ent}}\, t_{\text{ent}} \cdot dt_{\text{ent}} \tag{4.9}$$

After integrating with respect to t_{ent} (this can be done within the differentials in equation (4.8)) we arrive at the following transport equation for t_{entp} :

$$\frac{\partial t_{\text{entp}}}{\partial t} = -u\frac{\partial t_{\text{entp}}}{\partial x} - v\frac{\partial t_{\text{entp}}}{\partial y} - w\frac{\partial t_{\text{entp}}}{\partial z} + D_{\text{m}}\left(\frac{\partial^2 t_{\text{entp}}}{\partial x^2} + \frac{\partial^2 t_{\text{entp}}}{\partial y^2} + \frac{\partial^2 t_{\text{entp}}}{\partial z^2}\right) \tag{4.10}$$

However as described in equation (4.1), at a specific time t the relation between age and t_{ent} is:

$$\tau_a = t - t_{entp} \tag{4.11}$$

and by differentiating (4.11) as regards t we get:

$$\frac{\partial \tau_{\text{a}}}{\partial t} = 1 - \frac{\partial t_{\text{entp}}}{\partial t} \tag{4.12}$$

Substituting for t_{entp} from equation (4.11) into (4.10) gives the transport equation for the local mean age of air:

$$1 - \frac{\partial \tau_{\text{a}}}{\partial t} = u\frac{\partial \tau_{\text{a}}}{\partial x} + v\frac{\partial \tau_{\text{a}}}{\partial y} + w\frac{\partial \tau_{\text{a}}}{\partial z} - D_{\text{m}}\left(\frac{\partial^2 \tau_{\text{a}}}{\partial x^2} + \frac{\partial^2 \tau_{\text{a}}}{\partial y^2} + \frac{\partial^2 \tau_{\text{a}}}{\partial y^2}\right) \tag{4.13}$$

Although this equation applies in unsteady flow, most applications in building ventilation use steady flows where the source term is fixed. Thus, in steady flows we get:

$$\frac{\partial \tau_{\text{a}}}{\partial t} = 0 \tag{4.14}$$

which leads to the following expression:

$$1 = u\frac{\partial \tau_{\text{a}}}{\partial x} + v\frac{\partial \tau_{\text{a}}}{\partial y} + w\frac{\partial \tau_{\text{a}}}{\partial z} - D_{\text{m}}\left(\frac{\partial^2 \tau_{\text{a}}}{\partial x^2} + \frac{\partial^2 \tau_{\text{a}}}{\partial y^2} + \frac{\partial^2 \tau_{\text{a}}}{\partial z^2}\right) \tag{4.15}$$

4.5 Boundary Conditions

We define the following boundary conditions.

- The gradient of the local mean AOA in the direction normal to the solid surfaces is equal to zero:

$$\frac{\partial \bar{\tau}_a}{\partial n} = 0 \tag{4.16}$$

where n denotes the normal direction

- The local mean AOA at the inlet is zero, since every particle entering the building for the first time has zero age.

$$\bar{\tau}_a = 0 \tag{4.17}$$

- The gradient of the local mean AOA in the direction normal to the exit is equal to minus the area A of the outlet over the ventilation rate at the exit. This condition assumes that the velocity profile is uniform at the outlet and the negative sign represents that the air is exiting the building. It can be simplified using the definition of velocity as follows:

$$\frac{\partial \bar{\tau}_a}{\partial n} = -\frac{A}{Q} = -\frac{1}{u} \tag{4.18}$$

  where n denotes the normal direction

4.6 Transport Equations for Turbulent Flow

We have already expressed the transport equation for a contaminant in turbulent flow in section (3.5) by equation (3.23). This equation is an extension of equation (3.15), where c is replaced by the mean value $\bar{c}$, the velocities are replaced by their mean values and there are some additional turbulent diffusion coefficients. This extension was conducted by assuming that c can be expressed as $\bar{c}$ plus a fluctuating component caused by turbulence. We can use the same approach to individual concentrations of molecules with a given entry time. By replacing $\bar{c}$ in equation (3.23) we get the transport equation for $\bar{n}_{\text{ent}}$:

$$\frac{\partial \bar{n}_{\text{ent}}}{\partial t} + \bar{u}\frac{\partial \bar{n}_{\text{ent}}}{\partial x} + \bar{v}\frac{\partial \bar{n}_{\text{ent}}}{\partial y} + \bar{w}\frac{\partial \bar{n}_{\text{ent}}}{\partial z} = \frac{\partial}{\partial x}\left(D_{\text{ex}}\frac{\partial \bar{n}_{\text{ent}}}{\partial x}\right) + \frac{\partial}{\partial y}\left(D_{\text{ey}}\frac{\partial \bar{n}_{\text{ent}}}{\partial y}\right) + \frac{\partial}{\partial z}\left(D_{\text{ez}}\frac{\partial \bar{n}_{\text{ent}}}{\partial z}\right) \tag{4.19}$$

The effective diffusion coefficients D_{ex}, D_{ey}, D_{ez} represent the sum of the molecular and turbulent diffusion coefficients. Using the assumption of isotropic turbulence, like we did in section (3.5), these coefficients are equal.

In turbulent flows the local mean age of air is denoted by $\bar{\tau}_a$. The analysis in Section 3.5 can be applied in the same way to give the following equation for $\bar{\tau}_a$ for steady turbulent flow:

$$1 = \left(\bar{u}\frac{\partial \bar{\tau}_a}{\partial x} + \bar{v}\frac{\partial \bar{\tau}_a}{\partial y} + \bar{w}\frac{\partial \bar{\tau}_a}{\partial z}\right) - \frac{\partial}{\partial x}\left(D_{ex}\frac{\partial \bar{\tau}_a}{\partial x}\right) - \frac{\partial}{\partial y}\left(D_{ey}\frac{\partial \bar{\tau}_a}{\partial y}\right) - \frac{\partial}{\partial z}\left(D_{ez}\frac{\partial \bar{\tau}_a}{\partial z}\right) \tag{4.20}$$

It is worth remembering that equation (4.20) is approximate because it makes use of empirical diffusion coefficients.

Chapter 5: Proposed Computational Approach to Age of Air

5.1 Introduction

As described in the previous chapter, in order to determine the local mean age of air $\bar{\tau}_a$, we need to solve the transport equation (4.20).

In this equation the known variables are:

- the velocity field $(\bar{u}, \bar{v}, \bar{w})$
- the diffusion co-efficient, which is the sum of the turbulent diffusion coefficient $D_j$and the molecular diffusion coefficient D_m

$$D_{ej} = D_j + D_m \quad for\ j = x, y, z \tag{5.1}$$

According to Etheridge [35] the Schmidt number for (low rise) building ventilation applications can be set to $Sc_t = 0.7$ and according to Montazeri et al [36] the suggested expression for the diffusion coefficient is:

$$D_{ej} = \frac{v_t}{Sc_t} + (2.88 * 10^{-5}) * \rho \tag{5.2}$$

where v_t is the turbulent viscosity, Sc_t is the turbulent Schmidt number and ρ $\left[\frac{kg}{m^3}\right]$ is the air density.

Equation (4.20) can also be written in the following form:

$$\vec{u} \cdot \mathrm{div}(\bar{\tau}_a) = \mathrm{div}\left(\mathrm{D}_{e_j}\,\mathrm{grad}(\bar{\tau}_a)\right) + 1 \Rightarrow \mathrm{div}(\vec{u} \cdot \bar{\tau}_a) = \mathrm{div}\left(\mathrm{D}_{e_j}\,\mathrm{grad}(\bar{\tau}_a)\right) + 1 \tag{5.3}$$

5.2 Discretization

Figure (4) shows a 3D representation a cell with a cell center P. This cell has six faces, each of which is adjacent to a neighboring cell. The faces normal to the x-axis are called west and east, the faces normal to the y-axis are called north and south and the faces normal to the z-axis are called up and down.

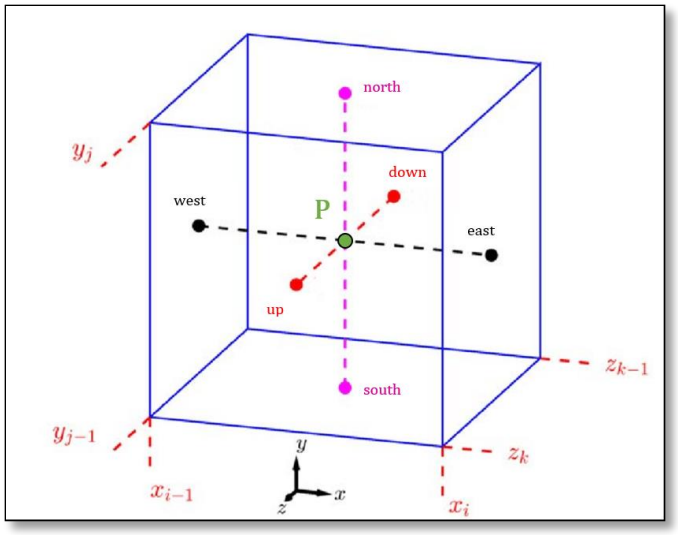

Figure 4: Notation of a 3D cell

For the notation of the six faces we will use the lower-case letters e, w, n, s, u, d for the eastern, western, northern, southern, upper, lower face of the cell respectively. Whereas, the notation used for the neighboring cells is W, E, N, S, U, D for the cell on the western, eastern, northern, southern, upper, lower side respectively. A 2D representation of neighboring cells is shown in figure (5).

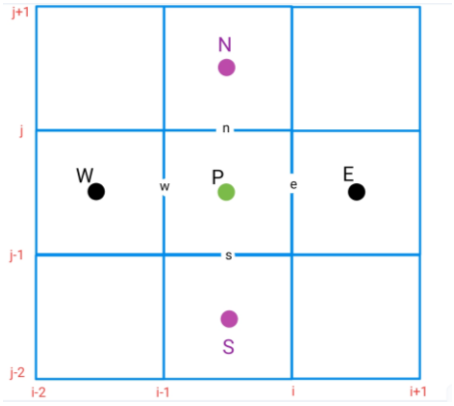

Figure 5: 2D representation of neighboring cells

Having established the used notations, we can move on to the discretization of Equation (5.2) over the volume cell of center P, shown in figures 6 and 7.

If we integrate equation (5.2) over the cell volume V_p we get:

$$\int_{V_P} \mathrm{div}(\vec{u} \cdot \bar{\tau}_a) dV = \int_{V_P} \mathrm{div}\big(D_{ej}\, \mathrm{grad}(\bar{\tau}_a)\big) dV + \int_{V_P} 1 dV \qquad (5.4)$$

Applying the Gauss Divergence Theorem for the convection and diffusion term we get:

$$\int_{A_P} \hat{n} \cdot (\vec{u}\ \bar{\tau}_a) dA = \int_{A_P} \hat{n} \cdot \left(D_{ej}\ \text{grad}\ (\bar{\tau}_a)\right) dA + V_P \tag{5.5}$$

$$\left(u\bar{\tau}_a - D_{ex}\frac{\partial \bar{\tau}_a}{\partial x}\right)_e A_e - \left(u\bar{\tau}_a - D_{ex}\frac{\partial \bar{\tau}_a}{\partial x}\right)_w A_w + \left(v\bar{\tau}_a - D_{ey}\frac{\partial \bar{\tau}_a}{\partial y}\right)_n A_n - \left(v\bar{\tau}_a - D_{ey}\frac{\partial \bar{\tau}_a}{\partial y}\right)_s A_s + \\ + \left(w\bar{\tau}_a - D_{ez}\frac{\partial \bar{\tau}_a}{\partial z}\right)_u A_u - \left(w\bar{\tau}_a - D_{ez}\frac{\partial \bar{\tau}_a}{\partial z}\right)_d \cdot A_d = V_P \tag{5.6}$$

For the diffusion terms $\left(D_{ej}\frac{\partial \bar{\tau}_a}{\partial j}\right)_f A_f$, where $j = x, y, z$ and $f = faces\ (w, e, n, s, u, d)$, we apply the central differencing scheme in the volume cell of center P, shown in figure 7.

- For the eastern face:

$$-A_e\left(D_{ex}\frac{\partial \bar{\tau}_a}{\partial x}\right)_e = -D_{ex(e)}\frac{\left(\bar{\tau}_{a(E)} - \bar{\tau}_{a(P)}\right)}{\Delta x_{PE}} \cdot A_e = \bar{\tau}_{a(P)}\left(\frac{D_{\text{ex(e)}} \cdot A_e}{\Delta x_{PE}}\right) - \bar{\tau}_{a(E)}\left(\frac{D_{\text{ex(e)}} \cdot A_e}{\Delta x_{PE}}\right) \tag{5.7}$$

- For the western face:

$$A_w\left(D_{ex}\frac{\partial \bar{\tau}_a}{\partial x}\right)_w = D_{ex(w)}\frac{\left(\bar{\tau}_{a(P)} - \bar{\tau}_{i(W)}\right)}{\Delta x_{PW}} \cdot A_w = \bar{\tau}_{a(P)}\left(\frac{D_{\text{ex(w)}} \cdot A_w}{\Delta x_{PW}}\right) - \bar{\tau}_{a(W)}\left(\frac{D_{\text{ex(w)}} \cdot A_w}{\Delta x_{PW}}\right) \tag{5.8}$$

- For the northern face:

$$-A_n\left(D_{ey}\frac{\partial \bar{\tau}_i}{\partial y}\right)_n = -D_{ey(n)}\frac{\left(\bar{\tau}_{i(N)} - \bar{\tau}_{i(P)}\right)}{\Delta y_{PN}} \cdot A_n = \bar{\tau}_{i(P)}\left(\frac{D_{\text{ey(n)}} \cdot A_n}{\Delta \text{y}_{\text{PN}}}\right) - \bar{\tau}_{i(N)}\left(\frac{D_{\text{ey(n)}} \cdot A_n}{\Delta \text{y}_{\text{PN}}}\right) \tag{5.9}$$

- For the southern face:

$$A_s\left(D_{ey}\frac{\partial \bar{\tau}_i}{\partial y}\right)_s = D_{ey(s)}\frac{\left(\bar{\tau}_{i(P)} - \bar{\tau}_{i(S)}\right)}{\Delta y_{PS}} \cdot A_s = \bar{\tau}_{i(P)}\left(\frac{D_{\text{ey(s)}} \cdot A_s}{\Delta \text{y}_{\text{PS}}}\right) - \bar{\tau}_{i(S)}\left(\frac{D_{\text{ey(s)}} \cdot A_s}{\Delta \text{y}_{\text{PS}}}\right) \tag{5.10}$$

- Analogously to the above we apply the scheme for the remaining faces

For the convection terms $\left(u_j\ \bar{\tau}_i\right)_f A_f$, where $j = x, y, z$ and $f = faces\ (w, e, n, s, u, d)$, we apply a hybrid differencing scheme based on the Péclet number Pe. In mass transfer, the Péclet number compares the rate of convective mass transfer to the rate of molecular diffusion. In this context, a high Péclet number implies that mass transfer is primarily due to convection, whereas a low Péclet number suggests that diffusion plays a more significant role. In this hybrid scheme Péclet number can also take negative values depending on the direction of convection. For small values of Péclet

number (between -2 and 2), where diffusion is strong, a central differencing scheme is selected for increased stability. The hybrid scheme is applied on each face in the following way.

- For the eastern face:

$$u_e\bar{\tau}_{a(e)} \cdot A_e = \begin{cases} u_e A_e \bar{\tau}_{a(P)}, & P_{e(e)} > 2 \\ u_e A_e \cdot \left(f \cdot \bar{\tau}_{a(E)} + (1-f)\bar{\tau}_{a(P)}\right), & P_{e(e)} \in (-2,2) \\ u_e A_e \bar{\tau}_{a(E)}, & P_{e(e)} < -2 \end{cases} \quad (5.11)$$

$$where \qquad Pe_{(e)} = \frac{u_e * \Delta x_{PE}}{D_{ex(e)}} \qquad and \qquad f = \frac{\Delta x_{Pe}}{\Delta x_{PE}}$$

- For the western face:

$$u_w\bar{\tau}_{i(w)} \cdot A_w = \begin{cases} u_w A_w \bar{\tau}_{a(P)}, & P_{e(w)} > 2 \\ u_w A_w \cdot \left(f \cdot \bar{\tau}_{a(W)} + (1-f)\bar{\tau}_{a(P)}\right), & P_{e(w)} \in (-2,2) \\ u_w A_w \bar{\tau}_{a(W)}, & P_{e(w)} < -2 \end{cases} \quad (5.12)$$

$$where \qquad Pe_{(w)} = -\frac{u_w * \Delta x_{PW}}{D_{ex(w)}} \qquad and \qquad f = \frac{\Delta x_{Pw}}{\Delta x_{PW}}$$

- For the upper face:

$$w_u\bar{\tau}_{i(u)} \cdot A_u = \begin{cases} w_u A_u \bar{\tau}_{a(P)}, & P_{e(u)} > 2 \\ w_u A_u \cdot \left(f \cdot \bar{\tau}_{a(U)} + (1-f)\bar{\tau}_{a(P)}\right), & P_{e(u)} \in (-2,2) \\ w_u A_u \bar{\tau}_{a(U)}, & P_{e(u)} < -2 \end{cases} \quad (5.13)$$

$$where \qquad Pe_{(u)} = \frac{w_u * \Delta z_{PU}}{D_{ez(u)}} \qquad and \qquad f = \frac{\Delta z_{Pu}}{\Delta z_{PU}}$$

- For the downward face:

$$w_d\bar{\tau}_{a(d)} \cdot A_d = \begin{cases} w_d A_d \bar{\tau}_{a(P)}, & P_{e(d)} > 2 \\ w_d A_d \cdot \left(f \cdot \bar{\tau}_{a(D)} + (1-f)\bar{\tau}_{a(P)}\right), & P_{e(d)} \in (-2,2) \\ w_d A_d \bar{\tau}_{\mathrm{a}(D)}, & P_{e(d)} < -2 \end{cases} \quad (5.14)$$

$$where \qquad Pe_{(d)} = -\frac{w_d * \Delta z_{PD}}{D_{ez(d)}} \qquad and \qquad f = \frac{\Delta z_{Pd}}{\Delta z_{PD}}$$

- Analogously to the above we apply the scheme for the remaining faces

The discretized equation can be written in the following form

$$\boldsymbol{a_P\,\bar{\tau}_{a(P)} = a_E\bar{\tau}_{a(E)} + a_w\bar{\tau}_{a(w)} + a_N\bar{\tau}_{a(N)} + a_S\bar{\tau}_{a(s)} + a_U\bar{\tau}_{a(U)} + a_D\bar{\tau}_{a(D)} + S} \quad (5.15)$$

where:

- $a_P = \left(\frac{D_{ex(e)} \cdot A_e}{\Delta x_{PE}} + \frac{D_{ex(w)} \cdot A_w}{\Delta x_{PW}}\right) + \left(\frac{D_{ey(n)} \cdot A_n}{\Delta y_{PN}} + \frac{D_{ey(s)} \cdot A_s}{\Delta y_{PS}}\right) + \left(\frac{D_{ez(u)} \cdot A_u}{\Delta z_{PU}} + \frac{D_{ez(d)} \cdot A_d}{\Delta z_{PD}}\right) + \begin{pmatrix} Convection\ Terms \\ if\ Pe > -2 \end{pmatrix}$
- $a_E = \left(\frac{D_{ex(e)} \cdot A_e}{\Delta x_{PE}}\right) - \begin{pmatrix} Convection\ Term \\ if\ Pe < 2 \end{pmatrix}$
- $a_W = \left(\frac{D_{ex(w)} \cdot A_w}{\Delta x_{PW}}\right) + \begin{pmatrix} Convection\ Term \\ if\ Pe < 2 \end{pmatrix}$
- $a_N = \left(\frac{D_{ey(n)} \cdot A_n}{\Delta y_{PN}}\right) - \begin{pmatrix} Convection\ Term \\ if\ Pe < 2 \end{pmatrix}$
- $a_S = \left(\frac{D_{ey(s)} \cdot A_s}{\Delta y_{PS}}\right) + \begin{pmatrix} Convection\ Term \\ if\ Pe < 2 \end{pmatrix}$
- $a_U = \left(\frac{D_{ez(u)} \cdot A_u}{\Delta z_{PU}}\right) - \begin{pmatrix} Convection\ Term \\ if\ Pe < 2 \end{pmatrix}$
- $a_D = \left(\frac{D_{ez(d)} \cdot A_d}{\Delta z_{PD}}\right) + \begin{pmatrix} Convection\ Term \\ if\ Pe < 2 \end{pmatrix}$
- $S = V_P$

5.3 Grid Structure

Before we numerically solve for the AOA, we need to define a computational grid. We assume a 3-dimensional orthogonal grid, generated by Ni nodes in the x-direction, Nj nodes in the y-direction and Nk nodes in the z-direction. We choose a cell-centered approach, which means that values will be stored at the center of the formed 3D cells, as shown in figure (6).

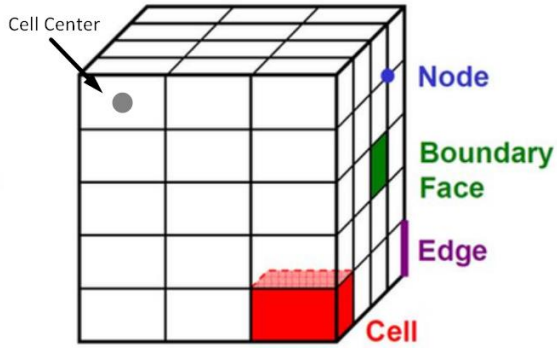

Figure 6: Schematic of the 3D Mesh

On the grid boundaries (i.e. for $i = 1, Ni$ and $j = 1, Nj$, and $k = 1, Nk$) we assign cells of zero thickness. As a result, the number of cells on a horizontal line is one more than the number of

gridlines that are perpendicular to that line. A 2D illustration of the grid is shown in figure (7).

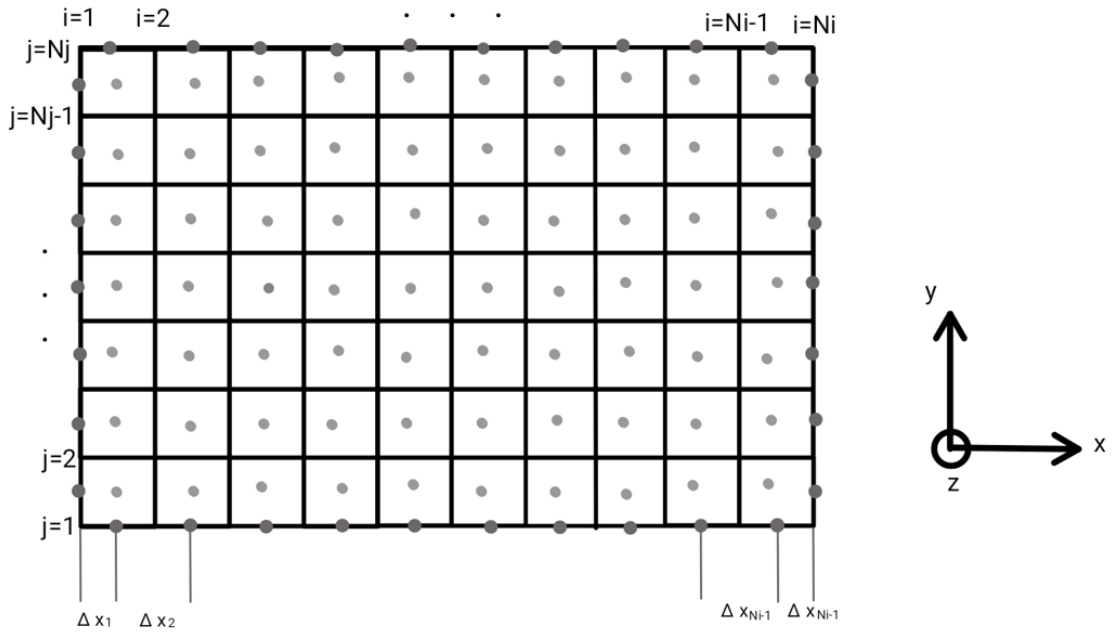

Figure 7: A 2D schematic of the 3D mesh

5.4 Numerical Method for Solving the System of Equations

The system of linear equations described in (5.17) can be solved using the ADI (alternating direction implicit) method. ADI is an iterative method, where the key idea is to split each numerical iteration into multiple steps, each of which solves the problem in one spatial direction while holding the others constant. At each step, you end up with a set of tridiagonal systems of linear equations. The user can choose to solve these systems either by using Thomas' algorithm or LU decomposition. After completing each step in one direction, the process is repeated for all spatial directions. After that, the next numerical iteration starts and the same steps are followed. Convergence is reached when the solution of the current iteration converges to that of the previous one, according to a user-defined convergence criterion.

The number of steps selected were three, one for each dimension (x, y, z). After some experimentation it was clear that the sequence in which the spatial directions are solved influences the accuracy of the solution and the speed of convergence. For example, ADI in X-Y-Z order (i.e. the first step solves in x-dimension, second in y-dimension, third in z-dimension) gave different results from ADI in Z-X-Y order or Y-X-Z order. It was found that sequences that started with the spatial direction of the flow performed better than others that didn't. Since most of the test cases involved flow along the z-axis, each ADI step starts with that direction. After some further experimentation and tuning the sequence Z-Y-X was selected on account of its increased accuracy and relatively high convergence speed.

An overview of the process is shown below.

a) Solving a TDMA along the z-axis

$$a_P\,\bar{\tau}_{a(P)} - a_U\bar{\tau}_{a(U)} - a_D\bar{\tau}_{a(D)} = a_E\bar{\tau}_{a(E)} + a_w\bar{\tau}_{a(w)} + a_N\bar{\tau}_{a(N)} + a_S\bar{\tau}_{a(S)} + S \tag{5.16}$$

For each $i = 2{:}\,Ni$ and for each $j = 2{:}\,Nj$ we solve a tridiagonal matrix of dimension $[Nk+1]x[Nk+1]$ where:

$$Source = V_P + a_E\bar{\tau}_{i(E)} + a_w\bar{\tau}_{i(w)} + a_N\bar{\tau}_{i(N)} + a_S\bar{\tau}_{i(S)} \Rightarrow$$

$$\Rightarrow Source = V_P + \left(\frac{D_{\text{ex(e)}}\cdot A_e}{\Delta x_{PE}}\right)\bar{\tau}_{a(E)} + \left(\frac{D_{\text{ex(w)}}\cdot A_w}{\Delta x_{PW}}\right)\bar{\tau}_{a(W)} +$$

$$+\left(\frac{D_{\text{ez(u)}}\cdot A_u}{\Delta z_{PU}}\right)\bar{\tau}_{a(N)} + \left(\frac{D_{\text{ez(d)}}\cdot A_d}{\Delta z_{PD}}\right)\bar{\tau}_{a(S)} \pm \begin{pmatrix} Convection\ Terms \\ with\ Pe < 2 \end{pmatrix} \tag{5.17}$$

- For j=1
  $a_P = 1, \quad a_E = -1, \quad Source = 0$
- For j=Nj+1
  $a_P = 1, \quad a_W = -1, \quad Source = 0$
- For i=1
  $\bar{\tau}_{a(P)} = 0$
- For i=Ni+1
  $\bar{\tau}_{a(P)} = \bar{\tau}_{a(W)} - \dfrac{\Delta XC(Ni)}{u(Ni+1,j,k)}$

b) Solving a TDMA along the y-axis

$$a_P\,\bar{\tau}_{a(P)} - a_N\bar{\tau}_{a(N)} - a_S\bar{\tau}_{a(s)} = a_E\bar{\tau}_{a(E)} + a_w\bar{\tau}_{a(w)} + a_U\bar{\tau}_{a(U)} + a_D\bar{\tau}_{a(D)} + S \tag{5.18}$$

For each $i = 2{:}\,Ni$ and for each $k = 2{:}\,Nk$ we solve a tridiagonal matrix of dimension $[Nj+1]x[Nj+1]$ where:

$$Source = V_P + a_E\bar{\tau}_{a(E)} + a_w\bar{\tau}_{a(w)} + a_U\bar{\tau}_{a(U)} + a_D\bar{\tau}_{a(D)} \Rightarrow$$

$$\Rightarrow Source = V_P + \left(\frac{D_{\text{ex(e)}}\cdot A_e}{\Delta x_{PE}}\right)\bar{\tau}_{a(E)} + \left(\frac{D_{\text{ex(w)}}\cdot A_w}{\Delta x_{PW}}\right)\bar{\tau}_{a(W)} +$$

$$+\left(\frac{D_{\text{ez(u)}}\cdot A_u}{\Delta z_{PU}}\right)\bar{\tau}_{a(U)} + \left(\frac{D_{\text{ez(d)}}\cdot A_d}{\Delta z_{PD}}\right)\bar{\tau}_{a(D)} \pm \begin{pmatrix} Convection\ Terms \\ with\ Pe < 2 \end{pmatrix} \tag{5.19}$$

- For j=1
  $a_P = 1, \quad a_E = -1, \quad Source = 0$
- For j=Nj+1
  $a_P = 1, \quad a_W = -1, \quad Source = 0$
- For i=1
  $\bar{\tau}_{a(P)} = 0$

- For i=Ni+1

$$\bar{\tau}_{a(P)} = \bar{\tau}_{a(W)} - \frac{\Delta XC(Ni)}{u(Ni+1,j,k)}$$

c) Solving a TDMA along the x-axis

$$a_P\,\bar{\tau}_{a(P)} - a_E\bar{\tau}_{a(E)} - a_w\bar{\tau}_{a(w)} = a_N\bar{\tau}_{a(N)} + a_S\bar{\tau}_{a(s)} + a_U\bar{\tau}_{a(U)} + a_D\bar{\tau}_{a(D)} + S \quad (5.20)$$

For each $j = 2: Nj$ and for each $k = 2: Nk$ we solve a tridiagonal matrix of dimension $[Ni+1]x[Ni+1]$ where the source term is equal to:

$$Source = S + a_N\bar{\tau}_{a(N)} + a_S\bar{\tau}_{a(s)} + a_U\bar{\tau}_{a(U)} + a_D\bar{\tau}_{a(D)} \Rightarrow$$

$$\Rightarrow Source = V_P + \left(\frac{D_{ey(N)}\cdot A_N}{\Delta y_{PN}}\right)\bar{\tau}_{a(N)} + \left(\frac{D_{ey(s)}\cdot A_s}{\Delta y_{PS}}\right)\bar{\tau}_{a(s)} + \left(\frac{D_{ez(u)}\cdot A_u}{\Delta z_{PU}}\right)\bar{\tau}_{a(U)} + \left(\frac{D_{ez(d)}\cdot A_d}{\Delta z_{PD}}\right)\bar{\tau}_{a(D)} \pm \begin{pmatrix} Convection\ Terms \\ with\ Pe < 2 \end{pmatrix} \quad (5.21)$$

- For $i = 1$
  $a_P = 1, \quad a_E = 0, \quad Source = 0$

- For $i = Ni + 1$
  $a_P = 1, \quad a_W = -1, \quad Source = -\frac{\Delta XC(Ni)}{u(Ni+1,j,k)}$

- For $j = 1$
  $\bar{\tau}_{a(P)} = \bar{\tau}_{a(N)}$

- For $j = Nj + 1$
  $\bar{\tau}_{a(P)} = \bar{\tau}_{a(S)}$

Chapter 6: Key Aspects of the Age of Air Software

The main objective for this thesis was to develop a software that calculates the age of air at all points of a 3-dimensional grid. The age of air Software is a FORTRAN code (REVISED_VENTILATION.f95), that was developed for the Laboratory for Innovative Environmental Technologies (LIET) as a tool to evaluate the ventilation efficiency of buildings.

6.1 Compatibility with Existing Software

As we have shown in the equations of Chapter 2, finding the age of air at a point, requires knowledge of the velocity at that point. In computational terms, the developed software solves for the age of air at any point of a given 3-dimensional grid using given values of the velocity vector at that point. Thus, a solved velocity field is required as an input in the developed software.

Obtaining a solution for the velocity field, is a matter of either another CFD Solver or experimental data i.e. from a wind-tunnel. In most cases a solved velocity field was obtained using the LIET's own in-house CFD code. This Software allows the user to generate grids, adjust their density, insert solid geometries like buildings and solve for steady turbulent flows using the k-ε model. For a given flow field, age of air can be calculated using the age of air Software. In the present realization, the format of the input and output files was constructed to be compatible with the in-house software. However, this is not restrictive as to the application of the methodology

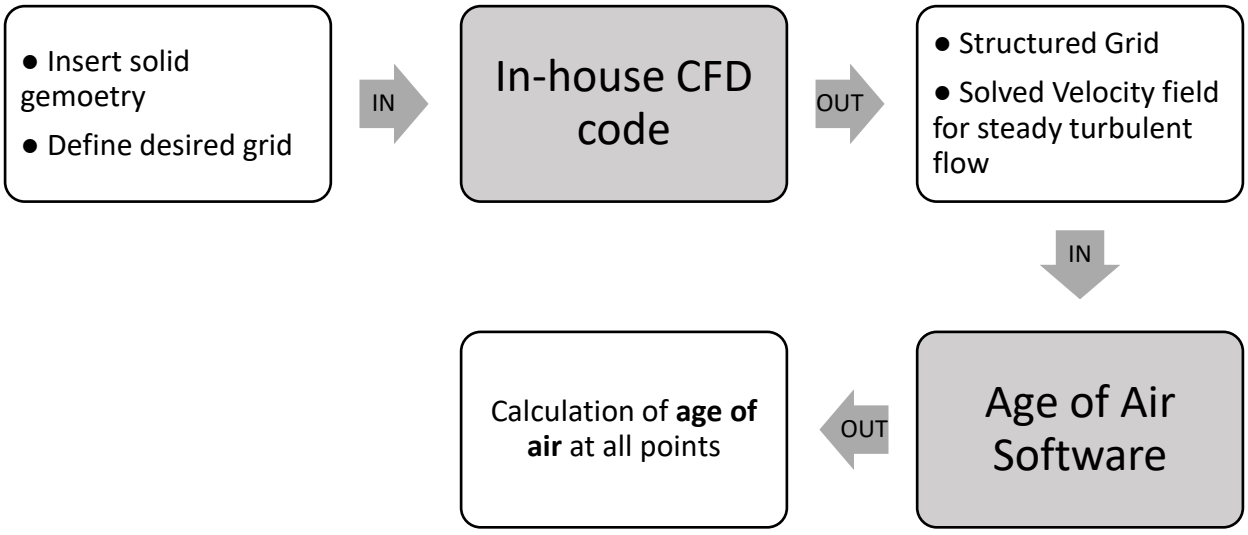

Flowchart 1: Compatibility flowchart of the AOA Software with the in-house CFD code

6.2 Main Code Structure

The structure of the developed code is outlined below:

Flowchart 2: Overview of the main AOA code

6.3 Post-processing of Results

After the solver converges, the results are stored in a file (MY_PRE_RESULTS.dat). These results describe the age distribution in the whole domain. However, we are only interested in the region of the domain that corresponds to the inside of the building. This is one of the main tasks that we need to do in the post-processing phase. In addition to that we may need to do some additional calculations and data clean up. Since this process can be repetitive, it was decided to outsource the post-processing phase to another program (POST_PROCESS.f95).

This Fortran program is essentially a post-processing tool designed to analyze and manipulate simulation results generated by the main program. The primary goal of this program is to process and represent the simulation results using Tecplot, a popular software for visualization and analysis of numerical simulation data.

What follows is a flowchart of the key components and functionalities of the program:

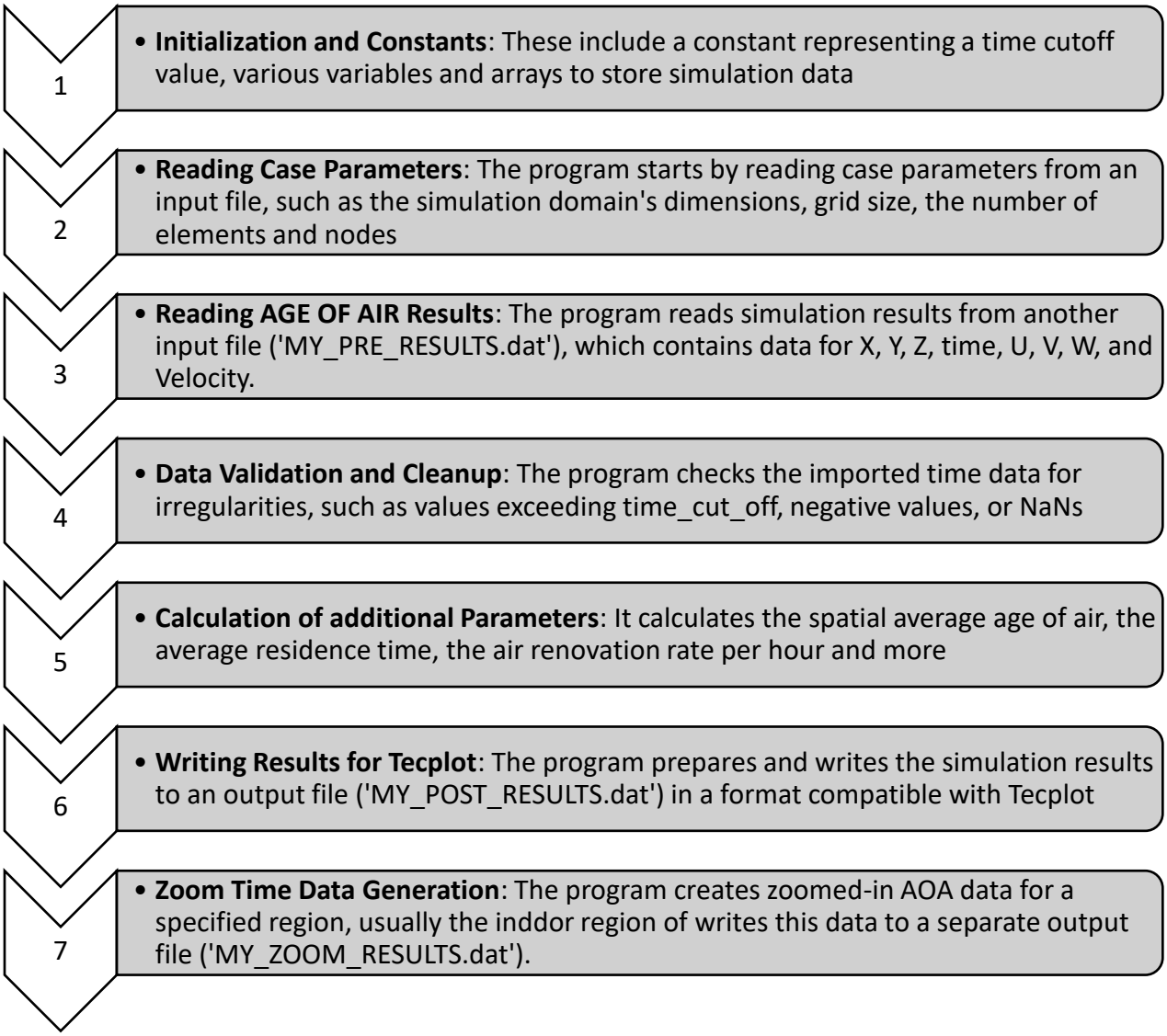

Flowchart 3: Overview of the post-processing code

Chapter 7: Validation Cases for Basic Flows

7.1 Introduction

The following cases serve as simple test cases that validate the functionality of our code. Each case is described by a different velocity field and has different analytical solution to the AOA. This analytical solution is then compared with the computational solution reached by the AOA Software. The selected cases are described below:

- The first three cases represent the problem of the age of air in its simplest form: determination of the AOA in a uniform flow along a single dimension. For each case the direction of the flow is different with the purpose of checking the directional independence of the solution.
- A flow along the z-axis with a varying velocity profile. This is a case of non-uniform flow, where the velocity w is a function of the height x.

7.2 Uniform Flow

All three cases of uniform flow will be tested on the same domain size (shown in figure (8)) with dimensions $(50\ x\ 50\ x\ 5)m\ = (Length\ x\ Width\ x\ Height)$. The velocity along the direction of the flow is constant and equal to $50\ m/s$.

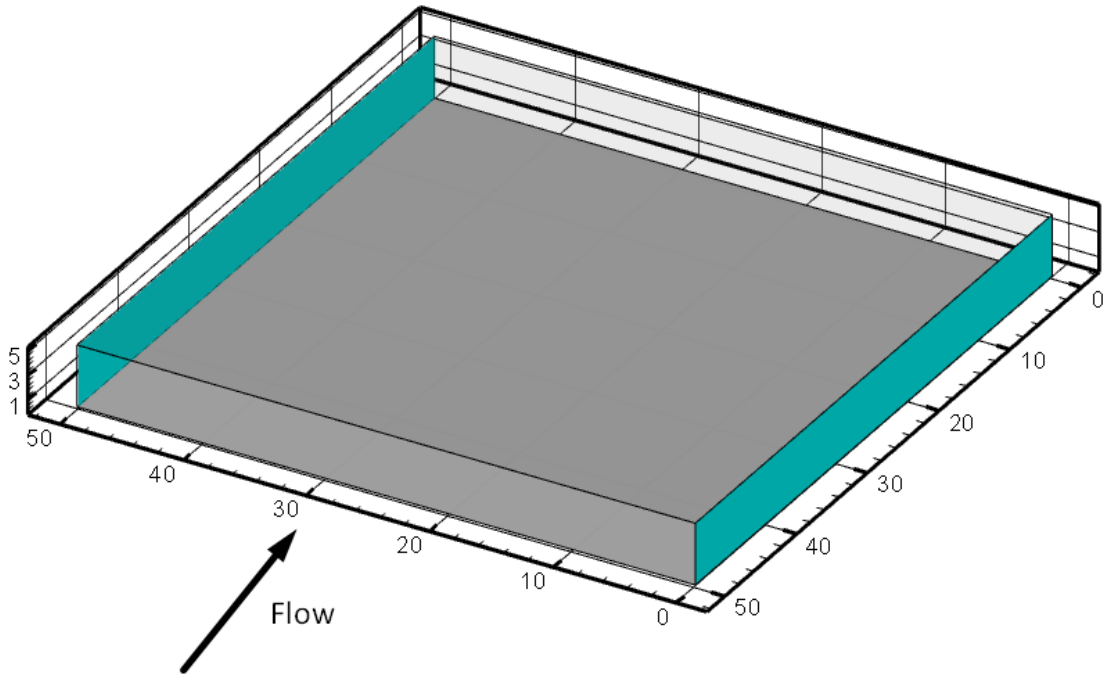

Figure 8: Schematic of the Domain

7.2.1 Uniform Flow along the x-axis

In this case we have a constant velocity $u = 50\frac{m}{s}$ and the remaining components of the velocity are zero ($v = w = 0$). The boundary faces normal to the x-axis represent the inlet and outlet faces whereas the boundary faces normal to the y-axis and z-axis are considered symmetry planes, as shown in figure (9).

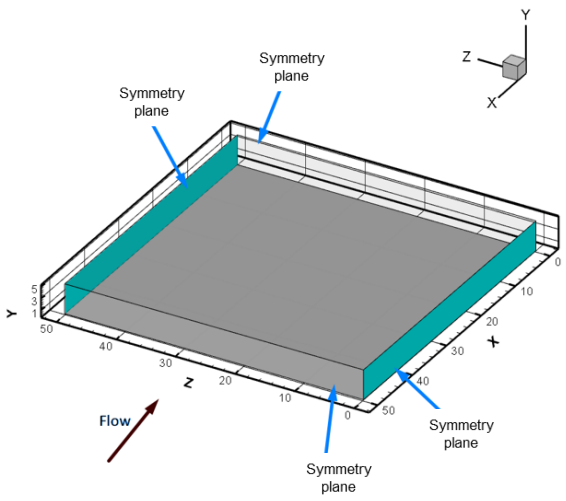

Figure 9: Domain for flow along the x-axis

The following boundary conditions apply:

- $\frac{\partial \tau_a}{\partial y} = 0$ *for the planes normal to the* $y-$ *axis*
- $\frac{\partial \tau_a}{\partial z} = 0$ *for the planes normal to the* $z-$ *axis*
- $\tau_a = 0$ *at the inlet*
- $\tau_a = -\frac{1}{u}$ *at the outlet*

The analytical solution for the AOA will be derived from the transport equation (4.15). This equation can be further simplified if we take into consideration that the y and z components of the velocity are zero. So, (4.15) can be written as:

$$1 = u\frac{\partial \tau_a}{\partial x} - D_m\left(\frac{\partial^2 \tau_a}{\partial x^2} + \frac{\partial^2 \tau_a}{\partial y^2} + \frac{\partial^2 \tau_a}{\partial z^2}\right) \tag{7.1}$$

Further simplification can be made if we consider the geometry of the domain. More specifically, the length of the domain in the z-dimension is much bigger than the length in the y-dimension. This means that the effect of the side planes normal to the z-direction can be neglected, which allows us to make the diffusion term $\frac{\partial^2 \tau_a}{\partial z^2}$ zero, thus reducing this 3-dimensional problem to two dimensions. All calculations will be made at half the z-length, $z_{mean} = \frac{z_{tot}}{2}$, where the effect of the side planes is most negligible. This leads us to the following form:

$$1 = u\frac{\partial \tau_a}{\partial x} - D_m\left(\frac{\partial^2 \tau_a}{\partial x^2} + \frac{\partial^2 \tau_a}{\partial y^2}\right) \tag{7.2}$$

It can also be said that in the direction of the flow (x-dimension), the effect of convection, as a result of a high flow velocity, is much stronger than that of molecular diffusion. It is therefore reasonable to assume that the diffusion term $\frac{\partial^2 \tau_a}{\partial x^2}$ negligible. This allows us to write equation (7.2) as follows:

$$1 = u\frac{\partial \tau_a}{\partial x} - D_m\left(\frac{\partial^2 \tau_a}{\partial y^2}\right) \tag{7.3}$$

The only remaining diffusion term is the one which corresponds to the vertical direction y. This direction has smaller length and is bounded by two symmetry planes. In a uniform flow, where the

velocity gradient is zero, it is safe to assume that the AOA gradient in the y-direction remains constant. However, we have already established the boundary conditions on symmetry planes, according to which the AOA gradient in the y-direction $\frac{\partial \tau_a}{\partial y}$ is zero. Thus, this gradient is zero throughout the length of the y-dimension and as a result the diffusion term $\frac{\partial^2 \tau_a}{\partial y^2}$ is zero as well. This means that all diffusion terms can be neglected in the case of a uniform flow and the equation (7.3) can be written as follows:

$$1 = u\frac{\partial \tau_a}{\partial x} \tag{7.4}$$

In our case $u = 50\frac{m}{s}$ and $\tau_a(x = 0) = 0$, so the analytical solution for the AOA is:

$$\tau_a = 0.02 * x \tag{7.5}$$

The computational solution to the problem will be found using the age of air Software. The selected grid size is (50 x 50 x 50) nodes and the contour of the AOA is shown in figure (10).

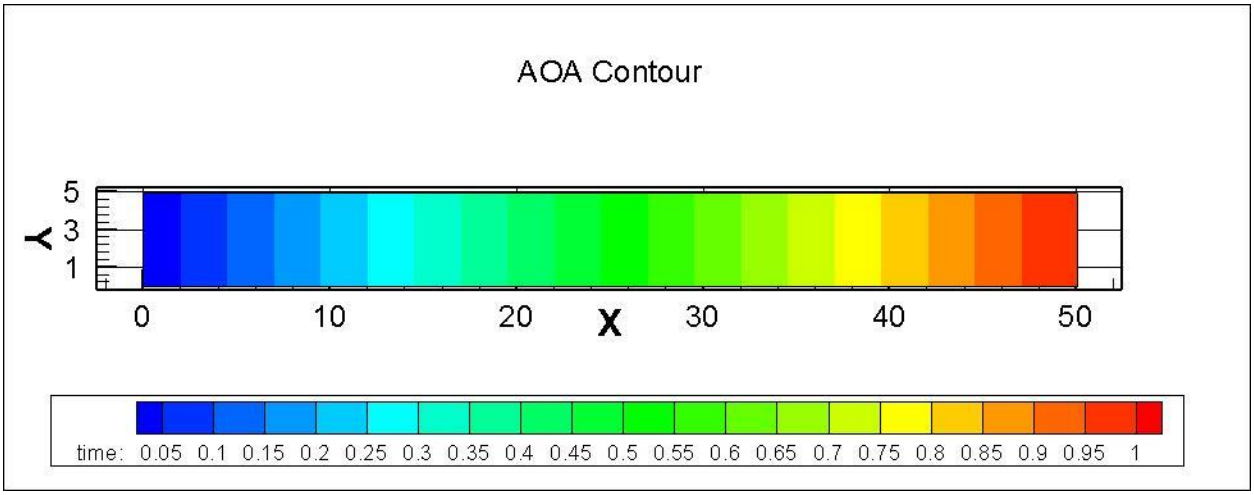

Figure 10: AOA contour for uniform flow in x-dimension

The contour appears consistent with the linear nature of the analytical solution. A better comparison between the analytical and the computational solution can be made by plotting the AOA at $y_{mean} = \frac{y_{tot}}{2}$ and $z_{mean} = \frac{z_{tot}}{2}$. The results are shown in the figure (11).

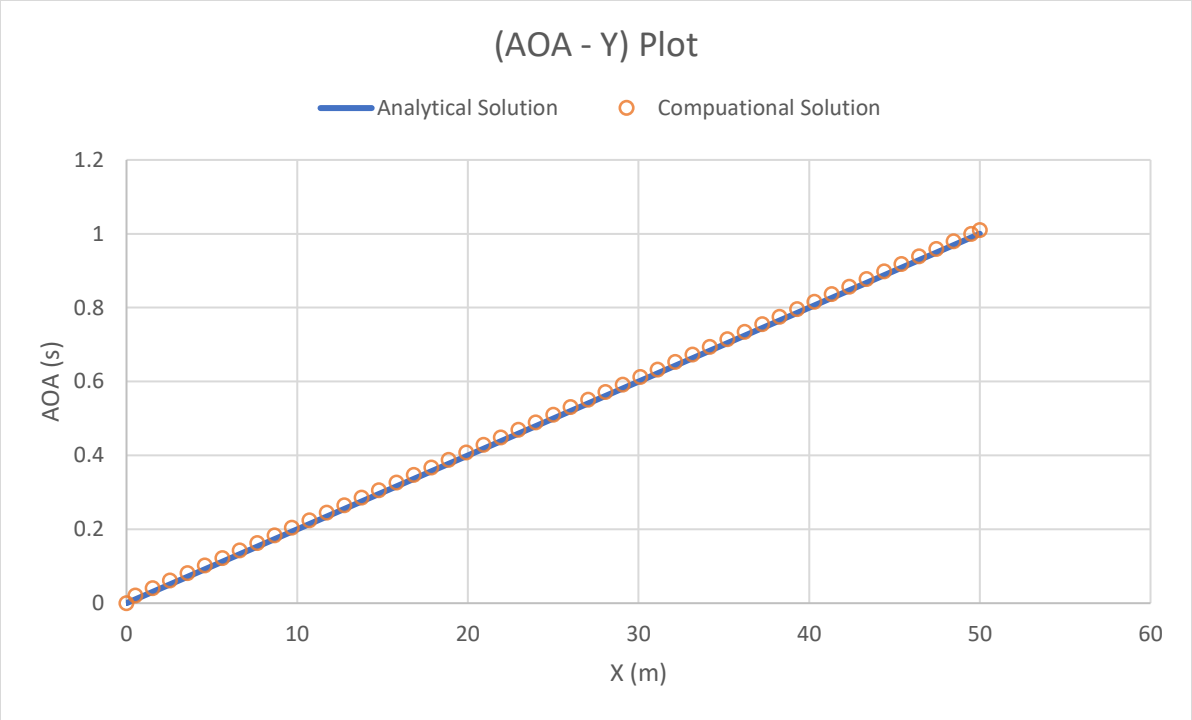

Figure 11: AOA plot for uniform flow in x-dimension

From the graph, it is clear that the results obtained through the computational solution are aligning with the expected linear results obtained through the analytical solution. This suggests that the computational method is producing accurate and reliable results.

7.2.2 Uniform Flow along the y-axis

In this case we have a constant velocity $v = 50\frac{m}{s}$ and the remaining components of the velocity are zero ($u = w = 0$). The boundary faces normal to the y-axis represent the inlet and outlet faces whereas the boundary faces normal to the x-axis and z-axis are considered symmetry planes, as shown in figure (12).

The following boundary conditions apply:

- $\frac{\partial \tau_a}{\partial x} = 0 \quad for\ the\ planes\ normal\ to\ the\ x-axis$
- $\frac{\partial \tau_a}{\partial z} = 0 \quad for\ the\ planes\ normal\ to\ the\ z-axis$
- $\tau_a = 0 \quad at\ the\ inlet$
- $\tau_a = -\frac{1}{v} \quad at\ the\ outlet$

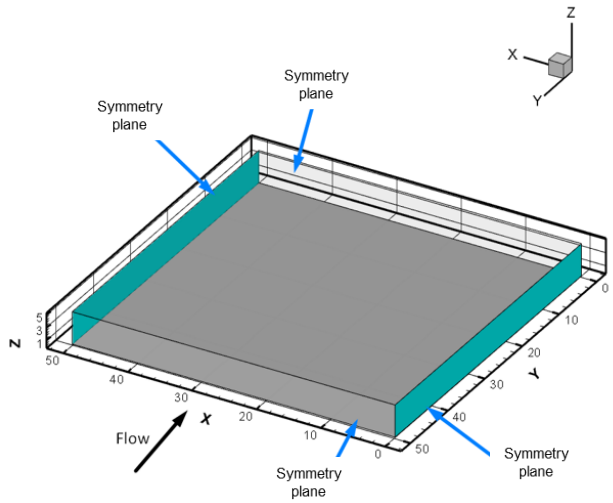

Figure 12:Domain for flow along the y-axis

The analytical solution for the uniform flow along the y-axis can be obtained in the same way as for the uniform flow along the x-axis. By making similar assumptions about the effect of diffusion, we can eliminate the diffusion terms and arrive at the final form:

$$\tau_a = 0.02 * z \tag{7.6}$$

The computational solution to the problem will be found using the age of air Software. The selected grid size is (50 x 50 x 50) nodes and the contour of the AOA is shown in figure (13).

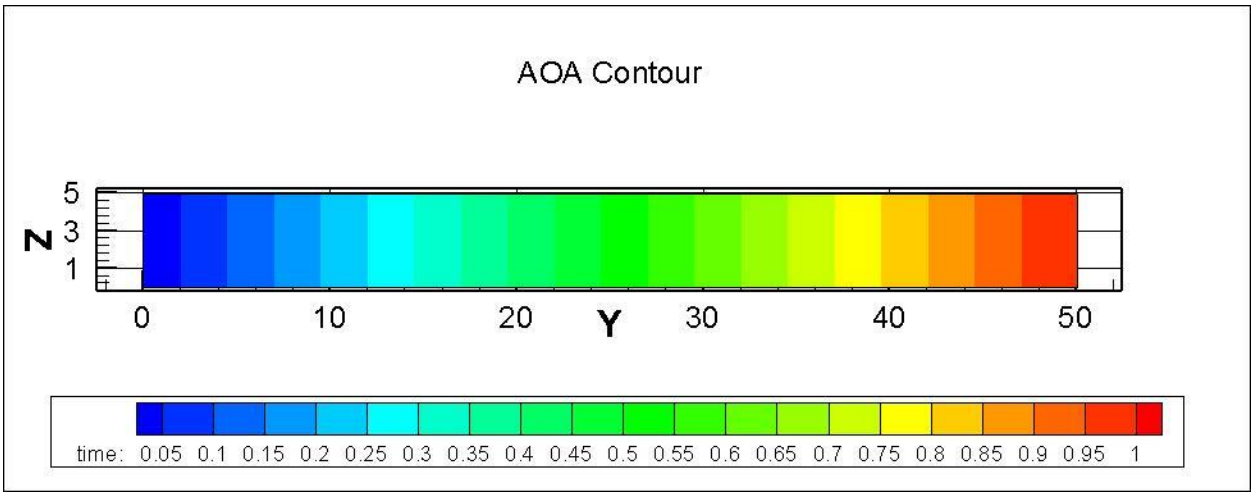

Figure 13: AOA contour for uniform flow in y-dimension

Once again, the linear form of the contour is consistent with the analytical solution. A better comparison between the analytical and the computational solution can be made by plotting the AOA at $x_{mean} = \frac{x_{tot}}{2}$ *and* $z_{mean} = \frac{z_{tot}}{2}$. The results are shown in the figure (14).

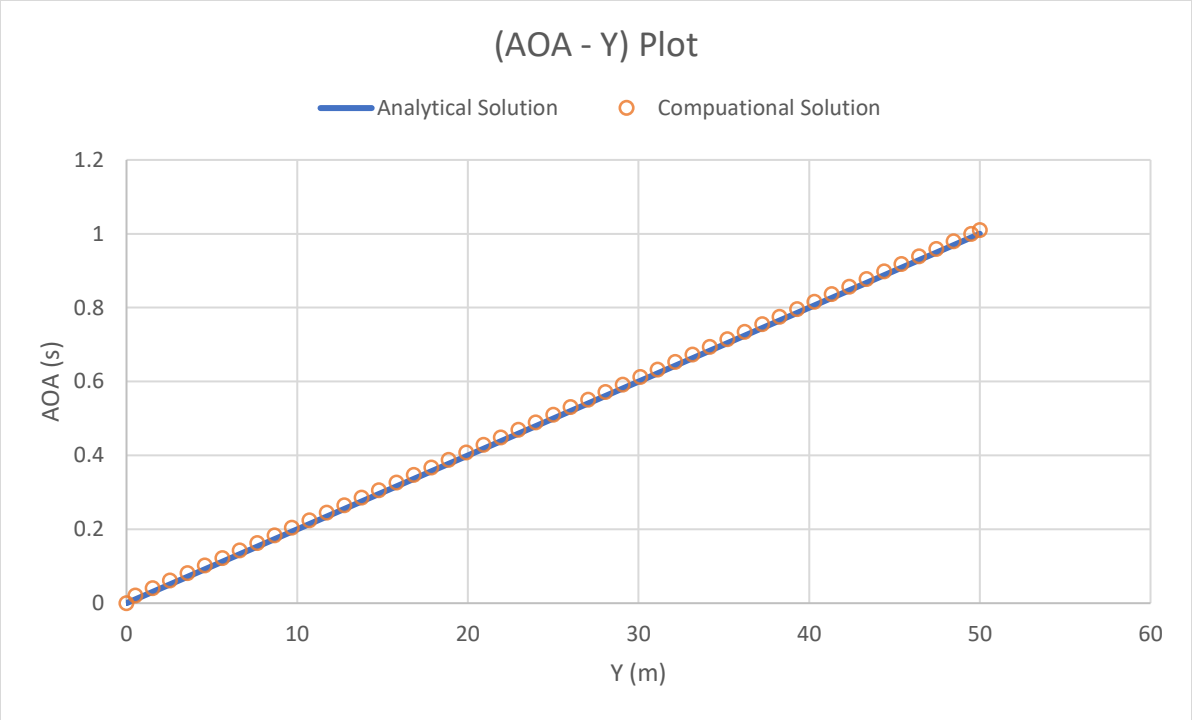

Figure 14: AOA plot for uniform flow in y-dimension

From the graph, it is clear that the computational solution aligns with the analytical one.

7.2.3 Uniform Flow along the z-axis

In this case we have a constant velocity $w = 50\frac{m}{s}$ and the remaining components of the velocity are zero ($u = v = 0$). The boundary faces normal to the z-axis represent the inlet and outlet faces whereas the boundary faces normal to the x-axis and y-axis are considered symmetry planes, as shown in figure (15).

The following boundary conditions apply:

- $\frac{\partial \tau_a}{\partial x} = 0 \quad for\ the\ planes\ normal\ to\ the\ x-axis$
- $\frac{\partial \tau_a}{\partial y} = 0 \quad for\ the\ planes\ normal\ to\ the\ y-axis$
- $\tau_a = 0 \quad at\ the\ inlet$
- $\tau_a = -\frac{1}{w} \quad at\ the\ outlet$

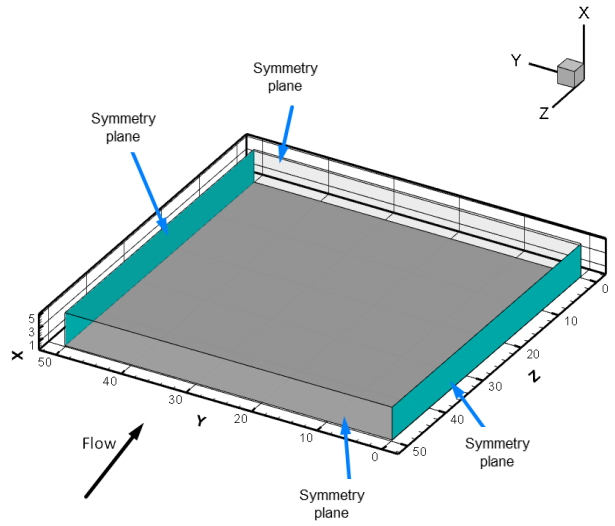

Figure 15: Domain for flow along the z-axis

The analytical solution for the uniform flow along the z-axis can be obtained in the same way as for the uniform flow along the x-axis. By making similar assumptions about the effect of diffusion, we can eliminate the diffusion terms and arrive at the final form:

$$\tau_a = 0.02 * y \tag{7.7}$$

The computational solution to the problem will be found using the age of air Software. The selected grid size is (50 x 50 x 50) nodes and the contour of the AOA is shown in figure (16).

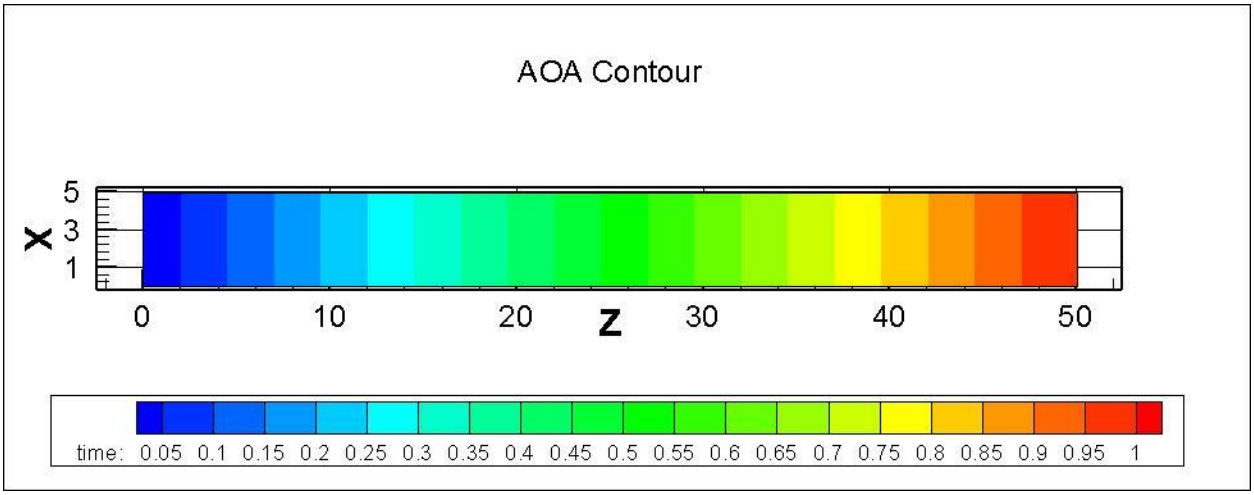

Figure 16: AOA contour for uniform flow in z-dimension

The computational solution has the expected linear form. We will also compare the computational solution with the analytical by plotting the AOA at $x_{mean} = \frac{x_{tot}}{2}$ *and* $y_{mean} = \frac{y_{tot}}{2}$. The results are shown in the figure (17).

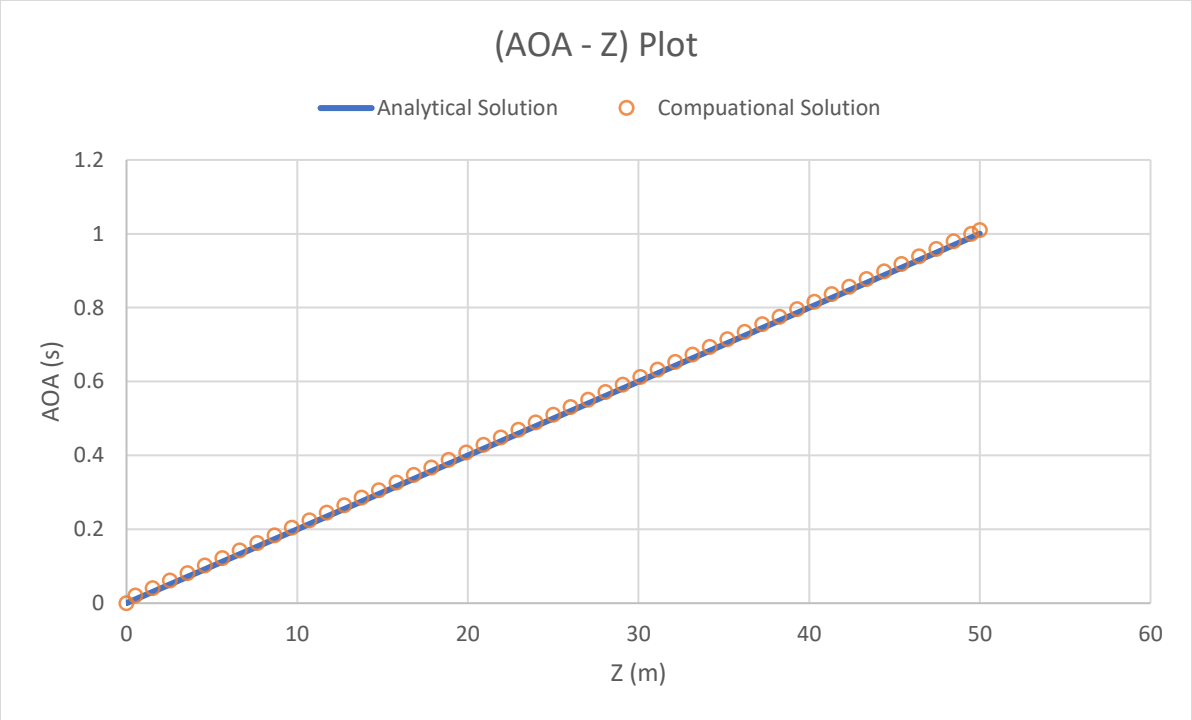

Figure 17: AOA plot for uniform flow in z-dimension

The graph sows a clear alignment of the computational solution with the analytical solution, ensuring once again the validity of our code.

Overall, all three test-cases produced the expected linear results and proved the directional independency of our code.

7.3 Non-uniform Flow between Parallel Plates

In this case we assume a flow along the z-axis with a non-uniform velocity profile. The selected domain (figure (18)) has the same dimensions as the one in the previous cases, $(50\ x\ 50\ x\ 5)m\ = (Length\ x\ Width\ x\ Height)$. The boundary faces normal to the y-axis and z-axis are considered walls and the appropriate boundary conditions apply.

The following boundary conditions apply:

- $\frac{\partial \tau_a}{\partial x} = 0 \quad for\ the\ walls\ normal\ to\ the\ x-axis$
- $\frac{\partial \tau_a}{\partial y} = 0 \quad for\ the\ walls\ normal\ to\ the\ y-axis$
- $\tau_a = 0 \quad at\ the\ inlet$
- $\tau_a = -\frac{1}{w} \quad at\ the\ outlet$

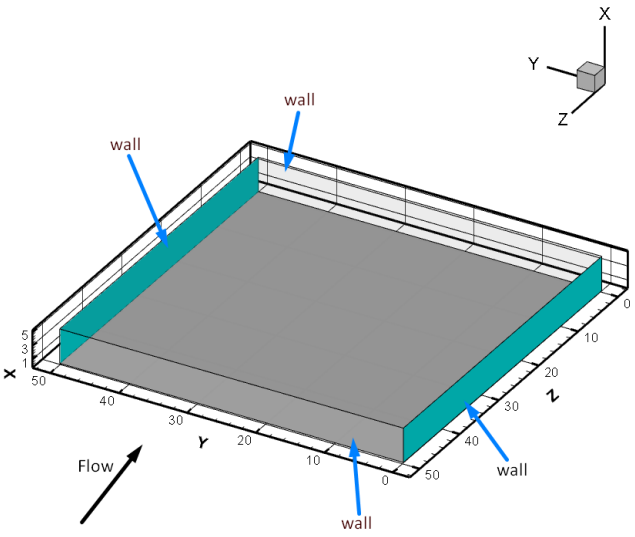

Figure 18: Domain for flow along the z-axis

At the inlet, the x any y components of the velocity are zero ($u = v = 0$), whereas the z-component w is a function of height x:

$$w(x) = 0.5 + 0.5 * |x^2 - 5x| \tag{7.8}$$

where $x \in [0,5]$. This velocity profile is represented in the figure (19).

The analytical solution for the AOA can be obtained by the transport equation (4.20).

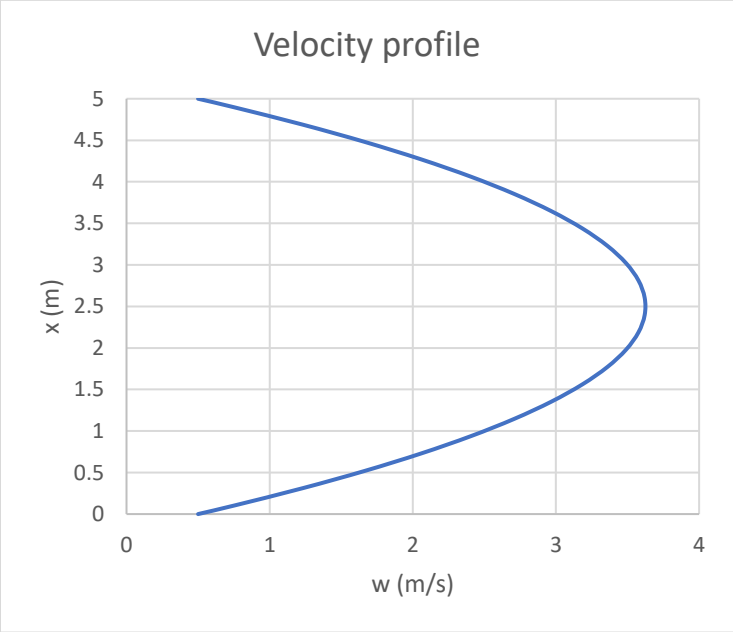

Figure 19: Velocity profile for the "tube" like flow

The analytical solution for the AOA, will be derived from the transport equation (4.15). Since, $u = v = 0$ the equation can be simplified in the following form:

$$1 = w\frac{\partial \tau_a}{\partial z} - D_m\left(\frac{\partial^2 \tau_a}{\partial x^2} + \frac{\partial^2 \tau_a}{\partial y^2} + \frac{\partial^2 \tau_a}{\partial z^2}\right) \quad (7.9)$$

Some diffusion terms in equation (7.7) can be considered negligible. More specifically:

- In the y-direction the distance between the two boundary walls is big enough to assume that their effect on the characteristics of the flow are minimal. Especially at half distance $y_{mean} = \frac{y_{tot}}{2}$ these effects can be neglected, allowing us to eliminate the diffusion term $\frac{\partial^2 \tau_a}{\partial y^2}$. As a result, this 3-dimensional problem can be reduced to two dimensions (x and z) and all calculations can be made at distance y_{mean}.
- In the z direction, which is the direction of the flow, the impact of diffusion on AOA is negligible compared to convection. This means that the diffusion term $\frac{\partial^2 \tau_a}{\partial z^2}$ can also be eliminated.

After these eliminations, we can write equation (7.7) as:

$$w\frac{\partial \tau_a}{\partial z} = D_m\left(\frac{\partial^2 \tau_a}{\partial x^2}\right) + 1 \quad (7.10)$$

At this point, we could also make the assumption that the last diffusion term $\frac{\partial^2 \tau_a}{\partial x^2}$ is also negligible compared to the convection term. An analytical solution that disregards the impact of diffusion in x-dimension as insignificant, is an approximation but we estimate that it is an adequate approximation for the specific problem. This approximate solution can be derived by solving the following simple differential equation:

$$\frac{\partial \tau_a}{\partial z} = \frac{1}{w(x)} \quad (7.11)$$

Substituting the form of $w(x)$ in (7.11) and solving the resulting equation would yield the following approximate analytical solution:

$$\tau_a(x,z)_{approx} = \frac{z}{0.5 + 0.5 * |x^2 - 5x|} \quad (7.12)$$

At this point, we will compare the analytical solution to computational solutions generated by the developed code in three different grid densities:

- 25 grid lines along each axis (grid size 25*25*25)
- 50 grid lines along each axis (grid size 50*50*50)
- 100 grid lines along each axis (grid size 100*100*100)

The results are illustrated using contour plot of the age of air and can be shown in figure (20).

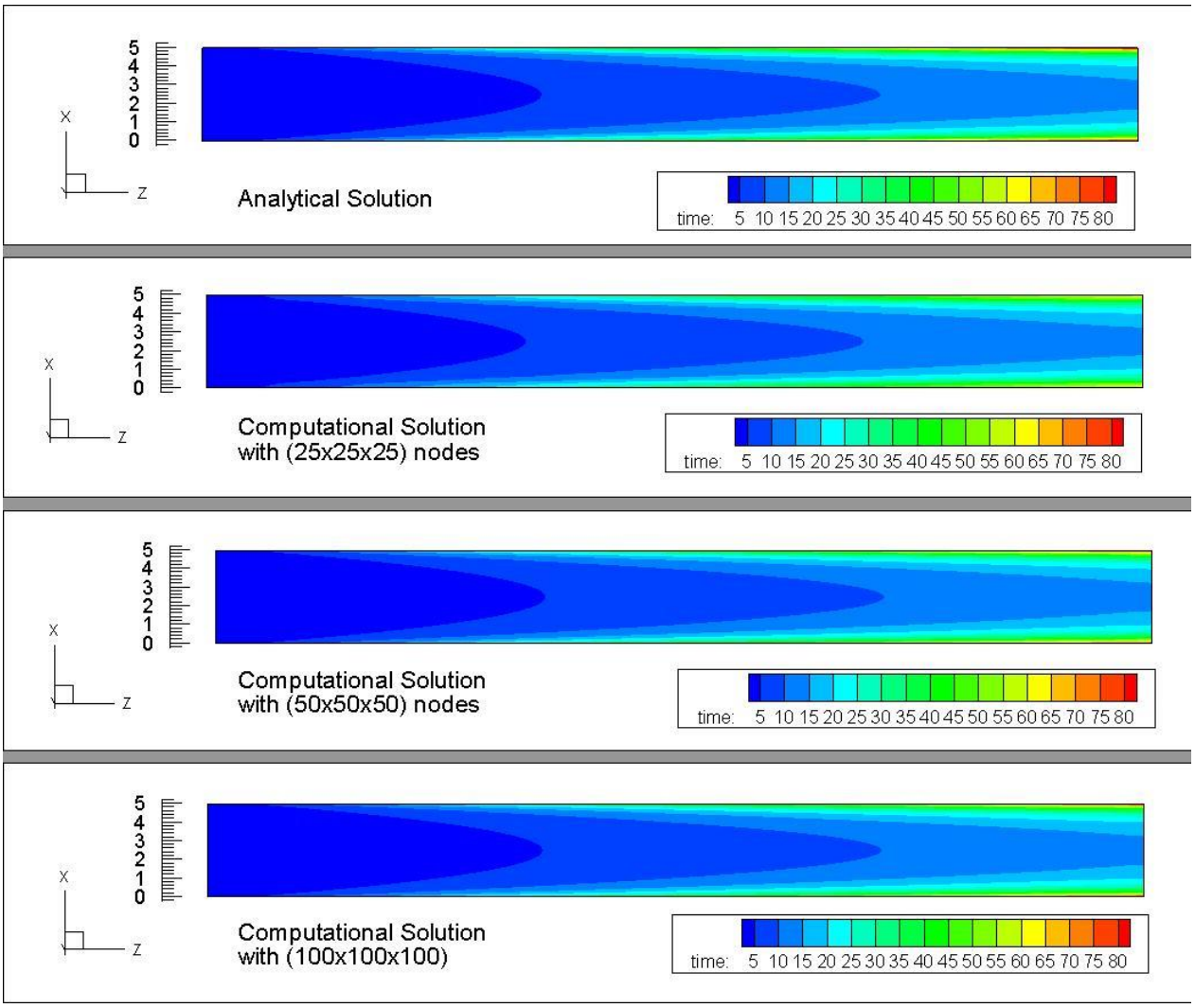

*Figure 20: Solutions of age of air from top to bottom: Analytical, Computational Solutions for grid size (25*25*25), (50*50*50), (100*100*100)*

The figure illustrates that all the computational solutions closely resemble the analytical solution. A more meaningful comparison of the solutions can be made by plotting the AOA values along the x-axis. These measurements have been taken at distances $z_1 = \frac{Z_{tot}}{2}$ *and* $y_1 = \frac{Y_{tot}}{2}$. The results are shown in figure (21).

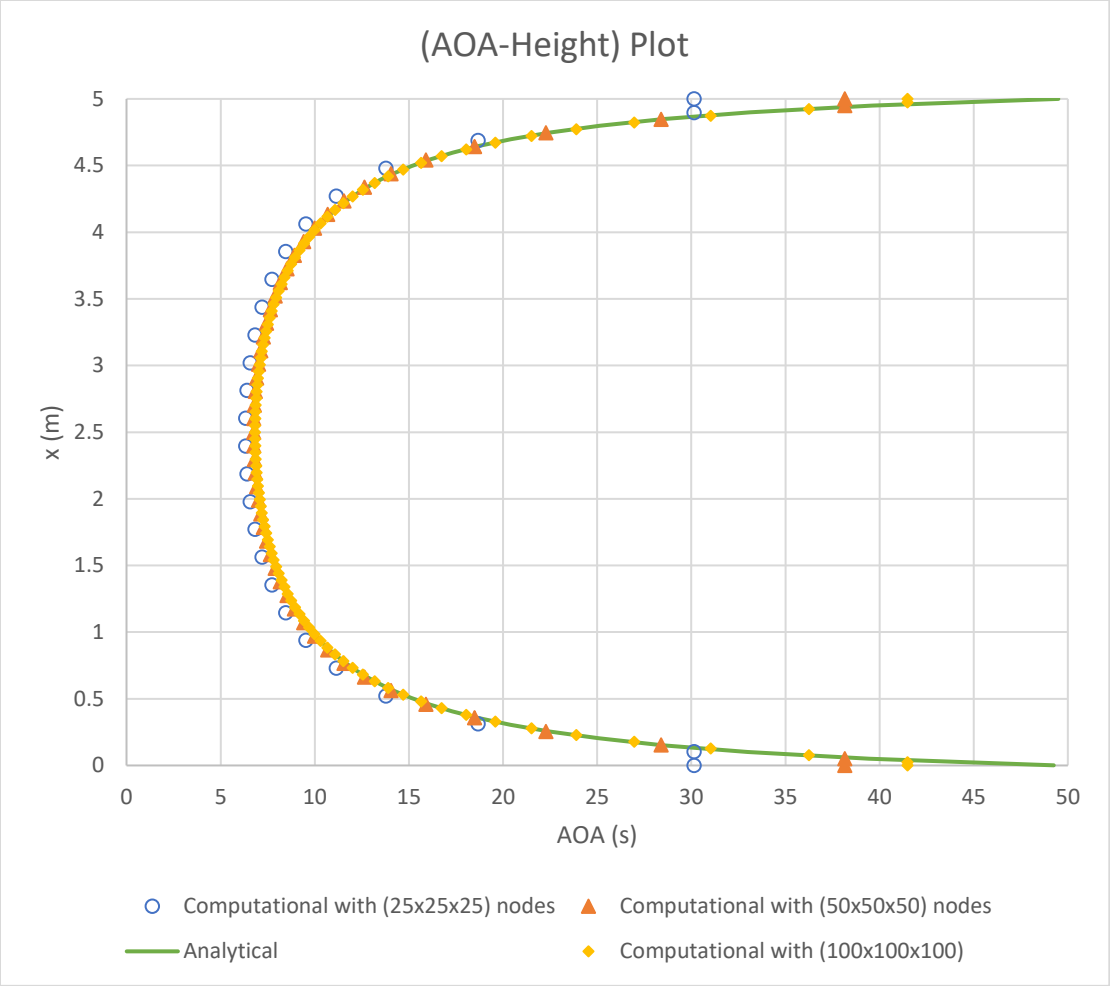

Figure 21: Comparison of computational and analytical AOA results along the x-axis

We can observe that all computational solutions converge towards the analytical one. At the smallest grid density (25x25x25), values of AOA seem to be slightly underestimated compared to the other solutions (both computational and analytical). This is most evident close to the walls, where the values of AOA are considerably lower than those in the analytical solution. By increasing the grid density and therefore the resolution, this difference between the computational solution and the analytical one, is minimized. Overall, the fact that the computational solutions closely align with the analytical solution, serves as compelling evidence that the code has been successfully validated.

Chapter 8: Test Cases for the Flow past a Building

8.1 Introduction

The following cases are more complex and are used to apply the developed software to flows around and inside buildings. In these test cases, the primary goal is not to assess or analyze air quality or ventilation efficiency but to ensure that the age of air software can be applied in more complex building geometries and produce meaningful results.

The geometry of the buildings is based on existing model cubes that have been used for experimental tests in the wind tunnel of the School of Mechanical Engineers in National Technical University of Athens [38].

They are all based on a model cube shape, which we will call "**Full-Full Cube**" and it is shown in figure (22).

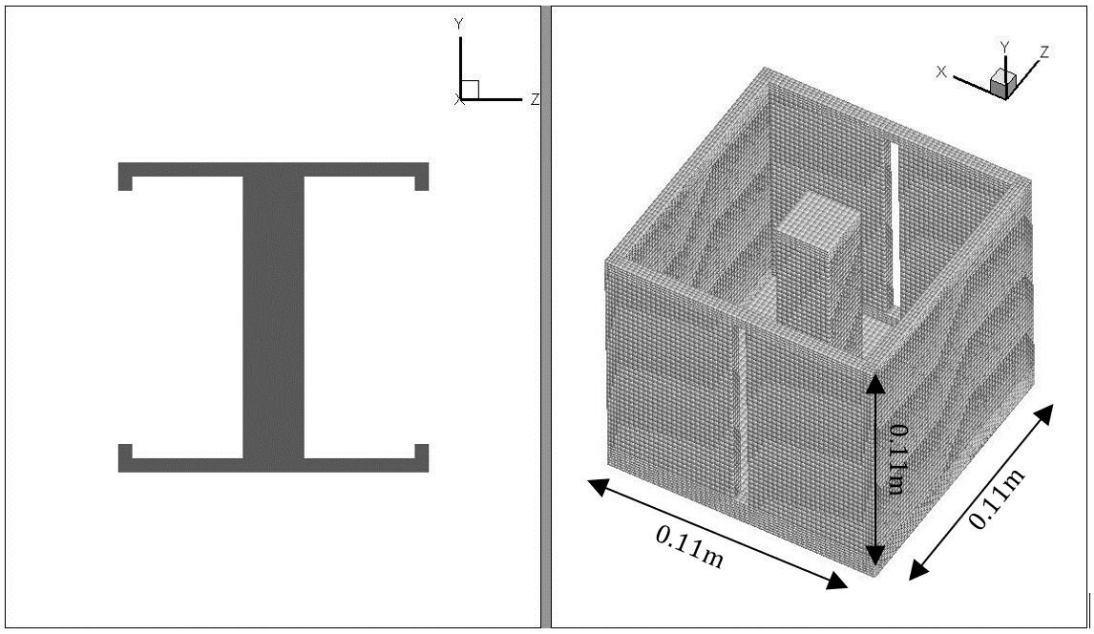

Figure 22: Full-Full Cube. Middle Slice view (left), Trimetric view without the roof (right)

All the buildings have:

- the same basic dimensions, (0.11x0.11x0.11)m.
- two openings, one upstream and one downstream (of width 0.006 m)
- one square column at the center (0.022x0.022)m

They are only differentiated by the height of their opening. More specifically:

1. **Full-Full Cube**: Both openings have a full length of 0.09m (Figure (23A)).
2. **Up-Full Cube**: We only keep the upper half of the upstream opening. The downstream opening remains unchanged (Figure (23B)).

3. **Down-Full Cube**: We only keep the lower half of the upstream opening. The downstream opening remains unchanged (Figure (23C)).
4. **Full-Down Cube**: We only keep the lower half of the downstream opening. The upstream opening remains unchanged (Figure (23D)).
5. **Down-Down Cube**: We only keep the lower half of the upstream opening and the lower half of the downstream opening (Figure (23E)).
6. **Down-Up Cube**: We only keep the lower half of the upstream opening and the upper half of the downstream opening (Figure (23F)).

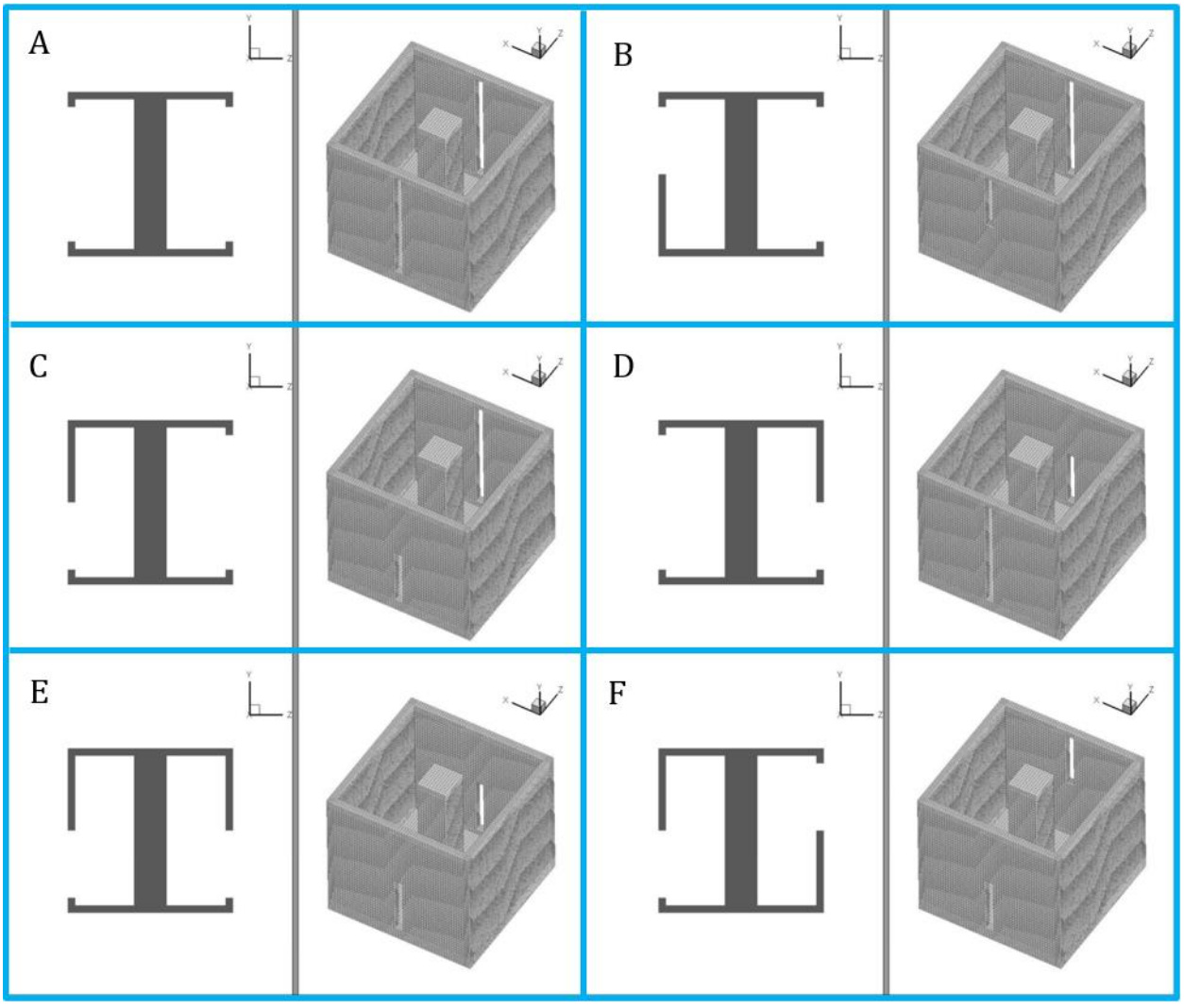

Figure 23: Full-Full (A), Up-Full (B), Down-Full (C), Full-Down (D), Down-Down (E), Down-Up (F)

All the test cases are performed using the same grid and the same initial conditions (Figure 24). The selected grid size is 1.210 x 1.430 x 2.750 m (length along x-axis, length along y-axis, length along z-axis). It has 180 grid lines along the x-axis, 87 along the y-axis and 190 along the z-axis (more than 2.9 million cells), which are arranged more densely around the building. The domain is 3-dimensional so it has 6 boundary planes. The air enters normal to the XY plane and flows along

the z-axis. The remaining boundary planes, normal to the x-axis and y-axis, are considered walls and the appropriate boundary conditions are applied. The building is positioned at x=0.55-0.66m, y=0-0.11m, z=0.66-0.77m. Although, the determination of age of air will only be conducted inside the building, it is necessary to have a domain size considerably bigger than the cube dimensions, in order to accurately study the airflow around and inside the building.

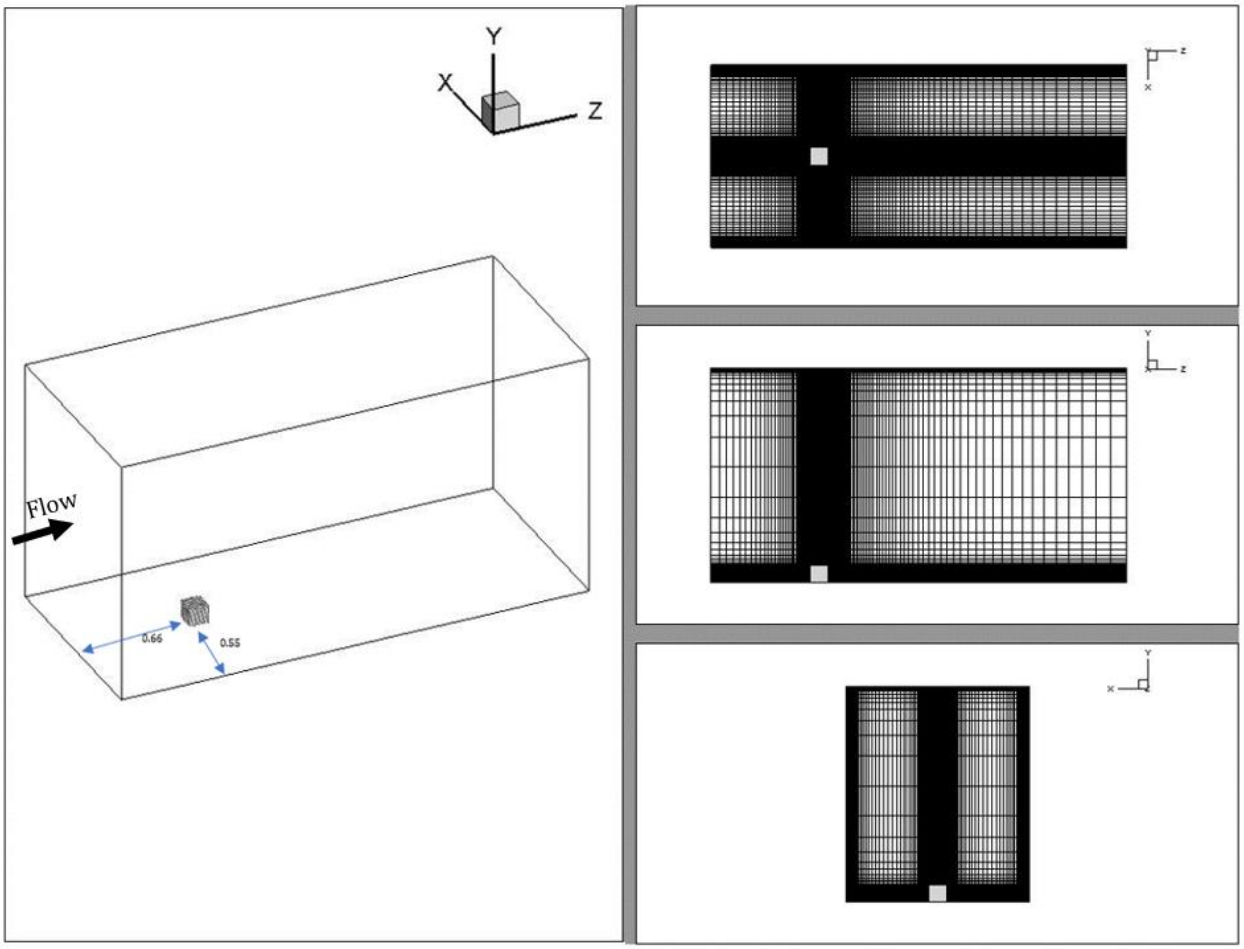

Figure 24: Left: Domain, Right: Top, Side and Front view of grid

For each test case we used the in-house CFD code to calculate the velocity field. All the simulations have been made using and the k-ε turbulence model. The inlet Velocity profile only has the w component i.e. $u = v = 0\ m/s$ and resembles a naturally occurring boundary layer (figure (25)), as measured by Pappa et al. [38]. Using the length of the building as reference length the Reynolds number is $Re = 0.36 * 10^5$.

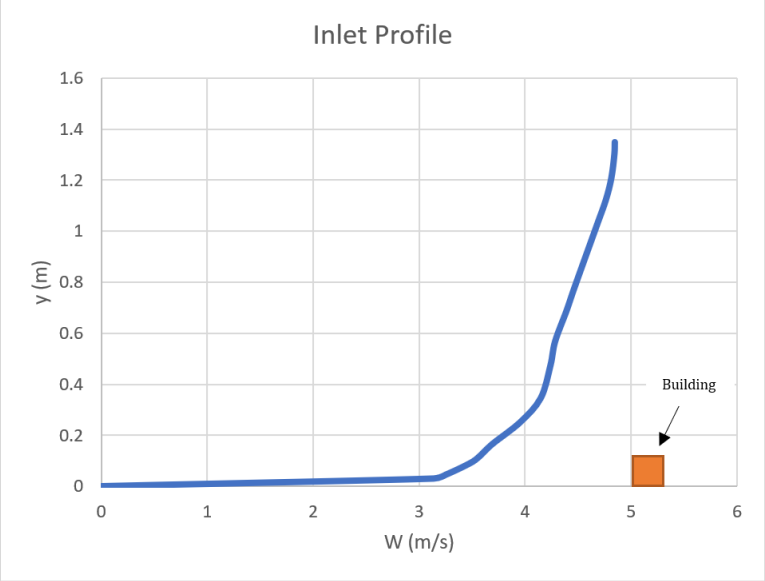

Figure 25: Inlet Velocity Profile

An example of a steady turbulent flow is that generated around a building by the wind, assuming that the wind speed and direction are constant. Similarly, flows inside enclosed spaces, such as rooms, are frequently described as both turbulent and steady. An illustrative scenario is the turbulent flow established within large openings when subjected to high winds. In contrast, an unsteady turbulent flow occurs when there is a transition from one steady state to another, such as when gradually closing one of the openings, resulting in changing flow patterns over time.

In our test cases, the solved velocity field is considered to be a steady state solution for a turbulent flow around the building. Based on this solution, we can run the AOA Software and determine the AOA at all points in the domain. An example of these results can be shown in figure (26). The top plot is a contour of the magnitude of the velocity that was calculated using the in-house CFD code and the bottom plot is a contour of the AOA that was calculated using the AOA Software.

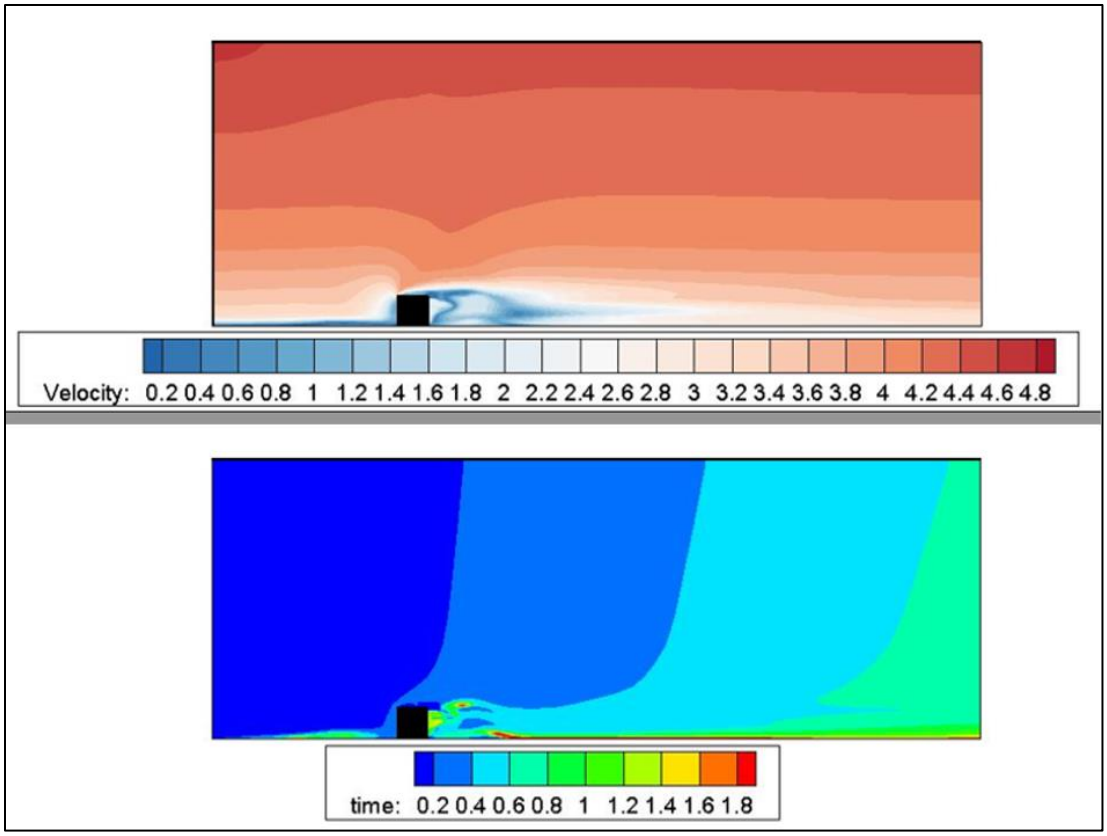

Figure 26:Top:Contour of Velocity Magnitude, Bottom: Contour of mean age of air

There is no need to evaluate the two plots in comparison to each other. Although the age of air is dependent upon the velocity field, there is no direct connection between the magnitude of the velocity and the AOA. From the top plot we can see that the velocity magnitude increases as we move along the y-axis, which is consistent with the form of the inlet profile. At the same time, it becomes zero near the walls, as a result of the no slip condition. As for the age of air, we can clearly see that its value increases as we move further towards the outlet. However, the distribution of the AOA outside the building offers no information about the indoor air quality. That's why in the following test cases we will focus on the inside of the buildings and not the whole domain.

The AOA results will be shown in 2D contour plots normal to the y-axis for three distinct heights within the building (figure (27)):

- **Height A**: $y = 0.04m$ (36% of the building's total height)
- **Height B**: $y = 0.06m$ (55% of the building's total height)
- **Height C**: $y = 0.08m$ (73% of the building's total height)

In addition to that all plots will show the tangential velocity vector.

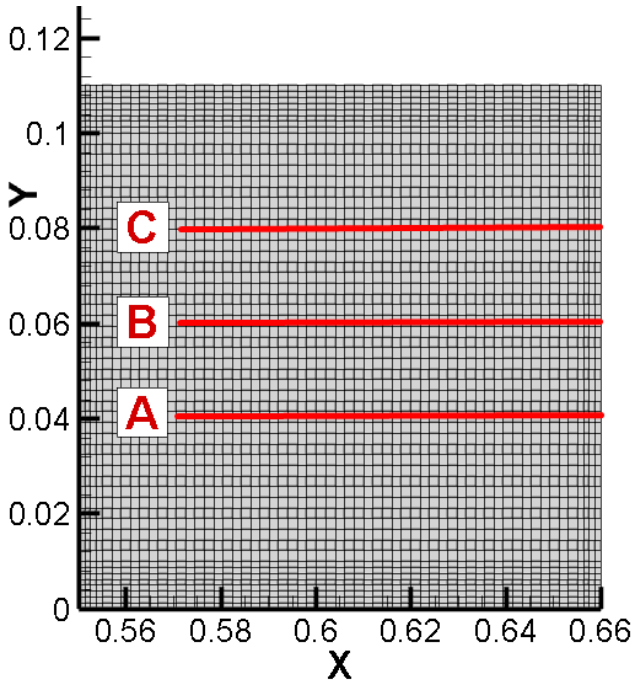

Figure 27: Height Positions

It is worth noting that areas of the building where air moves very slowly generate very high ages of air. These areas are called stagnation zones, they represent lack of fresh air and are associated with poor air quality. Representing these areas in a contour AOA plot can be challenging because they require a very big time-scale. If we included the true age values of stagnation zones in our plots, we would lose a great level of detail in the remaining areas. For that reason, in the post-processing stage, we chose to define a cut-off time. Any age of air higher than this constant cut-off time takes the value of the cut-off time. For our purposes the cut-off time was set to 2 seconds, which is twenty times the time it would take for an air particle to cover the distance of the building's length.

8.2 Test Case: **Full-Full Cube**

Running the age of air software for the Full-Full Cube yielded the results shown on figure (28).

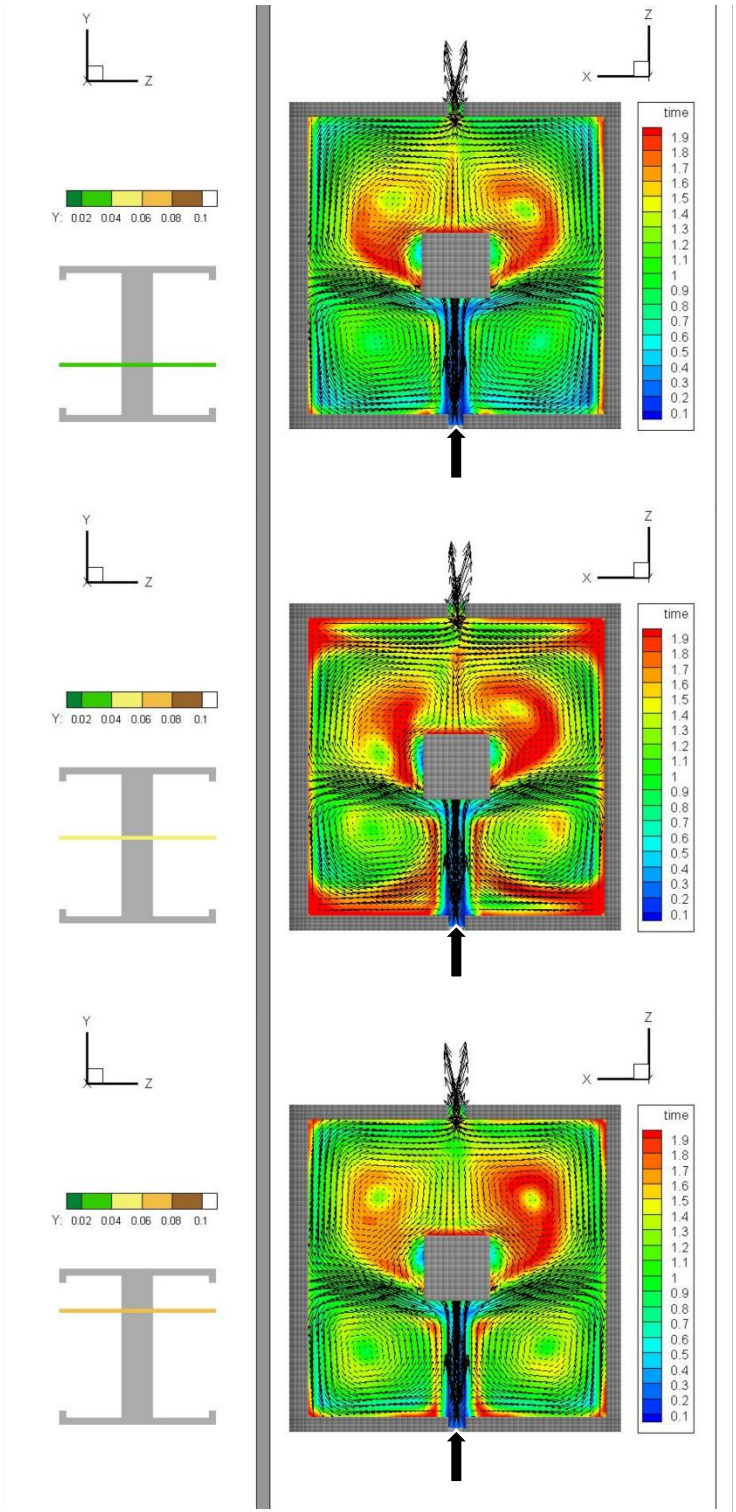

Figure 28:AoA results at heights A,B,C (from top to bottom) for Full-Full Case

From these plots we can observe some clear airflow patterns. Firstly, there is a high velocity stream of air entering from the front opening. As the air approaches the center column it changes direction and moves towards the walls. At this point some of it moves parallel to the wall until it finally exits from the rear opening and another part of it circles in the front area before rejoining the incoming air. The smallest velocity vectors can be observed on the left and right sides of the column as well as behind it. These appear to be areas of decreased air motion, increased age of air and therefore poorer air quality.

If we consider as symmetry plane the ZY plane that passes through the middle of the building, we can see a symmetry in the formed contours. This symmetry is evident at all heights and can be attributed to an analogously symmetrical velocity field. The symmetry of the velocity field is also clear when looking at the velocity vectors at each height. A symmetrical solution from the in-house CFD code is consistent with the desired steady-state turbulent flow around and inside a building. It is worth noting that at heights B and C there are some slight "imperfections" in the symmetry. This divergence from total mirroring is probably due to numerical issues related to convergence.

Another important symmetry can be found between heights A and C, since the AOA distribution in the upper half of the building resembles the AOA distribution in the lower half. This means that the air in the upper half

moves similarly to the lower half, which is to be expected for the Full-Full cube where the openings are of equal height and shape.

Moving on to the plot at height B one can observe slightly higher values of AOA near the corners of the building, compared to the results at A and C. It is possible that the top wall (i.e. the "ceiling") and the bottom wall (i.e. the "floor") influence the air flow, inducing vertical air motion near the corners. This is indeed true, as showcased by the contour of the y-component of velocity v in the figure (29). This effect is greater closest to the front corners and wanes as we move away from the "floor" and "ceiling". In that context, the increased age distribution at height B is a result of decreased vertical air motion.

Figure 29: Contour plot of v(m/s) taken at the midplane of the Full-Full building

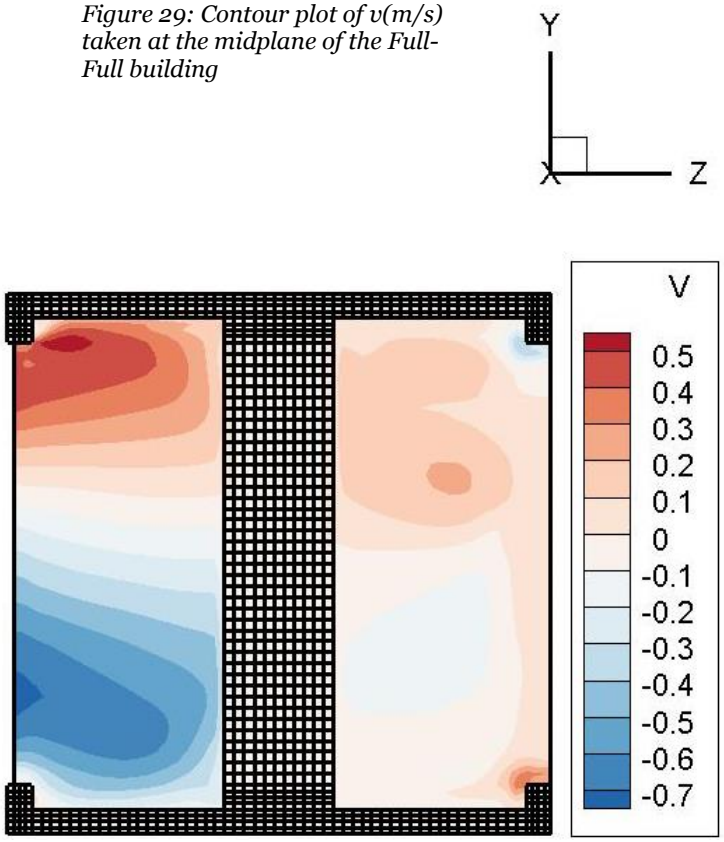

For a preliminary evaluation of indoor air quality, one can calculate the spatial average age of air of the building using the following equation:

$$\langle \tau_\alpha \rangle = \frac{1}{V_{tot}} \oint \tau_a dV = \frac{1}{V_{tot}} \sum_{p=0}^{n} \tau_{\alpha(p)} * V_p \quad (8.1)$$

where V_{tot} the total building volume, $\tau_{\alpha(p)}$ the AOA at a point P with a cell volume V_p. Based on this definition, the spatial average AOA is a measure of freshness of air in the entirety of the building. For the Full-Full case we get:

$$\langle \tau_\alpha \rangle = 1.468\ s$$

Overall, the Full-Full case displays airflow symmetry in multiple planes and seems to have a lot of areas with low ages of air.

8.3 Test Case: **Up-Full Cube**

Running the age of air software for the Up-Full Cube yielded the results shown on figure (30). Once again, we can see the symmetry around the column, associated with the steady-state solution of the velocity field.

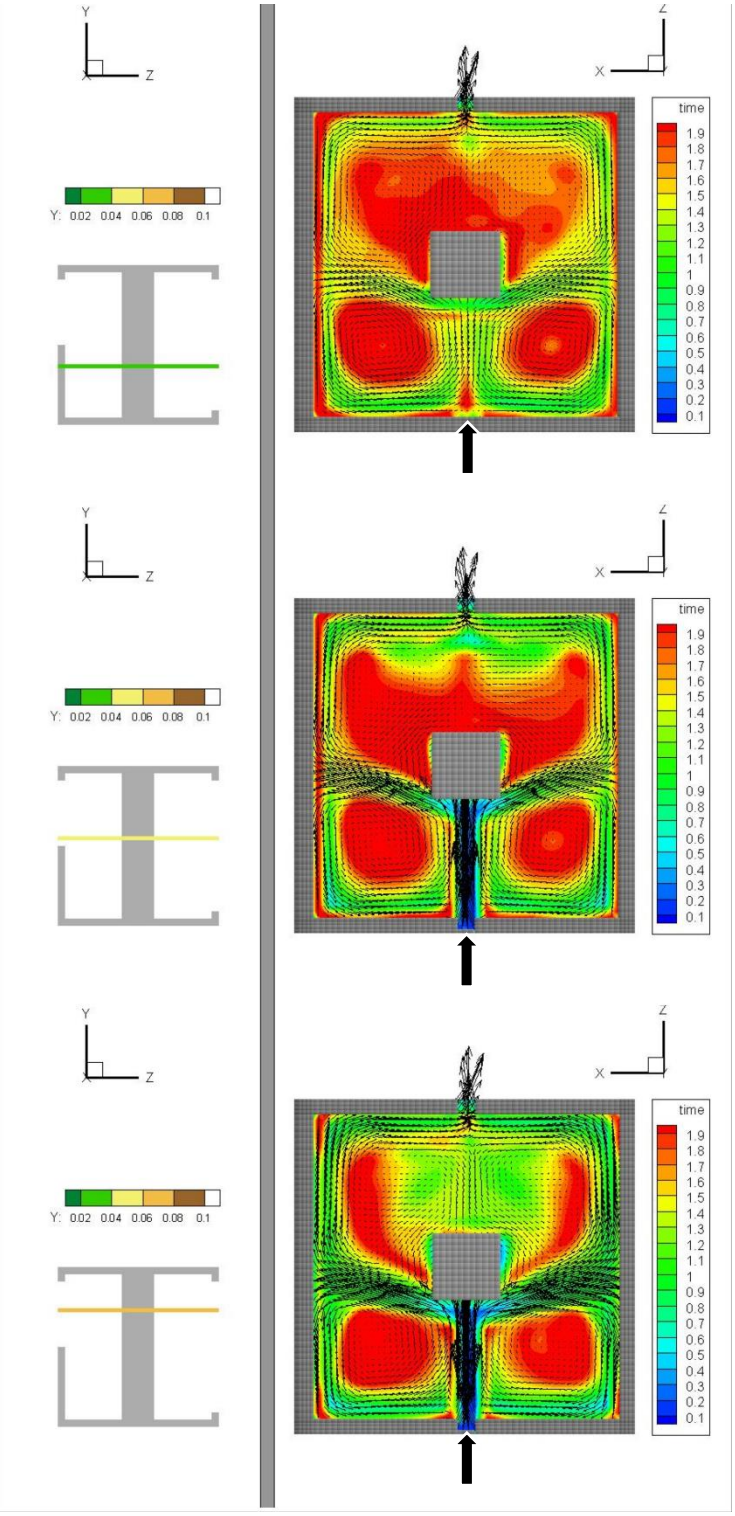

Figure 30: AOA results at heights A, B, C (from top to bottom) for Up-Full Case

Compared to the Full-Full case, the Up-Full case seems to generate overall higher values of AOA. The front area of the building has large stagnation zones (shown in red), where air is circulating very slowly. The rear area of the building also has large stagnation zones, especially at the lower heights A and B, where the front opening has been closed. Moving on to height C, the incoming jet of air helps reintroduce fresh air at the rear area.

The overall increase in the AOA is to be expected if we consider that by cutting the size of the front window in half, we have essentially limited the ventilation rate. This means that less fresh air enters the building and therefore the indoor ages increase more easily. In fact, this overall increase in age is also shown in the spatial average age which has increased by 17% compared to the Full-Full case.

$$\langle \tau_\alpha \rangle = 1.719\ s$$

Another interesting aspect of these results can be highlighted once again using a contour of the y-component of the velocity, as shown in figure (31). The vertical air motion is increased in the upper front area of the building, as a result of the incoming jet of air interacting with the ceiling of the building. The lower front area displays very weak downward vertical air motion, as a result of the absence of front opening at that level. In the rear area of the building vertical air motion remains weak, with some upward motion behind the lower half of the column. This is possibly created when air reflects on the lower edge of the rear opening.

Overall in the Up-Full case the incoming air in the upper half, fails to adequately ventilate the entirety of the building creating extensive areas of poor air circulation, especially at lower heights.

Figure 31: Contour plot of v(m/s) taken at the midplane of the Up-Full building

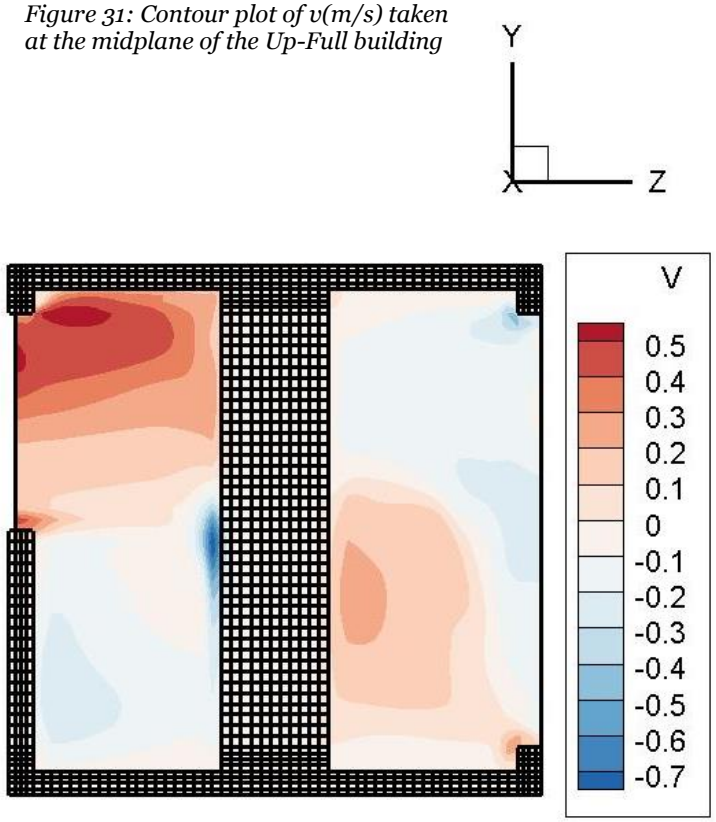

8.4 Test Case: **Down-Full Cube**

Running the age of air software for the Down-Full Cube yielded the results shown in figure (32).

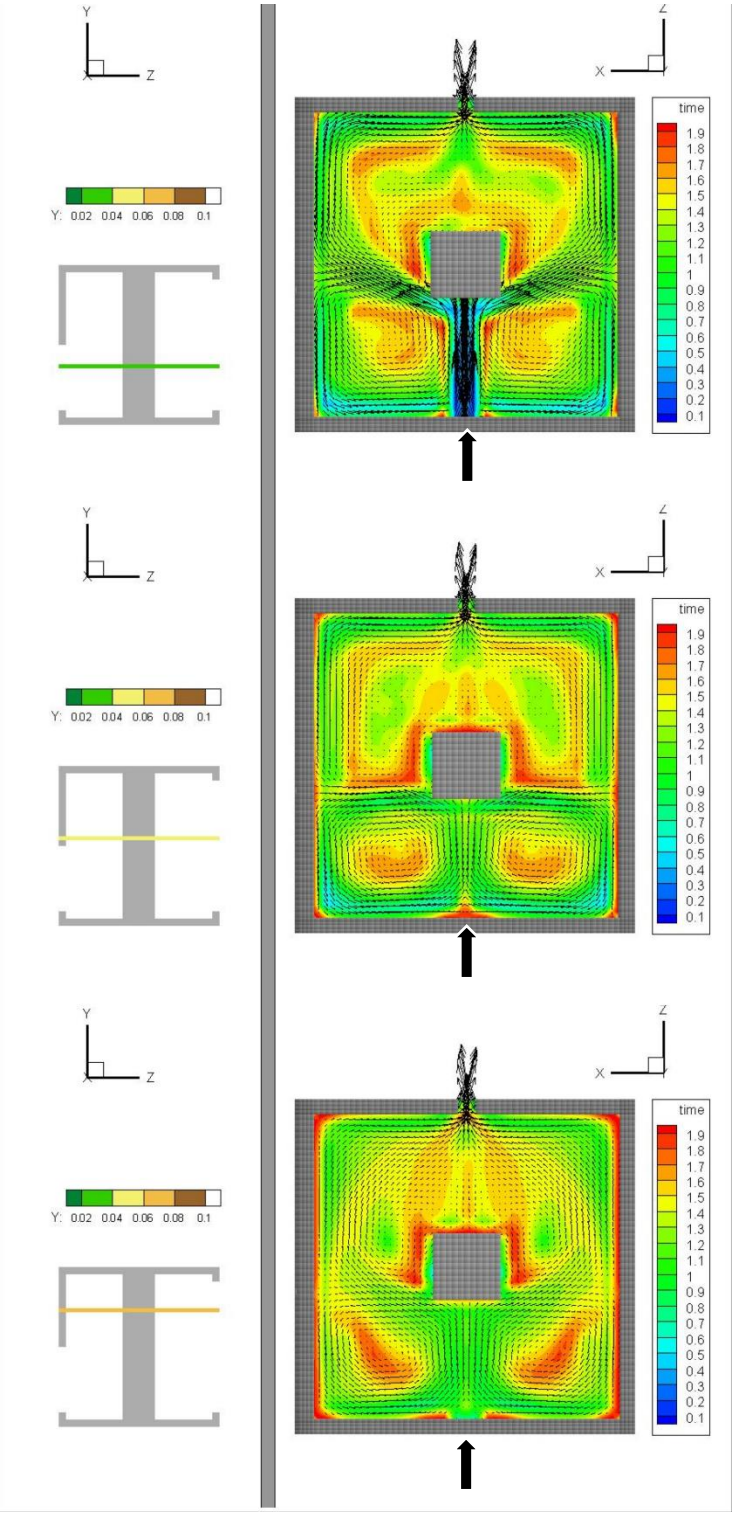

Figure 32: AOA results at heights A,B,C (from top to bottom) for Down-Full Case

This case offers the best representation of the steady state symmetry, we have seen so far. The calculation of both the velocity and the age of air appear to have converged to a realistic solution for a steady turbulent flow around this building.

In addition to that, this case has a comparatively low age distribution, with minimal stagnation zones. This is most apparent at height A, where the incoming jet directs air along the side walls of the building at high speed. However, even at heights above the front opening, the air circulation is maintained reasonably well. This means that more areas of the building have a good supply of fresh air.

Its spatial average was calculated:

$$\langle \tau_\alpha \rangle = 1.308\ s$$

which is 24 % lower than the one in the Up-Full case. This profound improvement in ventilation effectiveness proves that the lower upstream opening is much more effective in evenly distributing fresh air compared to the upper upstream opening. What is even more surprising however, is that the spatial average AOA in the Down-Full case is 11% lower than the one in the Full-Full case. Although the Full-Full case has larger upstream opening, it creates circulation zones behind the column where a substantial level of flow reversal takes place. This flow reversal prolongs the time air molecules stay in those areas and thus it increases the values of AOA. This pattern, is much milder in the Down-Full cube, where the circulation zones behind the

column appear to be much smaller in size. At the same time, the contours of age, display a lot of variation depending on the height of the building. This is indicative of strong vertical air motion, which can be illustrated using the contour of the y-component of the velocity (figure (33)). We can see that air entering the building has a strong downward velocity, which as discussed earlier is a result of interaction with the floor. Additionally, strong vertical air motion is also observed at the front upper area. Despite the absence of the upper half of the opening, this area is adequately supplied with air by incoming air which is directed upwards. Considerable upward air motion is also generated by the lower edge of the rear opening.

Figure 33: Contour plot of v(m/s) taken at the midplane of the Down-Full building

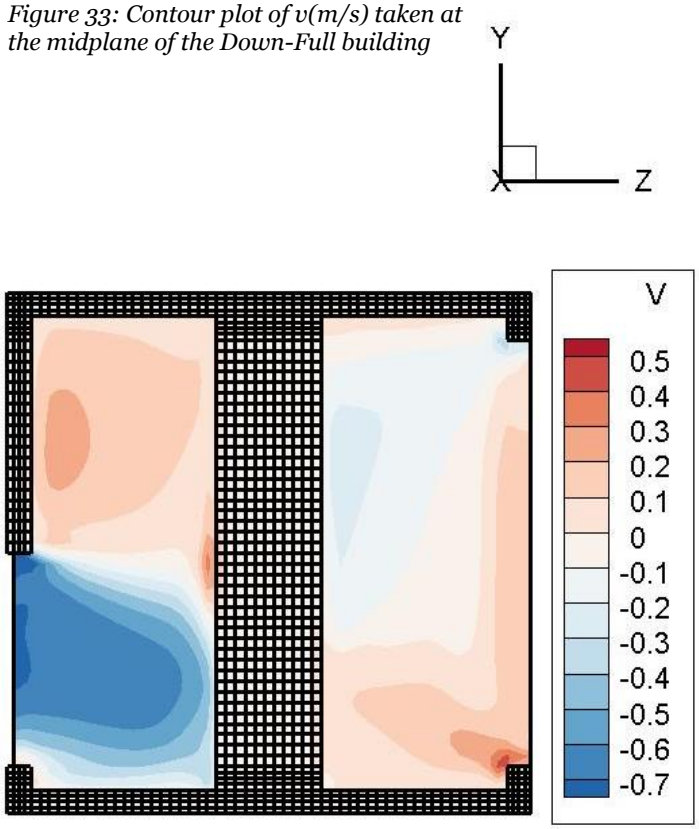

All in all, this configuration results in a very effective natural ventilation with minimal stagnation zones while sustaining strong air circulation both in the horizontal as well as the vertical direction.

8.5 Test Case: **Full-Down Cube**

The AOA results from for the Full-Down case are shown in figure (34). The symmetrical distribution of AOA is evident in all contours, showcasing the steady state nature of our solution.

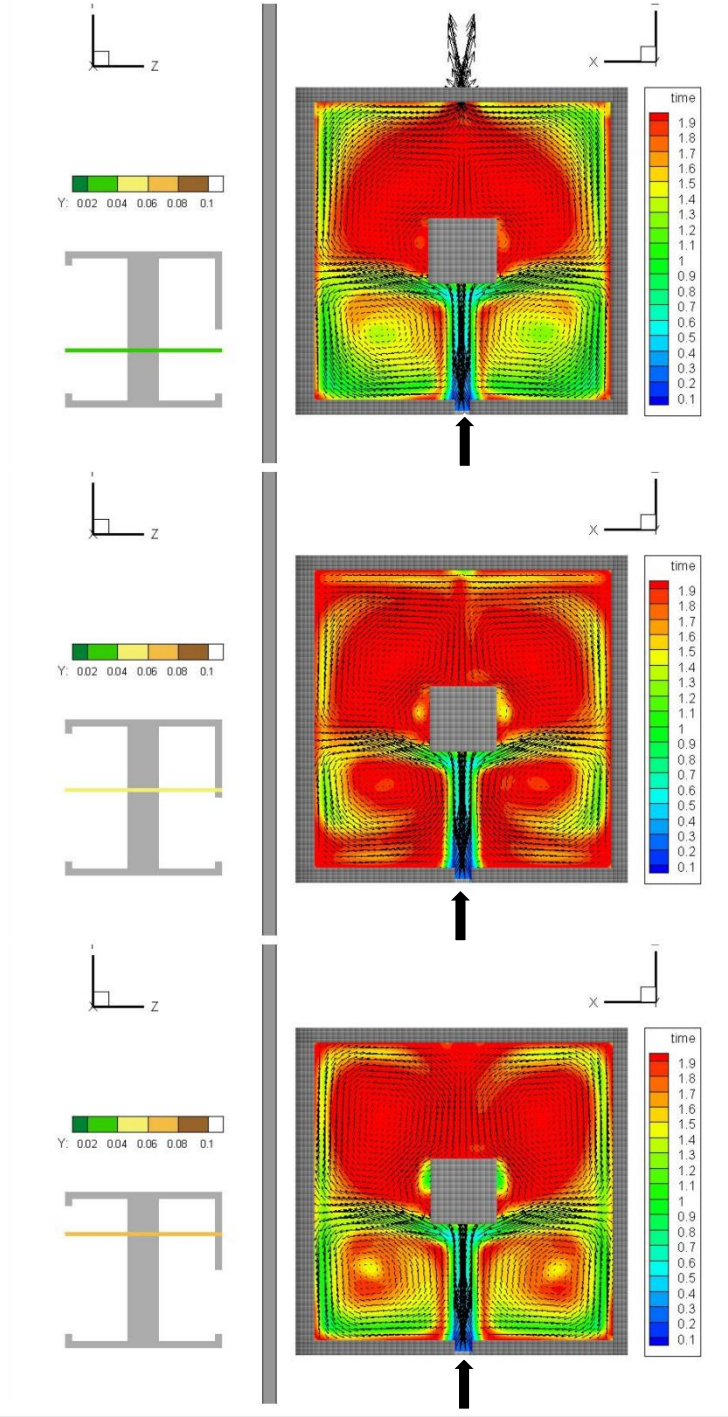

The Full-Down case can be considered as the reverse configuration of the Down-Full case, since the lower opening is now downstream instead of upstream. From the contours we observe a significant increase in the values of AOA compared to not only the Down-Full case but also the Up-Full and Full-Full cases. The area behind the column has wide stagnation zones at all heights indicating that the ventilation rate of exiting air is poor. In fact, this decrease in ventilation rate is stronger than it was for the Down-Full case, as also shown by the spatial average AOA which increased by 42.7% compared to the Down-Full case.

$$\langle \tau_\alpha \rangle = 1.867\ s$$

This highlights the impact of the size of the rear opening in drawing air outside, as a result of the lower pressure behind the building.

Figure 34:AOA results at heights A, B, C (from top to bottom) for Full-Down Case

The contour of the y-component of the velocity is shown in figure (35). Because of the full size of the upstream opening, incoming air in the upper half of the building is directed upwards and air in the lower half is directed downwards. At the rear there is very slow vertical air motion with the exception of the small areas surrounding the corners of the opening. Air close to the upper corner is reflected downwards and air close to the lower corner is reflected upwards.

Overall, blocking the downstream opening in the Full-Down case has significantly reduced the outflow rate in the building, created extensive stagnation zones and resulted in limited air circulation.

Figure 35: Contour plot of v(m/s) taken at the midplane of the Full-Down building

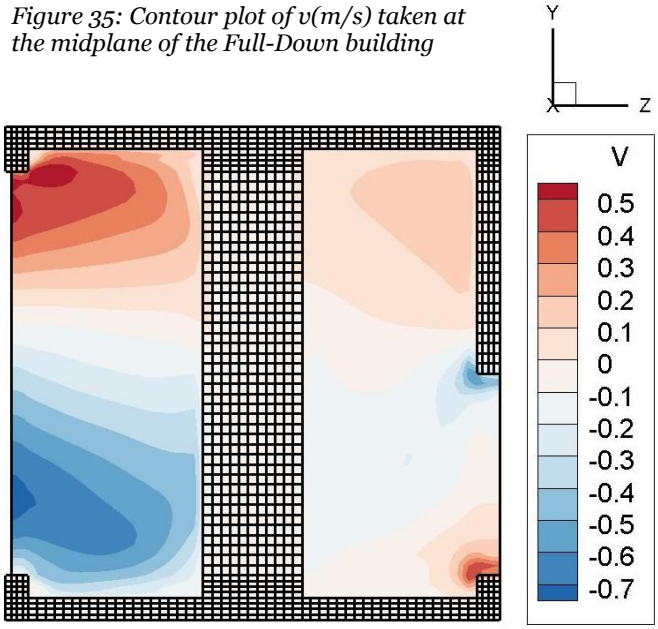

8.6 Test Case: **Down-Down Cube**

The Down-Down case is the first case where the size of both openings has been cut in half. This means that the ventilation rate has decreased even further, resulting in an overall increase in the age of air values. As a result, the existing time-scale is too small to distinctly illustrate the age of air distribution in the building. In order to increase the detail of our plots we increased the cut-off age to 3 seconds. This time-scale proves to be more fitting for the test cases where both openings have been cut in half.

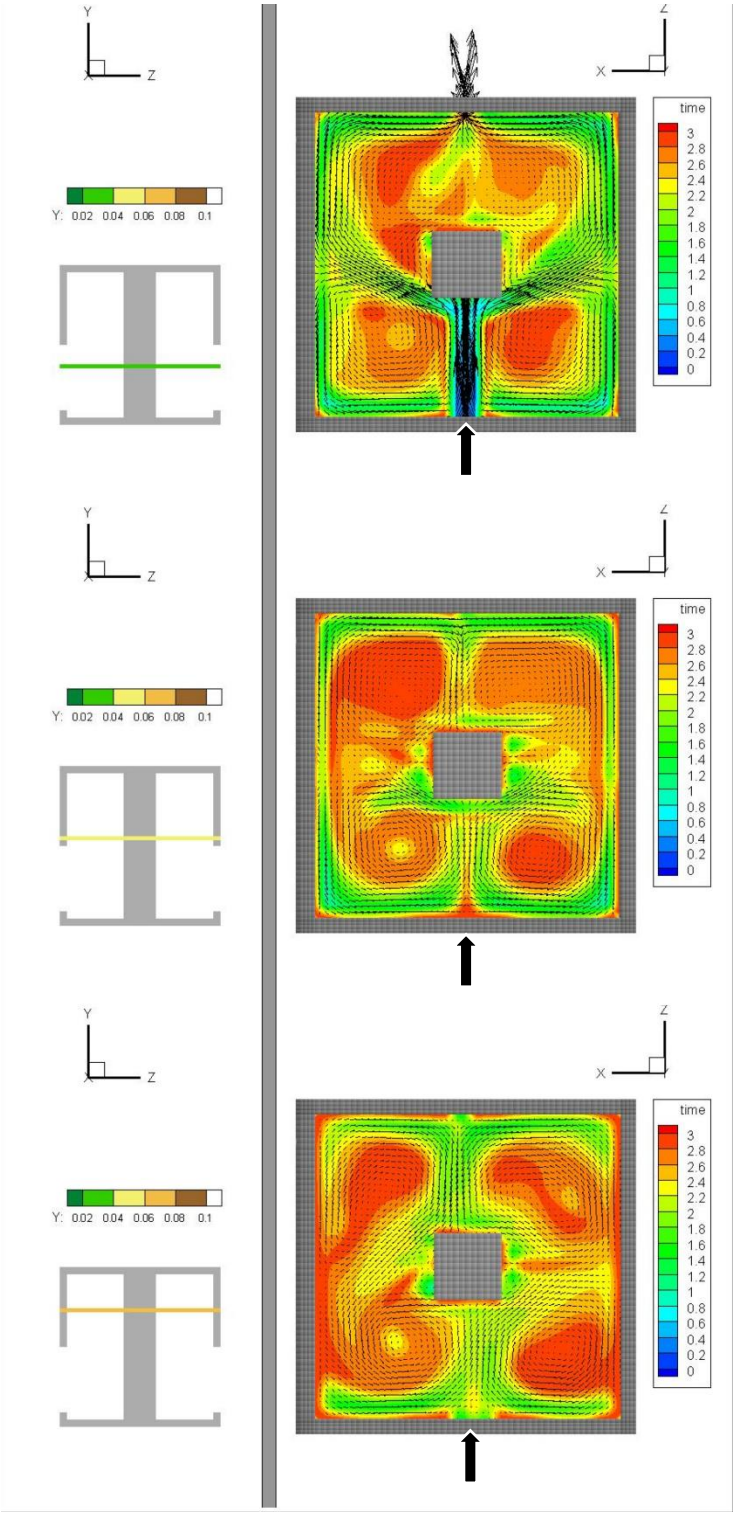

Figure 36: AoA results at heights A,B,C (from top to bottom) for Down-Down Case

The expected steady-state symmetry, although evident in figure (36), is not perfect. This can be attributed to the way the post processing tool (Tecplot) interpolates the results on the contour plot. Most probably however, it is caused by numerical issues related to the convergence of the velocity field.

From the extensive red zones, it is also clear that we have a lot of points in the building with AOA higher than 3s. At heights B and C which are above the level of the front opening, air is not supplied well enough, creating large stagnation zones along the whole length of the building. At height A, incoming air increases the circulation but the stagnation zones are not eliminated.

The spatial average age is:

$$\langle \tau_\alpha \rangle = 2.598\ s$$

Once again, we will use the contour of the y-component of the velocity to gain a better understanding of the airflow patterns inside the building. As we can see from figure (37) there are multiple areas of the building with high vertical velocity. In the front area incoming air is directed downwards while air near the ceiling is moving upwards. At the rear we have upward air motion both near the floor and near the ceiling.

Figure 37: Contour plot of v(m/s) taken at the midplane of the Down-Down building

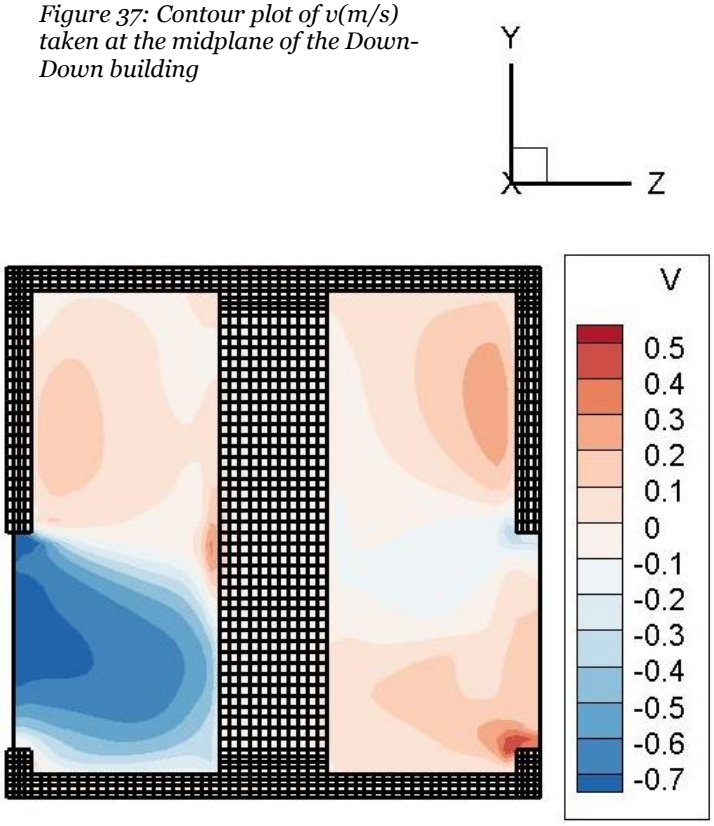

8.7 Test Case: **Down-Up Cube**

The Down-Up case is another case where the size of both openings has been cut in half. By using the same time scale (3 seconds) as the one used in the Down-Down case, we get the results shown in figure (38).

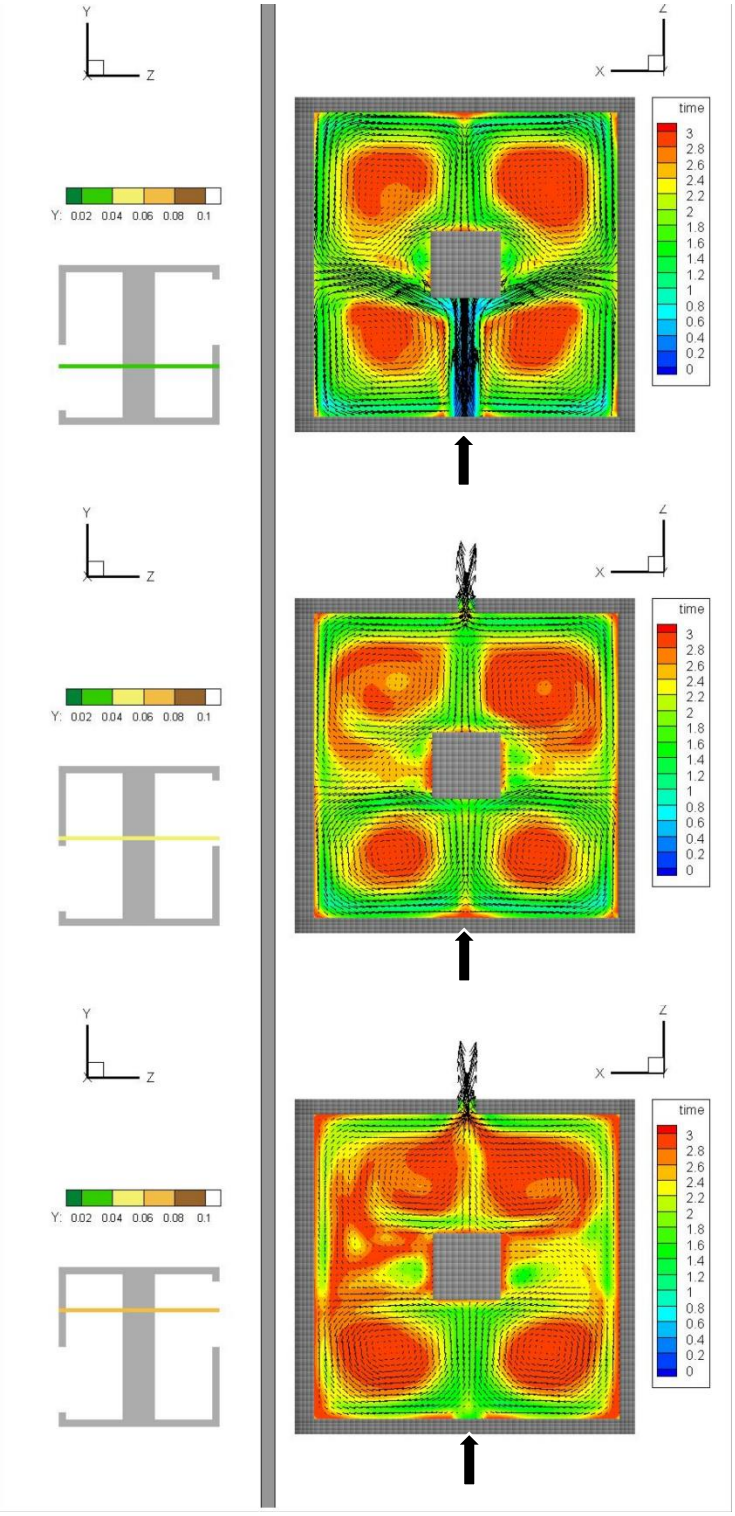

Figure 38: AoA results at heights A,B,C (from top to bottom) for Down-Up Case

The Down-Up case is another example of good steady state symmetry, albeit with some imperfections.

The values of AOA appear to be slightly lower compared to the Down-Down case. When the air entering from the lower half of the building encounters the column it is directed towards the side walls and creates four big circulation zones, two in the front and two in the rear area of the building. Although the circulating air has a high velocity it does not reach all the points in the domain, creating stagnation zones. These zones increase in size as we move upwards where the front opening is closed and fresh air is not in good supply.

The spatial average is equal to:

$$\langle \tau_\alpha \rangle = 2.551\ s$$

and is 1.8% lower than in the Down-Down case.

The contour of the y-component of the velocity will give us some more insight into the airflow inside the Down-Up building (Figure (39)). In the front area we have strong vertical motion which has a downward trajectory at the lower half and an upwards trajectory at the upper half. The strongest vertical air motion occurs at the rear of the building around the lower edge of the opening. There, air is deflected upwards, creating increased airflow and thus limiting the stagnation zones.

The Down-Up configuration appears to aid vertical air motion, although the limited ventilation rate is not enough to supply all the areas of the building with fresh air.

Figure 39: Contour plot of v(m/s) taken at the midplane of the Down-Up building

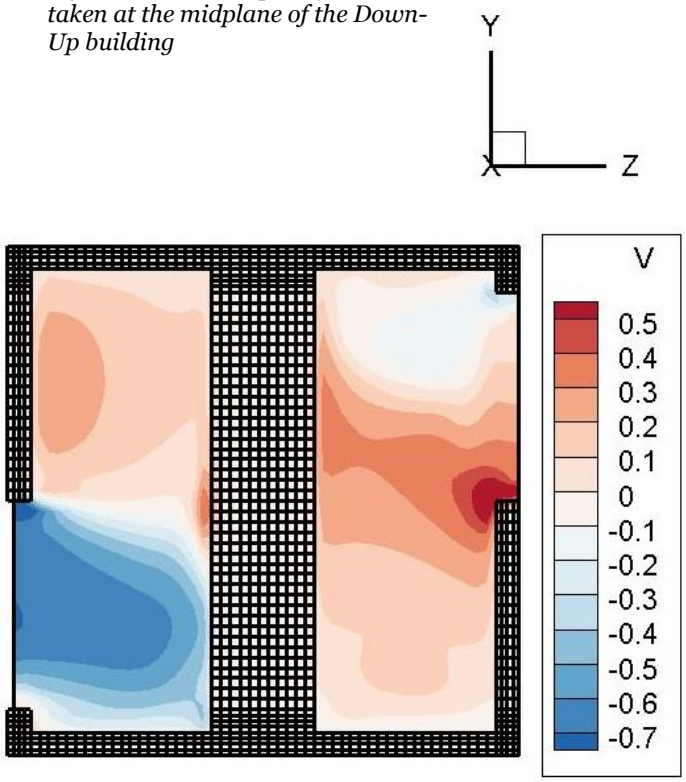

8.7 Results and Comments

Overall the results are consistent with the anticipated steady state symmetry and depending on the time scale they can accurately highlight complex patterns of airflow and age distribution.

The use of the spatial average AOA can help us quantify our AOA calculations and serve as a parameter for comparative analysis between the selected cases. In general, low values of the spatial average AOA, can be associated with "fresher", faster moving air and more efficient natural ventilation. As we can see from table (1), the case with the lowest spatial average AOA is the Down-Full configuration, followed by the Full-Full and Up-Full configuration. The remaining cases have much smaller size of openings, which means much lower ventilation rate. At the same time, a larger rear opening can create a suction effect, thus further increasing the exiting airflow rate. For these reasons, any type of comparison between the cases should take into consideration the size and position of the openings.

Table 1: Spatial average AOA for the selected cases

Test Case	Total size of the openings (as a fraction of the total size in "Full-Full")	Spatial Average AOA (s)
Full-Full	100%	1.468 (0%)
Up-Full	75%	1.719 (+17%)
Down-Full	75%	1.308 (-11%)
Full-Down	75%	1.867 (+27%)
Down-Down	50%	2.598 (+77%)
Down-Up	50%	2.551 (+74%)

In that context, we can create two separate groups of comparison:

A. The cases with no more than one half-blocked opening, namely the Full-Full, the Up-Full, the Down-Full and the Full-Down case.

B. The cases with both openings half-blocked, namely the Down-Down and the Down-Up case

Starting with group A, our observations on the provided contours, showed a clear advantage of the Down-Full case in circulating fresh air throughout the building while minimizing stagnation zones. This belief was confirmed by the value of spatial average AOA of the Down-Full case which is 11 % lower than the one in the Full-Full case. The positioning of the upstream opening in the lower half of the building allows for powerful airflow near the side walls and its upper corner induces strong vertical air motion. As a result, stagnant zones around the column are "broken-up" and they are resupplied with constantly moving fresh air. Overall, it appears that incoming air can be more efficiently distributed in the building when it's entering from the lower half.

A significant comparison can be made between the Down-Full and Full-Down case. These cases have the same total size of openings but in the Down-Full case the half opening is positioned upstream, whereas in the Full-Down case it is positioned downstream. Based on our results, reducing the size of the upstream opening, reduces the spatial average AOA by 11%, but reducing the size of the downstream opening yields 17% higher spatial average AOA. This profound effect of the downstream opening in the AOA, indicates the existence of a suction effect created by the lower pressure behind the building. When the size of the downstream opening is maximized, more air is exposed to the outside lower pressure and is therefore more effectively drawn outwards and renewed.

Moving on to group B, the Down-Down case was identified as having poor supply of fresh air and large stagnation zones in the upper half of the building. Incoming air from the lower half failed to adequately ventilate the upper half leading to increased values of AOA. As a result, its spatial average AOA distribution was lower than the one in the Down-Up case. The latter configuration proved to induce strong vertical air motion patterns that positively affected the natural ventilation of the building.

Chapter 9: Conclusions and Suggestions

The developed software has demonstrated its capability to accurately determine the age of air at all points inside a building through a series of successful test cases. These positive outcomes from the test cases provide confidence in the software's ability to model and predict the age of air distribution within indoor spaces.

As a result of the software's accurate predictions, it can be used in the future to calculate various parameters associated with the age of air, which are essential for evaluating indoor air quality. Unlike some simplified models that assume ideal piston flow (uniform mixing), the developed software takes into account the complexities of real-world indoor environments. It considers factors such as imperfect mixing and molecular diffusion, which are critical for a more realistic assessment of indoor air quality. This approach allows for a better understanding of how different parts of the indoor space may have different air ages and pollutant concentrations, leading to more informed decisions and strategies for improving indoor air quality.

In summary, the developed software's ability to accurately determine the age of air at all points within a building, while considering factors like imperfect mixing and molecular diffusion, enhances its utility for evaluating indoor air quality.

Potential improvements to the developed software can enhance its capabilities for evaluating indoor air quality. These improvements aim to provide a more comprehensive assessment of air quality within indoor spaces. Here are some of the enhancements that could be incorporated:

- Calculation of additional Parameters: Incorporating calculations of parameters like ventilation efficiency, air renovations parameter, net escape velocity would allow users to make more normalized and comparative assessments of how fresh air is distributed fresh throughout the building.
- Experimental Data Integration: Instead of calculating the velocity field using other CFD software, integrating experimental data from sources like wind tunnel tests can provide more flexibility to data processing. This approach ensures that the simulation reflects real-world conditions more closely.
- Standardized Approach for Stagnant Zones: To address the issue of representing stagnant or very slow-moving air zones, it's essential to develop a standardized methodology. This would prevent such zones from disproportionately influencing the overall age of air evaluations. Proper handling of these regions will lead to more accurate and meaningful results.

By incorporating these improvements into the software, users can perform more accurate and comprehensive evaluations of indoor air quality, taking into account a wider range of factors and parameters. This enhanced capability will be invaluable for designing effective ventilation strategies and ensuring healthier indoor environments.

References

[1] E. Clancy, "Indoor air quality and Ventilation," CIBSE Knowledge Series: KS17, 2011.

[2] A. Ernst and J. Zibrak, "Carbon Monoxide Poisoning," *New England Journal of Medicine 339,* 1998.

[3] C. Weschler, "Ozone's impact on public health: contributions from indoor exposures to ozone and products of ozone-initiated chemistry," *Environ. Health Perspect. 114,* 2006.

[4] J. Samet, "Radon and Lung Cancer," *JNCI Journal of the National Cancer,* 1989.

[5] J. Adgate, T. Church, A. Ryan, G. Ramachandran, A. Fredrickson and T. Stock, "Outdoor, indoor, and personal exposure to VOCs in children," *Environ. Health Perspect. 112,* 2004.

[6] D. Layton and P. Beamer, "Migration of Contaminated Soil and Airborne Particulates to Indoor Dust," *Environmental Science & Technology 43,* 2009.

[7] E. Heseltine and J. Rosen, "World Health Organization guidelines for indoor air quality: dampness and mould," WHO, 2009.

[8] J.-P. Zock, E. Plana, D. Jarvis, J. Anto, H. Kromhout, S. Kennedy and N. Kunzli, " The Use of Household Cleaning Sprays and Adult Asthma: An International Longitudinal Study," *American Journal of Respiratory and Critical Care Medicine,* 2007.

[9] K. Hess-Kosa, Indoor Air Quality-The latest in Sampling and Analytical Methods, CRC press Taylor & Francis Group, 2011.

[10] World Health Organization. n.d., "Sick Building Syndrome".

[11] B. R., "Microbiological agents as health risks in indoor air," *Environ. Health,* 1991.

[12] Y. e. a. Li, "Role of ventilation in airborne transmission of infectious agents in the built environment - a multidisciplinary systematic review," *Indoor Air 17,* 2017.

[13] T. Myatt, S. Johnston, Z. W. M. Zuo, T. Kebadze, S. Rudnick and D. Milton, "Detection of Airborne Rhinovirus and Its Relation to Outdoor Air Supply in Office Environments," *American Journal of Respiratory and Critical Care Medicine 169,* 2004.

[14] L. Laret, I. Lebrun, D. Marret and P. Nusgena, "Etude experimentale sur l'efficacit6 de la ventilation mecanique control~e dans un local d'habitation," University of Li6ge, Belgium, 1976.

[15] O. Lidwell, "The evaluation of ventilation," Camb., 1960.

[16] D. Spalding, "A note on mean residence-times in steady flows of arbitrary complexity," *Chem. Engng. Sci., No. 9,* 1958.

[17] M. Sandberg, "What is ventilation efficiency?," *Build. Environ. 16,* pp. 123-135, 1981.

[18] M. Chen, L. Fan, C. Hwang and E. Lee, "Air flow models in a confined space a study in age distribution," *Build. Sci. 4 (3) ,* pp. 133-143, 1969.

[19] W. Chow, W. Fung and L. Wong, "Preliminary studies on a new method for assessing ventilation in large spaces," *Building and Environment 37,* p. 145–152, 2002.

[20] W. Fisk, D. Faulkner, D. Sullivan and F. Bauman, "Air change effectiveness and pollutant removal efficiency during adverse mixing conditions," *Indoor Air 7,* pp. 55-63, 1997.

[21] A. Jung and M. Zeller, "An analysis of different tracer gas techniques to determine the air exchange efficiency in a mechanically ventilated room," in *4th International Conference on Air Distribution in Rooms*, Krakow, Poland, 1994.

[22] G. G., "Effective depth of fresh air distribution in rooms with single-sided natural ventilation.," *Energy and Buildings 31,* p. 65–73, 2000.

[23] Y. Li, L. Fuchs and S. Holmberg, "Methods for predicting air change efficiency," in *3rd International Conference on Air Distribution in Rooms*, Aalborg, Denmark, 1992.

[24] S. Hu and Y. Chuah, "Deterministic simulation and assessment of air recirculation performance of unidirectional-flow cleanrooms that incorporate age of air concept," *Building and Environment 38,* p. 563–570, 2003.

[25] O. Rouaud and M. Havet, "Numerical investigation on the efficiency of transient contaminant removal from a food processing clean room using ventilation effectiveness concepts," *Journal of Food Engineering 68,* p. 163–174, 2005.

[26] P. Stankov, "CFD prediction of air flow in a ventilated room as a tool for emerging design," *.Journal of Theoretical and Applied Mathematics 29,* pp. 101-112, 1999.

[27] J. Abanto, D. Barrero, M. Reggio and B. Ozell, "Airflow modelling in a computer room," *Building and Environment 39,* p. 1393–1402, 2004.

[28] M. Parra, J. Villafruela, F. Castro and C. Méndez, "Numerical and experimental analysis of different ventilation systems in deep mines," *Building and Environment 41,* pp. 87-93, 2006.

[29] W. Chow, " On safety systems for underground car parks," *Tunnelling and Underground Space Technology 13,* p. 281–287, 1998.

[30] J. Shen and L. Haas, " Calculating age and residence time in the tidal York River using three-dimensional model experiments," *Estuarine, Coastal and Shelf Science 61,* pp. 449-461, 2004.

[31] S. Kato, K. Ito and S. Murakami, "Analysis of visitation frequency through particle tracking method based on LES and model experiment," *Indoor Air 13,* pp. 182-193, 2003.

[32] S. Murakami, "New scales for ventilation efficiency and their application based on numerical simulation of room airflow," in *International Symposium on Room Air Convection and Ventilation Effectiveness*, 1992.

[33] G. Gan, "Effective depth of penetration of fresh air distribution in rooms with single-sided natural ventilation," *Building and Environment, 31,* p. 65–73, 2000.

[34] G. Lube, T. Knopp, G. Rapin, R. Gritzki and M. Rosler, "Stabilized finite element methods to predict ventilation effectiveness and thermal comfort in buildings," *International Journal for Numerical Methods in Fluids 57,* p. 1269–1290, 2008.

[35] D. Etheridge, Natural Ventilation of Buildings: Theory, Measurement and Design, First Edition., John Wiley & Sons Ltd., 2012.

[36] H. Montazeri and F. Montazeri, *Renewable Energy 118,* pp. 502-520, 2018.

[37] S. Sokolfsky and G. H. Jirka, CVEN 489-501: Special Topics in Mixing and Transport Processes in the Environment, Texas A&M University, 2005.

[38] V.Pappa, M. M.Manolesos and D.Bouris, "Numerical and Experimental study of the flow past a generic cubic building with openings embedded in a turbulent boundary layer," *Building and Environment 141,* pp. 166-181, 2018.

[39] Y. Adachi, N. Ikegaya, H. Satonaka and A. Hagishima, "Numerical simulation for crossventilation flow of generic block sheltered by urban-like block array," *Build. Environ. 185,* 2020.

[40] S. Kato, K. Ito and S. Murakami, "Analysis of visitation frequency through particle tracking method based on LES and model experiment," *Indoor Air 13,* pp. 182-193, 2003.

[41] G. Csanady, "Dispersal by randomly varying currents," *J. Fluid Mech. 132,* pp. 375-394, 1983.

[42] M. Sandberg and M. Sjoberg, "The use of moments of air for assessing air quality in ventilated rooms," *Build. Environ. 22,* pp. 111-127, 1987.

[43] L. Davidson and E. Olsson, "Calculation of age and local purging flow rate in rooms," *Build. Environ. 22,* pp. 111-127, 1987.

[44] E. Lim, K. Ito and M. Sandberg, "New ventilation index for evaluating imperfect mixing conditions - analysis of net escape velocity based on RANS approach," *Build. Environ. 61,* pp. 45-56, 2013.

[45] N. Ikegaya, K. Ito and M. Sandberg, "Rigorous mathematical formulation of net escape velocity and net escape probability determining a macroscopic concentration," *Indoor Air 32,* 2022.

[46] E. Lim, K. Ito and M. Sandberg, "Performance evaluation of contaminant removal and air quality control for local ventilation systems using the ventilation index Net Escape Velocity," *Build. Environ. 79,* pp. 78-89, 2014.

[47] E. Lim, J. Chung, M. Sandberg and K. Ito, "Influence of chemical reactions and turbulent air quality control for local ventilation systems using the ventilation index Net Escape Velocity," *Build. Environ. 79,* p. 78–89, 2014.

[48] J. Chung, E. Lim, M. Sandberg and K. Ito, "Returning and net escape probabilities of contaminant at a local point in indoor environment," *Build. Environ. 125,* pp. 67-76, 2017.

[49] Σ. Τσαγκάρης, Μηχανική των Ρευστών-Θεωρία και Ασκήσεις, Αθήνα: Εκδόσεις Τσιότρας, 2016.

Appendix (A): A Guide to the Main Code

Before running the code, the user should write the domain dimensions (`X_tot, Y_tot, Z_tot`) and grid size (`Ni, Nj, Nk`) in a file named MY_DIMENSIONS.txt. If he/she intends to use data from the in-house CFD Software the following additional files are required: `DBASEGRID`, `tecgrid_00.dat`, `tecresults_00.dat`. After specifying the desired parameters (see below) the code is ready run. A more detailed overview of its structure (compared to the one given in Chapter 6) is given below:

[1] **Definition of Parameters:**

The code begins with parameter definitions that include options for

- the usage the in-house CFD code. The value of `CAFFCA` defines whether you will import results from the in-house CFD code (0 for not using in-house CFD code results, 1 for using in-house CFD code results),
- flow directions (X, Y, or Z). The value `FLOW`, defines the direction of the flow (for `FLOW =1` we have flow along the x-direction, for `FLOW =2` we have flow along the along the y-direction for `FLOW =3` we have flow along the along the z-direction
- maximum iteration count. The value `max_iter` defines the max number of iterations needed to solve the TDMA using ADI (usually set to 2000)
- density. The value `dens`, defines the air density (set to 1.1691 kg/m3)
- convergence criterion. The value `RES_LIMIT` defines convergence criterion of the solver (usually set to 10E-04 or any other small number depending on the desired accuracy.

[2] **Variable Declarations**: Various integer and real variables are declared to store information about grid dimensions, grid coordinates, velocity components, and matrices used in solving the time-dependent equation. Arrays are also allocated for these variables.

[3] **Reading Case Parameters:**

The code reads parameters related to the computational domain, such as the total grid dimensions (`X_TOT, Y_TOT, Z_TOT`), and assigns them to variables `Ni, Nj`, and `Nk`.

[4] **Grid Generation**:

Depending on the value of `CAFFCA`, the code either imports grid and velocity field data or generates its own grid and velocity field. In cases where we wish not to use the in-house CFD code (`CAFFCA=0`), a grid can be generated using the subroutine my_grid. However, since we often prefer to use the velocity field produced by in-house CFD code, it makes sense to import the in-house CFD code grid as well. So, when the parameter CAFFCA is set to 1, the program imports the grid and velocity field from the file tecresults_00.dat, using the subroutine dimensions, which imports the basic dimensions of the grid and the subroutine `CAFFCA_INPUT`, which imports the grid co-ordinates, the velocity field and viscosity.

[5] **Wall and Block Definitions**:

The code includes functions to create walls and blocks within the domain based on the in-house CFD code input. These structures represent physical barriers or obstacles within the computational domain. This part of the code is necessary in order to correctly apply the

boundary conditions on the surfaces of walls, at the entrance of the field as well as its exit. For that reason we introduce a variable named `IWALL(i,j,k)`,which has a different value for each cell and denotes one of the following things:

- If `IWALL=0`, cell in empty space
- If `IWALL=+1`, cell at the entrance of the domain
- If `IWALL= -1`, cell at the exit of the domain
- If `IWALL=+10` or `+100`, cell on the boundary face normal to the x-axis (+10 for the lower face and +100 for the higher)
- If `IWALL=+20` or `+200`, cell on the boundary face normal to the y-axis (+20 for the lower face and +200 for the higher)
- If `IWALL=+30` or `+300`, cell on the boundary face normal to the z-axis (+30 for the lower face and +300 for the higher)

[6] **Linear System Creation**:

The code creates a linear system of equations based on the grid, velocity field, and boundary conditions. It allocates matrices and computes coefficients for diffusion and convection terms for each cell in the grid.

[7] **ADI (Alternating Direction Implicit) Solver**:

The time-dependent equation is solved using the ADI method. Depending on the flow direction, the code iteratively calculates the age of air for each grid cell. The time evolution is handled in different directions (X, Y, or Z) based on the chosen flow direction. The code iterates until a convergence criterion is met or the maximum number of iterations is reached.

[8] **Convergence Check:**

The code continuously checks for convergence by calculating the residual error between successive iterations. If the convergence criterion is met, the code exits the loop. Otherwise, it continues iterating until convergence or until it reaches the maximum allowed iterations.

[9] **Results Output:**

The code includes functions to write various results, including the maximum age of air, parameters, and potentially visualization data. The AOA data for the whole domain are written in a file named `MY_PRE_RESULTS.dat`. Data describing the geometry of the grid are written in the file `MY_GRID.dat`. Data about the boundaries is written in file `MY_WALLS.dat`.

[10] **Subroutines:**

The code contains several subroutines that perform specific tasks such as cell geometry calculations, diffusion and convection term calculations, and boundary condition handling.

Appendix (B): A Guide to the Post-processing Code

This program takes input simulation data, processes it by zooming in specific regions, calculates relevant quantities, and prepares the data for visualization using Tecplot. In order to run the file `MY_PRE_RESULTS.dat` is required. A more detailed overview of the code is shown below:

[1] **Initialization and Constants**:

These include a constant representing a time cutoff value, various variables and arrays to store simulation data, such as coordinates (`X, Y, Z`), `time`, velocity components (`U, V, W`), and total velocity magnitude (`Velocity`).

[2] **Reading Case Parameters**:

The program starts by reading case parameters from an input file, such as the simulation domain's dimensions (`X_TOT, Y_TOT, Z_TOT`), grid size (`Ni, Nj, Nk`), the number of elements (`nelem`) and nodes (`nodes`), and element connectivity (`ielem, jelem, kelem`).

[3] **Reading AGE OF AIR Results**:

The program reads simulation results from another input file ('MY_PRE_RESULTS.dat'), which contains data for X, Y, Z, time, U, V, W, and Velocity. The format of the data appears to be in columns.

[4] **Data Validation and Cleanup**:

The program checks the imported time data for irregularities, such as values exceeding `time_cut_off`, negative values, or NaNs. It adjusts or replaces these values as necessary and counts the occurrences of such irregularities.

[5] **Calculations:**

It calculates the spatial average age of air (`T_a`) within the simulation domain based on volume-weighted averaging of time values. It calculates the average residence time (`T_r`), which is twice the average age of air. It calculates the air renovation rate per hour (`ARH`) as 3600 divided by `T_r`.

[6] **Writing Results for Tecplot:**

The program prepares and writes the simulation results to an output file (`MY_POST_RESULTS.dat`) in a format compatible with Tecplot. This includes defining variables and zones for Tecplot, writing coordinates, time, velocity components, and optionally specifying solid walls.

[7] **Zoom Time Data Generation**:

The program provides a subroutine `write_zoom_time` for generating zoomed-in time data for a specified region within the simulation domain. It calculates new coordinates, time, and velocity components for the specified zoomed region and writes this data to a separate output file (`MY_ZOOM_RESULTS.dat`).

[8] **Supporting Subroutines**:

Several supporting subroutines are provided, including 'parameters' (for reading case parameters), 'find' (for finding the closest value in an array), `TextSearch` (for searching for text within a file), and `Last_TextSearch` (for finding the last occurrence of a word within a file).